2017

The Effect of Corrosion Defects on the Failure of Oil and Gas Transmission Pipelines: A Finite Element Modeling Study

Jennet Orasheva
University of North Florida, orasheva.j@gmail.com

THE EFFECT OF CORROSION DEFECTS ON THE FAILURE OF OIL AND GAS TRANSMISSION PIPELINES: A FINITE ELEMENT MODELING STUDY

by

Jennet Orasheva

A thesis submitted to the School of Engineering

In partial fulfillment of the requirements for the degree of

Master of Science in Mechanical Engineering

UNIVERSITY OF NORTH FLORIDA

COLLEGE OF COMPUTING, ENGINEERING, AND CONSTRUCTION

July 2017

Acknowledgments

I would sincerely like to thank my advisor and supervisor, Dr. Murat Tiryakioglu, for many learning possibilities suggested through my studies, along with his excellent guidance and professional support. Also, I would like to thank him for the inspiration, friendship and encouragement throughout Master's program.

I would like to express my gratitude for committee members, Dr. Alexandra Schonning and Dr. Paul Eason. I am thankful to Dr. Schonning for willingness to help constantly and for her advice, and for the access to the rapid prototyping laboratory, which let me carry out my research productively.

I would like to thank, Dr. David Johnson, Director, Pipeline Safety from Energy Transfer, for providing complete report for real corrosion data of the oil and gas transmission pipelines. With help of the report this project could be implemented successfully.

I am wholeheartedly thankful to my friends and department faculty and staff for making my experience unforgettable.

I would like to thank my mother, who always believed in me and supported and supports emotionally.

Last, but certainly not least, I am thankful to my husband, who believed in me and supported throughout my studies.

Abstract

The transportation of oil and gas and their products through the pipelines is a safe and economically efficient way, when compared with other methods of transportation, such as tankers, railroad, trucks, etc. Although pipelines are usually well-designed, during construction and later in service, pipelines are subjected to a variety of risks. Eventually, some sections may experience corrosion which can affect the integrity of pipeline, which poses a risk in high-pressure operations. Specifically, in pipelines with long history of operation, the size and location of the corrosion defects need to be determined so that pressure levels can be kept at safe levels, or alternatively, a decision to repair or replace the pipe section can be made. To make this decision, there are several assessment techniques available to engineers, such as ASME B31G, MB31G, DNV-RP, software code called RSTRENG. These assessment techniques help engineers predict the remaining strength of the wall in a pipe section with a corrosion defect. The corrosion assessment codes in the United States, Canada and Europe are based on ASME-B31G criterion for the evaluation of corrosion defects, established based on full-scale burst experiments on pipes containing longitudinal machined grooves, initially conducted in 1960s. Because actual corrosion defects have more complex geometries than machined grooves, an in-depth study to validate the effectiveness of these techniques is necessary. This study is motivated by this need.

The current study was conducted in several stages, starting with the deformation behavior of pipe steels. In Phase 1, true-stress-true plastic strain data from the literature for X42 and X60 steel specimens were used to evaluate how well four commonly used constitutive equations, namely, those developed by Hollomon, Swift, Ludwik and Voce, fit the experimental data. Results showed that all equations provided acceptable fits. For simplicity, the Hollomon equation was selected to be used in the rest of the study.

In Phase 2, a preliminary finite element modeling (FEM) study was conducted to compare two failure criteria, stress-based or strain-based, performed better. By using data from the literature for X42 and X60 pipe steels, experimental burst pressure data were compared with predicted burst pressure data, estimated based on the two failure criteria. Based on this preliminary analysis, the stress-based criterion was chosen for further FEM studies.

In Phase 3, failure data from real corrosion pits in X52 pipe steels with detailed profiles were used to develop a FEM scheme, which included a simplified representation of the defect. Comparison of actual and predicted burst pressures indicated a good fit, with a coefficient of determination (R^2) level of 0.959.

In Phase 4, burst pressure levels were estimated for real corrosion pits for the experiments from the same study as in Phase 3, but only with corrosion pit depths and length and without corrosion widths. Widths were estimated from the data used in Phase 3, by using an empirical equation as a function of pit length. There was significant error between experimental and predicted burst pressure. Errors in Phases 3 and 4 were compared statistically. Results showed that there is a statistically significant difference in the error when the width of the corrosion pit is unknown. This finding is significant because none of the assessment techniques in the literature takes width into consideration. Subsequently, a parametric study was performed on three defect geometries from the same study in Phase 3. The pit depths and lengths were held constant but widths were changed systematically. In all cases, the effect of the pit width on burst pressure was confirmed.

In Phase 5, the three assessment techniques, ASME B31G, MB31-G and DNV-RP were evaluated by using experimental test results for X52 pipe. Synthetic data for deeper pits were developed by FEM and used along with experimental data in this phase. Two types of the error

were distinguished to classify defects. Type I errors (α) and Type II errors (β) were defined using Level 0 evaluation method. Results showed that although ASME B31G is the most conservative technique, it is more reliable for short defects than MB31G and DNV-RP. The least conservative technique was DNV-RP but it yielded β error, i.e., the method predicted a safe operating pressure and pipe section would fail. Therefore, DNV-RP is not recommended for assessment of steel pipes, specifically for X52 pipes.

Table of Contents

List of the figures

List of the tables

Nomenclature

α	Type I error
β	Type II error
σ_Y	Material yield strength (MPa)
ρ	Fluid density (kg/m^3)
$\bar{\sigma}$	Flow stress (MPa)
σ^2	Population variance
σ_e	Equivalent stress (MPa)
σ_H	Circumferential/hoop stress (MPa)
σ_L	Longitudinal stress (MPa)
σ_R	Radial stress (MPa)
σ_{TS}	True tensile strength (MPa)
$\sigma_{TS,(SM)}$	Specified minimum yield strength (MPa)
$\sigma_{Y,(SM)}$	Specified minimum tensile strength (MPa)
σ_{VM}	Von-Mises stress (MPa)
A_0	Original cross-sectional area of the pipe at the defect (m^2)
C	Constant used for approximation of corrosion profile
D	Pipe outer diameter (m)
d	Maximum defect depth (m)
$\frac{d}{t}$	Normalized defect depth
% e	Percent error
E	Elastic modulus (GPa)
E_L	Longitudinal joint factor in wall thickness calculation
$f_{\frac{\alpha}{2},n_1-1,n_2-1}$	Percentage points of the F distribution
f	Darcy friction factor
F	Design factor in wall thickness calculation
g	Gravitational acceleration (m/s^2)
$\frac{L}{\sqrt{Dt}}$	Normalized defect length
L	Maximum defect length (m)

L_p	Length of pipeline section (m)
n_1 and n_2	Number of data points with estimated and actual defect width
ΔP	Pressure drop (kPa)
$P_{f\text{-}exp}$	Experimental failure (burst) pressure (kPa)
$P_{f\text{-}FEM}$	Predicted failure (burst) pressure using FEA (kPa)
$P_{f\text{-}pred}$	Predicted failure (burst) pressure (kPa)
P_i	Internal pressure (kPa)
P_O	External atmosphere pressure; P_O = 1 atm.
Q	Flow rate (m^3/s)
r	Radius to the point of interest (m)
R^2	Coefficient of determination
R_e	Reynolds number
r_i	Pipe inside radius (m)
r_O	Pipe outside radius (m)
s^2	Sample variance
S_C	Circumferential space between corrosion defects (m)
SG	Specific gravity
S_L	Longitudinal space between corrosion defects (m)
SS_E	Residual sum of squares
SS_T	Total sum of squares
S_{TS}	Material tensile strength (MPa)
t	Pipe wall thickness (m)
T	Temperature derating factor in wall thickness calculation
v	Average velocity of the fluid (m/s)
w	Maximum defect width (m)

Abstract

The transportation of oil and gas and their products through pipelines is safe and economically efficient, when compared with other methods of transportation, such as tankers, railroad, trucks, etc. Although pipelines are usually well-designed, during construction and later in service, pipelines are subjected to a variety of risks. Eventually, some sections may experience corrosion that can affect the integrity of the pipeline, and which poses a risk in high-pressure operations. Specifically, in pipelines with long history of operation, the size and location of the corrosion defects need to be determined so that pressure levels can be kept at safe levels, or alternatively, a decision to repair or replace the pipe section can be made. To make this decision, there are several assessment techniques available to engineers, such as ASME B31G, MB31G, DNV-RP and software code called RSTRENG. These assessment techniques help engineers predict the remaining strength of the wall in a pipe section with a corrosion defect. The corrosion assessment codes in the United States, Canada and Europe are based on ASME-B31G criterion for the evaluation of corrosion defects, established based on full-scale burst experiments on pipes containing longitudinal machined grooves, initially conducted in 1960s. Because actual corrosion defects have more complex geometries than machined grooves, an in-depth study to validate the effectiveness of these techniques is necessary. This study is motivated by this need.

The current study was conducted in several stages, starting with the deformation behavior of pipe steels. In Phase 1, true stress-true plastic strain data from the literature for X42 and X60 steel specimens were used to evaluate how well four commonly used constitutive equation.

In Phase 2, preliminary finite element modeling (FEM) study was conducted on data from literature for X42 and X60 pipe steels to identify the best criterion to use to predict failure. Based on this preliminary analysis, the stress-based criterion was chosen for further FEM studies.

In Phase 3, failure data from real corrosion pits in X52 pipe steels with detailed profiles were used to develop a FEM model where comparison of actual and predicted burst pressures indicated a good fit.

In Phase 4, burst pressure levels were estimated for real corrosion pits for the experiments from the same study as in Phase 3, but only with corrosion pit depths and length and without corrosion widths. Widths were estimated from the data used in Phase 3, by using an empirical equation as a function of pit length. There was significant error between experimental and predicted burst pressure. Errors in Phases 3 and 4 were compared statistically. Results showed that there is a statistically significant difference in the error when the width of the corrosion pit is unknown. This finding is significant because none of the assessment techniques in the literature takes width into consideration. Subsequently, a parametric study was performed on three defect geometries from the same study in Phase 3. In all cases, the effect of the pit width on burst pressure was confirmed.

In Phase 5, the assessment techniques were evaluated by using experimental test results for X52 pipe. Synthetic data for deeper pits were developed by FEM and used along with experimental data in this phase. Type I errors (α) and Type II errors (β) were defined using Level 0 evaluation method. Results showed that although ASME B31G is the most conservative technique, it is more reliable for short defects than MB31G and DNV-RP. The least conservative technique was DNV-RP but it yielded β error. Hence, it is recommended that DNV-RP not be used to assess safety of pipelines based on corrosion pit size data.

1. Introduction

Pipeline systems are divided in three major categories based on the type of fluid transported: oil pipelines (both crude and refined petroleum), natural gas pipelines and others (water, chemical, slurry, etc.) [1]. When compared with other methods of transportation, such as tankers, railroad, trucks, etc., it has been stated that the transportation of oil, gas and their products through pipelines is still safe and economically efficient [2]. According to the Pipeline and Hazardous Materials Safety Administration of the United States Department of Transportation, the breakdown of the pipeline networks based on the fluid transported in 2015 is as follows:

- 2,527,165 miles of the natural gas pipeline network, (300,258 miles of transmission line, 2,209,228 miles of distribution line, 17,679 miles of gathering line)
- 208,658 miles of oil pipeline network, of which 204,413 miles are for transmission lines

The natural gas and crude oil pipeline networks in the contiguous United States and the state of Alaska in 2015 are shown in Figure 1-1 and Figure 1-2 respectively.

Although most pipes are made from steel, some oil pipelines and distribution lines can be also made from plastic materials. Pipe diameters vary from 4 to 48 inches (102-1219 mm) for oil pipelines and 2 to 60 inches (51-1524 mm) for gas pipelines, where small diameters are used for gathering and distribution lines.

Figure 1-1. Crude oil and petroleum products pipeline systems [3].

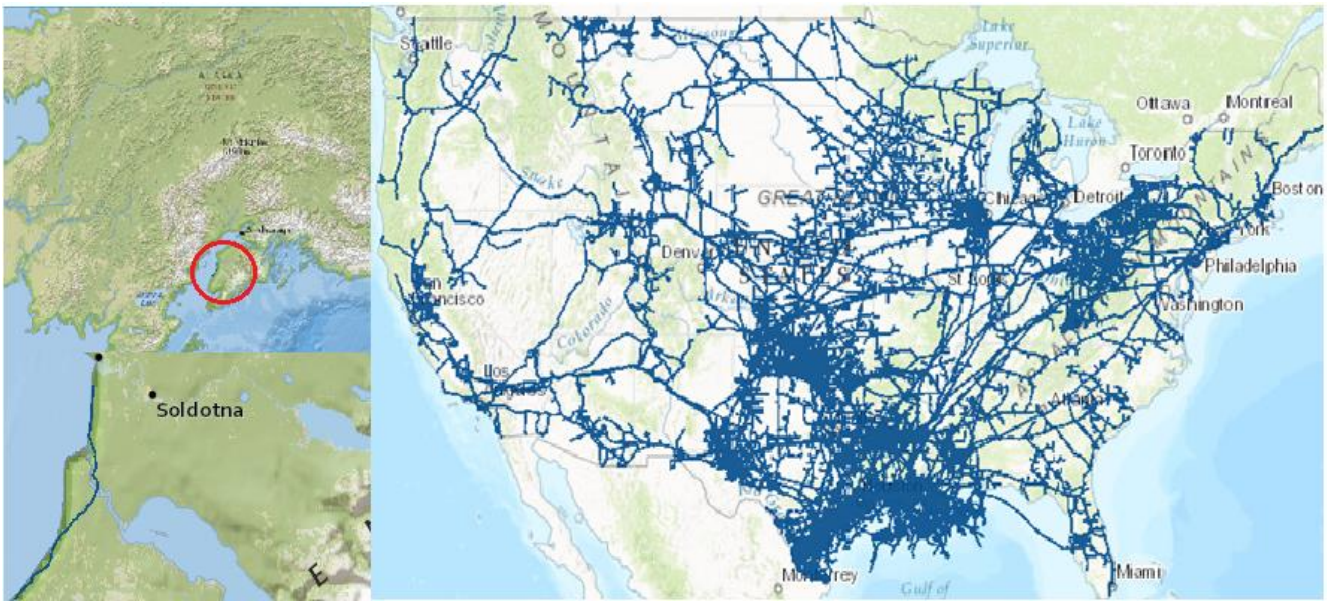

Figure 1-2. Natural Gas pipeline systems [3].

2. Pipeline engineering and design

Several standards, issued jointly by the American National Standards Institute (ANSI) and American Society of Mechanical Engineers (ASME), are used to design pipelines in the United States. The standards are:

- ANSI/ASME Standard B31.1, Power Piping [4]
- ANSI/ASME Standard B31.3, Chemical Plant and Petroleum Refinery Piping [5], which is applied to main onshore and offshore facilities worldwide.
- ANSI/ASME Standard B31.4, Liquid Transportation Systems for Hydrocarbons, Liquid Petroleum Gas, Anhydrous Ammonia, and Alcohols [6].
- ANSI/ASME Standard B31.8, Gas Transmission and Distribution Piping Systems [7].

The first step in the design of a new pipeline is projecting the route based on the original and destination points, so that topography of the pipeline route can be determined. Subsequent major steps in piping design require input parameters, such as [8]:

- Volumetric flow rate of the fluid carried by pipe
- Fluid type, temperature and quality
- Maximum operating pressure for the pipeline
- Minimum pressure required at the destination points
- Ambient temperature

Transmission pipelines are manufactured from the material conforming to the API 5LX standard, which consist of corrosion resistant alloys (for sour gas service), denoted as API 5LX-42, API 5LX-46, API 5LX-52, API 5LX-60, API 5LX-65, API 5LX-70, API 5LX-80 and API 5LX-100 [9]. The numbers following the dash represent the specified minimum yield

strength of the materials in ksi. X80 and X100 are new materials with high yield strength, where the ratio of yield to tensile strength can reached 0.979. A list of some of the materials with mechanical and chemical properties can be found in Table 2-1.

Table 2-1. API-5LX pipe materials

Grade	Chemical Composition (%)								$\sigma_{Y(SM)}$	$\sigma_{TS,(SM)}$	$\frac{\sigma_{Y(SM)}}{\sigma_{TS(SM)}}$	ε
	C	Si	Mn	P	S	V	Nb	Ti	MPa	MPa	max	%
X42*	0.22	0.45	1.3	0.025	0.015	0.05	0.05	0.04	290	420	0.93	23
X46*	0.22	0.45	1.3	0.025	0.015	0.05	0.05	0.04	320	435	0.93	22
X52	0.16	0.45	1.65	0.02	0.01	0.07	0.05	0.04	358.5	455	0.93	21
X60	0.16	0.45	1.65	0.02	0.01	0.08	0.05	0.04	413.7	517	0.93	19
X65	0.16	0.45	1.65	0.020	0.01	0.09	0.05	0.06	447.9	530	0.93	18
X70	0.17	0.45	1.75	0.02	0.01	0.10	0.05	0.06	482.3	565	0.93	17
X80**	0.03	0.21	1.76	0.016	0.004	0.09		0.02	555	625	0.93	20
X100	0.06	0.24	2	0.01	0.003		0.1		690	760	0.97	23.6

*Chemical composition is showed in maximum amount for each component
**Chemical composition is taken from Ref. [10]

Fluid Flow in Pipes

As liquids and gases are transported through the pipeline, the energy loss due to the friction between the fluid transported and the surface of the pipe will lead to a pressure drop, the magnitude of which is dependent on volumetric flow rate (Q), pipe diameter (D), the total length of the pipeline section (L_T), physical properties of the fluid and the pipe material. Because transmission pipelines are usually operated at high pressures, the flow can be considered as turbulent [8]. Therefore, further design equations and parameters need to be defined accordingly. In classical fluid mechanics, the pressure drop (expressed as feet in liquid head) can be evaluated using the Darcy-Weisbach equation [11]:

$$\Delta P = \frac{8 \rho f L_T}{\pi^2 D^3} Q^2 \qquad \text{Equation 2-1}$$

where

$$Q = \frac{\pi D^2}{4} . v \qquad \text{Equation 2-2}$$

The characteristics of the flow is determined by the dimensionless Reynold's number, R_e:

$$R_e = \frac{v\, D\rho}{\mu} \qquad \text{Equation 2-3}$$

For turbulent flow, i.e. R_e>4000, f can be estimated by the Colebrook equation [12] :

$$\frac{1}{\sqrt{f}} = -2\log\left(\frac{e}{3.7D} + \frac{2.51}{R_e\sqrt{f}}\right) \qquad \text{Equation 2-4}$$

To maintain a desired volumetric flow rate through the pipeline, the applied pressure should exceed the pressure drop, ΔP. However, applied pressure should not exceed the level that will lead to a fracture in the pipe, i.e., pipeline failure. To determine the optimum level, stresses developed in the pipelines, especially around stress concentrators such as corrosion pits need to be evaluated. These stresses will be discussed in detail in later sections.

Calculation of the wall thickness using ANSI/ASME B31.8 code

If the diameter of the pipe is calculated and the material type is known, the minimum required wall thickness can be calculated by using ANSI/ASME B31.8 code:

$$t = \frac{P . D}{2 . F . E . T . \sigma_{Y(SM)}} \qquad \text{Equation 2-5}$$

The design factor, F, is used to indicate the location class of the area where the pipe will be installed and operated, which ranges from 1(rural) to 4 (tightly populated) [13]. The F, E and T factors can be found in Tables 841.1.6-1, 841.1.7.-1 and 841.1.8-1, respectively, in the ANSI/ASME B31.8 Standard [7].

Construction and maintenance of pipelines

Construction

The basic construction steps can be found in literature related to pipeline installation [14], [15]. Before the construction of a pipeline begins, crew surveys the area to locate hydrologic features and equipment needed for construction. Utilities are marked to prevent any damage during the installation. Clearing any vegetation and grading is completed and a trenching machine excavates the trench needed to the design elevation of the pipe. In some rocky areas, blasting may be required to excavate the trench. Pipe sections, usually manufactured in 80 ft, 40 ft and 20 ft (as determined by design engineer), are bent, if needed, and welded into the long continuous sections. Each welding joint is verified with radiographic or ultrasonic technology. A protective coating is applied as soon as the welding process is finished. The welding joints and coating are electronically inspected to detect the presence of any external damage and are repaired (if needed) before lowering the pipe into the trench. Long pipeline sections are lowered into trench and placed on sandbags to prevent the damage to pipe coating. The coating is rechecked and the ends of the section are welded to form the line [7]. A layer of the rock-free dirt is used to cover all around the pipe for coat protection. A hydrostatic pressure test is conducted to check the overall integrity of the pipeline. Usually, that pressure is 1.5 times greater than MAOP [16] which is maintained for several hours. After trench is backfilled, the clean-up and restoration starts and continues until the area is restored and revegetated. The warning marks are placed to indicate the presence of underground pipeline. A picture from the site work can be found in Figure 2-1.

Figure 2-1. Pipeline construction: lowering the pipeline in a trench [17].

Operation and maintenance of pipelines

The main goal for pipeline company owners and operators is to transport maximum amount of oil (or gas) while preventing pipeline failures. In order to maintain the pressure and the flow of the fluid, conducted through the pipe, several pumping and compression stations are installed along its route.

Once pipelines are in service, they are continuously monitored for their integrity. One element of that program is pipeline in-line inspection, typically conducted by using a device that is widely known as "Smart Pipeline Intelligent Gadgets (PIGs)". The PIGs use the magnetic flux leakage technique, a non-destructive method, which allows for safe inspection of the pipeline from the inside for the presence of external, internal defects and corrosion. The inspection device is loaded through a hatch of the end of the pipe. Inside fluid pressure pushes the device through the pipe to gather data. During the PIG's journey, it creates continues magnetic circuits within the pipe

wall. When any defect is detected by the device, it changes the flux pattern and the data are stored for evaluation once the inspection is completed. The intervals for pigging is determined by an integrity management decision for each specific pipeline, which is based on a flow assurance analysis of the line and the Code of Federal Regulations, established by 49. CFR. §195.583 [18]. (see Table 2-2)

Table 2-2.Inspection frequency according the Code of Federal Regulations [18]

If the pipeline is located:	Then the frequency of inspection is:
Onshore	At least once every 3 calendar years, but with intervals not exceeding 39 months.
Offshore	At least once each calendar year, but with intervals not exceeding 15 months.

Also, PIGs can be used to apply internal pipe coating (epoxy) and for cleaning purposes from debris and wax in operating pipelines.

Figure 2-2. The Smart PIG [19].

Pipeline failures

Even when a pipeline has been properly designed and constructed, they may still be subjected to environmental abuse, coating disbandment, external damage, soil movements and third-party damage. Pipeline failures occur due to a combination of environment, stresses and material properties. Products released due to a pipeline failure can result in loss of property and environmental damage as well as injuries and fatalities. Released hazardous liquids may impact wildlife or pollute drinking water reserves. Moreover, pipeline failure can be the cause of interruption in supplies of natural gas and oil, which may lead to substantial economic loss [20]. According to US DoT Pipeline and Hazardous Materials Safety Administration (PHMSA), the economic and human loss due to significant pipeline incidents over a 20-year period (1996-2015) are $7 billion; 324 fatalities along with 1, 333 injuries, respectively [21].

Conservation of Clean Air and Water in Europe (CONCAWE) [22] categorizes the failure types that can occur in oil and gas pipelines into five groups:

1. *Mechanical:* this type of failure results from a material defect or construction fault. It is a localized[1] damage of pipelines which leads to either immediate or future pipeline failure. Immediate failure typically occurs by striking with mechanical equipment (e.g. backhoe) and produces a leak at the time of damage. This type of damage occurs in three broad categories: dents, gouges, and combined dent/gouge defects [23].
2. *Operational:* this kind of failure is a result of operational errors, break down or insufficiency of safeguarding systems (e.g. mechanical pressure relief system) or from operator inaccuracy/error.

[1] Localized means that the damage is limited to a part of the pipe's cross section and extends along a portion of the pipe's axis.

3. *Corrosion*: unprotected pipelines, whether buried in the ground, exposed to the atmosphere, or submerged in water, are prone to corrosion.
4. *Natural hazard:* this type of failure results from flooding, lightning strikes, shifting land, etc.
5. *Third party*: this type of failure results from accidental or intentional actions by a third party.

In Figure 2-3, the distribution of failures and their occurrence rates are presented. Note that failure due to corrosion represents 30% of all failures.

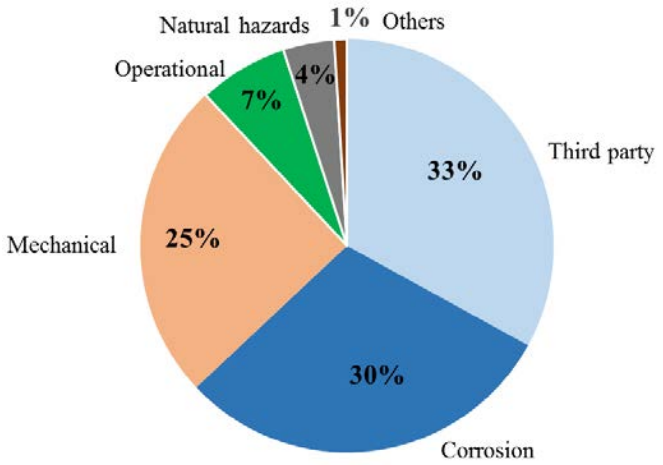

Figure 2-3 Different failure mechanisms (data from Ref. [22])

Stresses on Pipelines

When a pipeline or pressure vessel is pressurized, a two or three-dimensional stress state is developed within the pipe walls. For open-ended pipelines in service, radial and tangential (hoop) stress components will be present, while for closed-ended pressure vessels used in burst

experiments, a third component called longitudinal (axial) stress will also be present [24]. These are schematically shown in Figure 2-4.

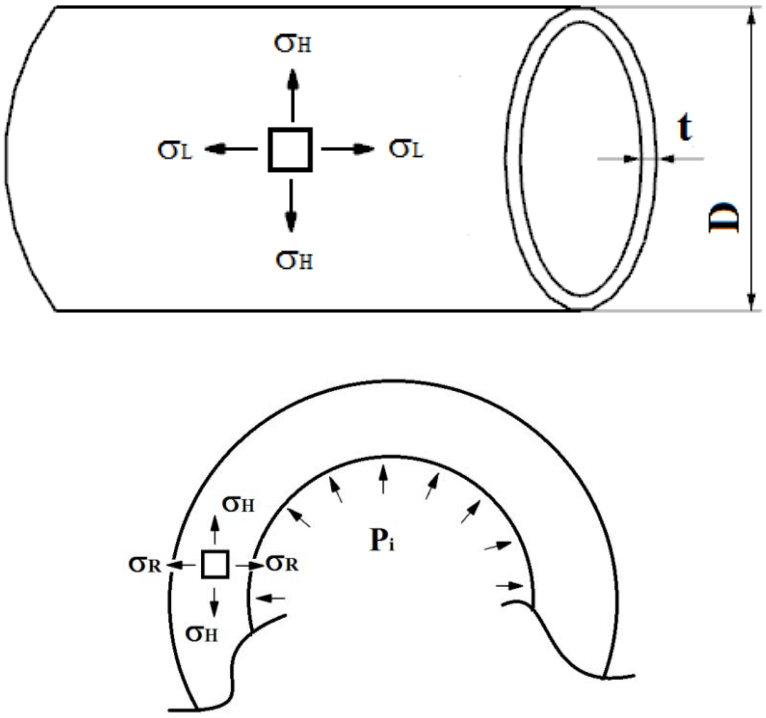

Figure 2-4 Stresses in pipe due to internal pressure

The hoop stress, σ_H, is found by:

$$\sigma_H = \frac{P_i r_i^2 - P_o r_o^2}{r_o^2 - r_i^2} + \frac{r_i^2 r_o^2 (P_i - P_o)}{r^2 (r_o^2 - r_i^2)} \qquad \text{Equation 2-6}$$

Radial stress, σ_R, is found by:

$$\sigma_R = \frac{P_i r_i^2 - P_o r_o^2}{r_o^2 - r_i^2} - \frac{r_i^2 r_o^2 (P_i - P_o)}{r^2 (r_o^2 - r_i^2)} \qquad \text{Equation 2-7}$$

Longitudinal stress, σ_L is found by:

$$\sigma_L = \frac{P_i r_i^2 - P_o r_o^2}{r_o^2 - r_i^2} \qquad \text{Equation 2-8}$$

When the ratio D/t > 20, the pipe is considered thin-walled, and the stress distribution through the wall thickness can be assumed to be uniform. Consequently, the stress equations can be simplified as:

$$\sigma_H = \frac{P_i r}{t} \qquad \text{Equation 2-9}$$

$$\sigma_R = 0 \qquad \text{Equation 2-10}$$

$$\sigma_L = \frac{P_i r}{2t} \qquad \text{Equation 2-11}$$

The overall effective von-Mises stress can then be found by [24].

$$\sigma_{VM} = \sqrt{\frac{1}{2}[(\sigma_H - \sigma_R)^2 + (\sigma_R - \sigma_L)^2 + (\sigma_L - \sigma_H)^2]} \qquad \text{Equation 2-12}$$

By examining Equation 2-6 through Equation 2-11, it can be seen that the hoop stress is the largest stress component. Therefore, when a pressurized pipe fails, failure results in a longitudinal tear. The hoop stress is the main design and operating stress of pipelines; pipe material is selected based on desired internal pressure and hence the hoop stress. When pipelines are in use, internal pressure is adjusted based on the calculated hoop stress, such that:

$$0.4 \le \frac{\sigma_h}{\sigma_{Y(SM)}} \le 0.8 \quad \text{for D} \ge 400\text{mm}$$

$$0.72 \le \frac{\sigma_h}{\sigma_{Y(SM)}} \le 0.8 \quad \text{for D} < 400\text{mm}$$

Corrosion defects in transmission pipelines

Some sections of high-pressure pipelines, especially with a long history of operation, may experience corrosion which can jeopardize the integrity of the pipeline. Corrosion defects can occur on either the external or internal surface of the pipelines (Figure 2-5). External corrosion can be the result of fabrication faults, coating or cathodic protection problems, residual stress, cyclic loading, temperature or local environment (soil chemistry). However, the most frequent root cause corrosion damage is coating failure. Corrosion on the internal surface of the pipeline occurs due to contaminants in the products such as small sand particles, amino acids, etc.

(a) (b)

Figure 2-5. Examples of pipes with (a) external [25] and (b) internal corrosion [26].

Defect measurement and interaction

Each method of assessing locally damaged areas is based on the assumptions of a simplified profile. The dimensions of the corrosion defect is defined by its maximum length and depth in the axial and longitudinal directions (Figure 2-6). The width of the corrosion pit is not taken into account.

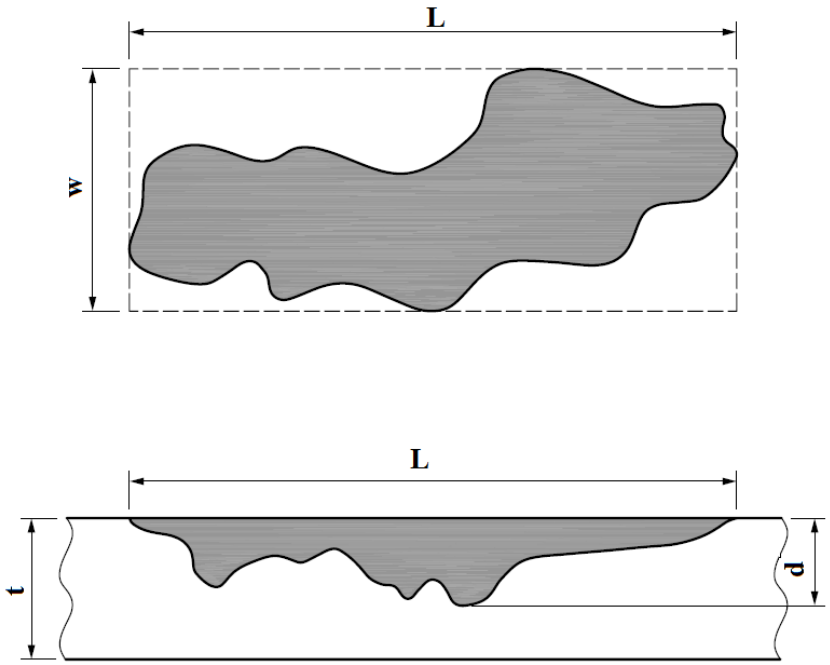

Figure 2-6 Dimensions of corrosion defect profile [27].

Corrosion defects may occur as a cluster of multiple corrosion pits. An example is provided in Figure 2-7. Note that the contour plot shows multiple pits with various depths.

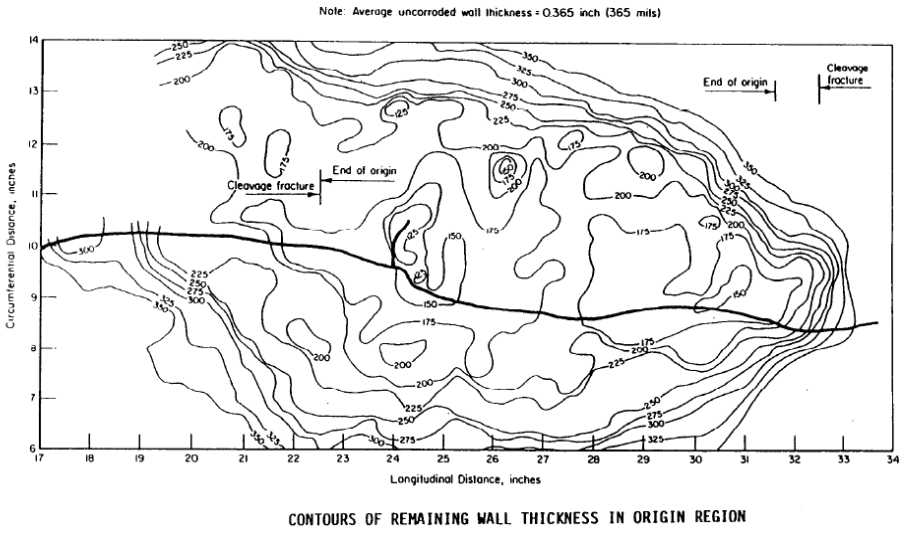

Figure 2-7 Contour plot of a corroded area in a pipe that fractured, showing multiple pits [28].

Defects in close proximity to each other usually act more like a single but larger defect. If these defects are not treated together in pressure calculations, the pipeline can fail at a lower pressure than predicted. Corrosion pits are considered interacting if the circumferential or/and longitudinal distance between flaws is equal to or less than three times of the pipe thickness. BS 7910 [27] has additional interacting rules for thinned areas:

- The axial distance between flaws is equal or less than the defect length or width of the smallest flaw;
- The circumferential distance between flaws is equal or less than the length or width of the smallest flaw.

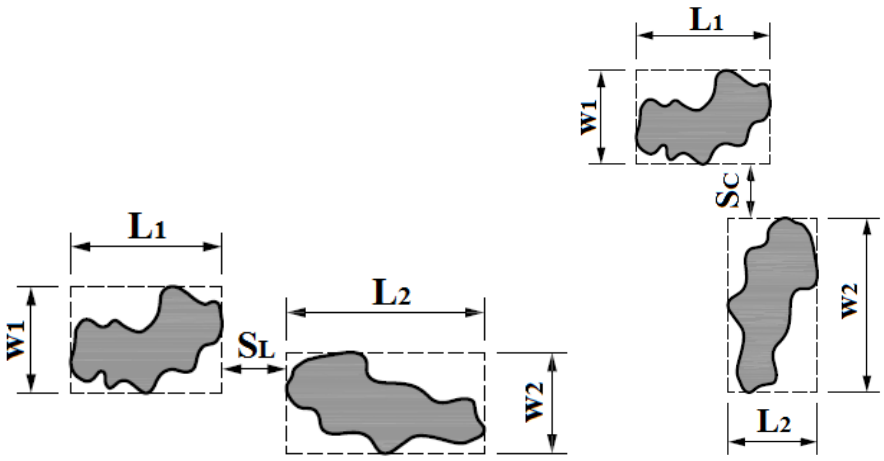

Figure 2-8 Interaction between flaws [27].

In such cases interacting defects should be evaluated as a single flaw with:

- $L=L_1+L_2+S_L$
- $w=w_1+w_2+S_C$

The depth will be equal to the deepest point of corrosion defect or cluster of pits.

The Effect of Corrosion Pits on Stresses Generated in Pipes

Corrosion pits act as stress concentrators [29] and contribute to premature failure of pipelines. An example of a failed pipe is presented in Figure 2-9. Note that the fracture, once initiated, propagated longitudinally at first, and subsequently deviated from its path due to the opening of the pipe along the crack.

To understand the effect of pits, a review of fracture mechanics principles is necessary. Such a review is provided in Ref. [30] for through-wall defects and is summarized below.

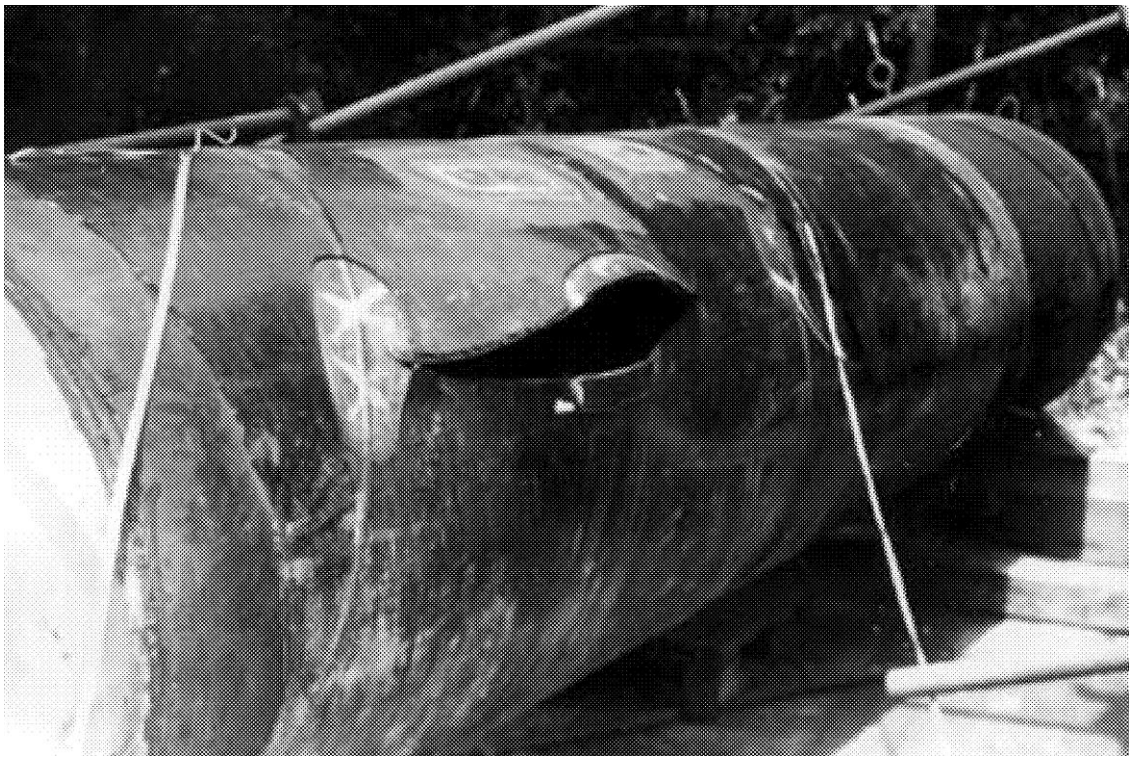

Figure 2-9. A pipe that failed due to surface defects [31]

In pressurized cylinders made of moderately tough to tough materials, the hoop stress is found by:

$$\sigma_H = \frac{K_c}{M\sqrt{\pi\gamma\frac{L}{2}}}$$ Equation 2-13

where γ is a correction factor to account for the plastic zone surrounding the defect upon loading that incorporates the model by Dugdale [32] for yielding in steels, and can be found as:

$$\gamma = \left(\frac{\pi M\sigma_h}{2\overline{\sigma}}\right)^2 \ln\left[\sec\left(\frac{\pi M\sigma_h}{2\overline{\sigma}}\right)\right]^2$$ Equation 2-14

The correction factor, γ, incorporates M which is a factor introduced by Folia to account for bulging around a crack tip in a pressurized cylindrical vessel [33], and is commonly referred to as Folia's factor:

$$M=\sqrt{1+0.8\left(\frac{L}{\sqrt{Dt}}\right)^2}$$ Equation 2-15

The flow stress of the material is an empirical number originally suggested by Hahn et al. [34] to represent the entire stress-strain curve and work hardening behavior with a single value, and is found as:

$$\overline{\sigma}=\xi\sigma_Y + \sigma_i$$ Equation 2-16

The parameters ξ and σ_i are empirical constants. In the original formulation, ξ and σ_i were taken as 1.1 and 0, respectively.

For extremely tough materials, i.e., those metals that can absorb large amounts of energy by plastic deformation prior to fracture,

$$\frac{K_c}{\sigma_y}\frac{2}{L}=7$$ Equation 2-17

The change in hoop stress as a function of crack length for X52 grade steel along with data by Duffy et al. [35] for machined pits is provided in Figure 2-10 [30].

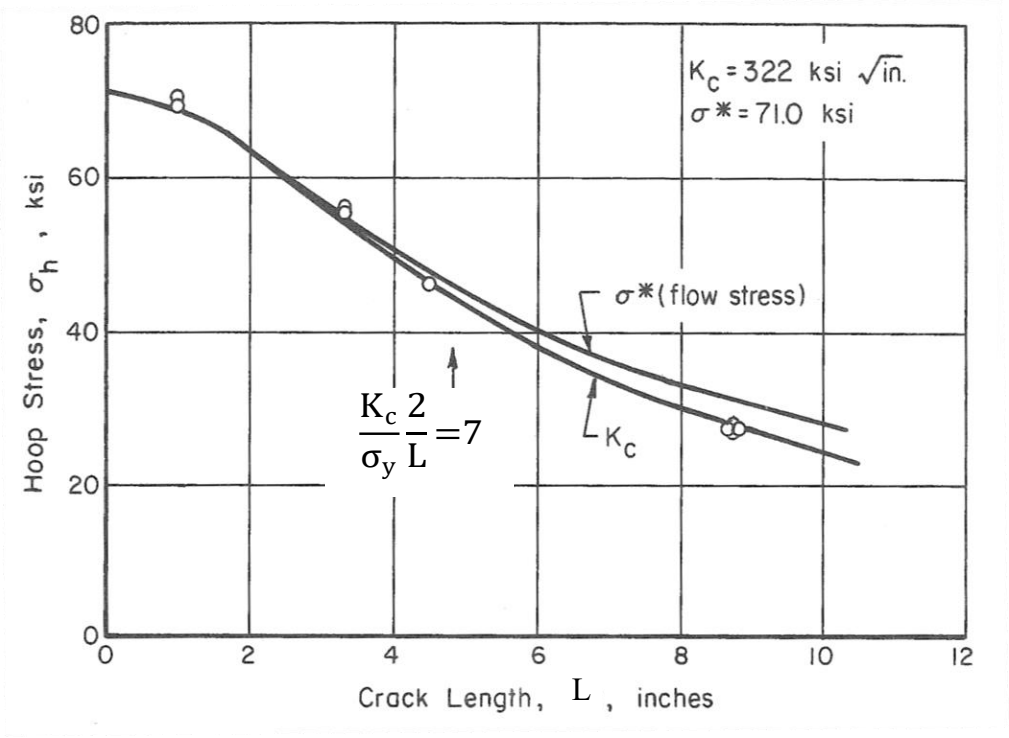

Figure 2-10 Hoop stress as a function of crack length for X52 grade pipe steel [30]

Figure 2-10 shows close agreement between predicted and measured hoop stress values for machined pits in X52 steel. This approach, commonly referred to as NG-18, has several weaknesses:

- The formulation has been deemed "complex and difficult to use" [36]. That is one of the reasons why easier assessment techniques have been developed and used in the pipeline industry. These assessment techniques are reviewed in the next section.
- Data were obtained by machined pits and not from actual corrosion pits.

- The flow stress approach proposed by Hahn et al. attempts to represent the entire stress-strain curve of the material with a single value, the flow stress.
- The correction for plastic zone extension in ductile materials is valid if the "correcting function predicts the plastic behavior" [30] i.e., work hardening in plastic deformation.

The last point implies that an accurate expression of the work hardening characteristics is important. Therefore, a review of constitutive equations in the literature that express the true stress-true strain relationships in metals is necessary.

Constitutive Equations for σ-ε Relationships

The true stress-true strain relationship in metals can be expressed by several constitutive equations. The most commonly used equations are those developed by Hollomon [37], Voce [38], Ludwik [39] and Swift [40], and are provided below:

Hollomon Equation:

$$\sigma = K_H \varepsilon_p^{\,n_H} \qquad \text{Equation 2-18}$$

Voce Equation:

$$\sigma = \sigma_\infty - (\sigma_\infty - \sigma_0)e^{-K_V \varepsilon_p} \qquad \text{Equation 2-19}$$

Ludwik Equation:

$$\sigma = \sigma_L + K_L \varepsilon_p^{\,n_L} \qquad \text{Equation 2-20}$$

Swift Equation:

$$\sigma = K_S(\varepsilon_p + \varepsilon_S)^{n_S} \qquad \text{Equation 2-21}$$

Note that the Voce, Ludwik and Swift equations have three parameters while the Hollomon equation has two that need to be estimated. The Voce equation was found to provide most accurate results for aluminum alloys [41] - [42], where all four equations provided very similar fits to a cast Mg alloy [43]. Choudhary et al. [44] found that the Voce equation provided a better fit than the Hollomon, Ludwik and Swift equations to 316 austenitic stainless steel, tested at room and elevated temperatures. Mok et al. [45] conducted tensile tests on several grades of pipe steel and used only the Hollomon equation in their analyses. Therefore, it is not clear which constitutive equation should be used for pipe steels.

Review of the previous FEM studies:

Several analyses and experiments have been done to determine the remaining strength of the pipe sections with external flow [25], [45], [46]. In these studies, the remaining thickness of the pipe after corrosion was modeled using a four elements through the remaining ligaments. For some studies, Finite Element Analysis (FEA) was performed as if the pipe had an open end, while in reality the actual pipe section was acting as a pressure vessel. Most of those studies have been conducted by using data obtained from machined grooves, which have much simpler geometries than actual corrosion pits. Additionally, all available assessment techniques and research reported in the literature have disregarded any possible effect of the corrosion pit width. Similarly, corrosion pit width has not been investigated in FEM studies.

Failure Criteria

In FEM studies, a criterion is needed to define when fracture takes place. In the literature, several criteria are used for predicting failure due to plastic collapse in steel pipes. The two most widely

used are (i) stress-based, and (ii) strain-based failure. The accuracy of results is affected by the initial selection of this criterion.

Stress-based failure criterion has been used by several researchers [47], [48], [49] to define the failure stress. Although fracture in the steel is known [31] to take place when stress reaches the ultimate tensile strength, S_T, some researchers modified this criterion to obtain better agreement between experimental and predicted results. For instance, Chiodo et al. [50] chose a stress level corresponding to 90% of ultimate tensile strength as failure stress. However, in most studies, the true stress at the ultimate tensile strength was taken as the failure criterion [47].

A number of strain-based failure criteria have been used in the literature in FEM studies, including the void growth model developed by Rice and Tracey [51], the model developed by Gurson [52], the continuum damage model proposed by Lemaitre [53], and the stress-modified critical strain (SMCS) model developed by Hancock and Mackenzie [54]. Among these models SMCS is easier to implement in FEM studies because of the lower number of parameters required.

Oh et al. [55], [56] have recently applied the SCMS model to X52 grade steel. Stress triaxiality, T_s, is found by;

$$T_s = \frac{\sigma_m}{\sigma_e} = \frac{\sigma_1 + \sigma_2 + \sigma_3}{3\sigma_e} \qquad \text{Equation 2-22}$$

where

$$\sigma_e = \frac{1}{\sqrt{2}}\left[(\sigma_1 - \sigma_2)^2 + (\sigma_2 - \sigma_3)^2 + (\sigma_3 - \sigma_1)^2\right]^{\frac{1}{2}} \qquad \text{Equation 2-23}$$

The value of stress triaxiality for round bars is roughly equal to 1/3 [57]. Similarly,

$$\varepsilon_e = \frac{\sqrt{2}}{3}\left[(\varepsilon_1 - \varepsilon_2)^2 + (\varepsilon_2 - \varepsilon_3)^2 + (\varepsilon_3 - \varepsilon_1)^2\right]^{\frac{1}{2}} \quad \text{Equation 2-24}$$

True fracture strain, as proposed by Rice and Tracey [51] can be found as;

$$\varepsilon_f = A_f e\left(-\frac{3}{2}\frac{\sigma_m}{\sigma_e}\right) \quad \text{Equation 2-25}$$

where A_f is an empirical constant, determined experimentally. If the true fracture strain in tensile testing, $\varepsilon_f{}^*$, is known, then:

$$\frac{\varepsilon_f}{\varepsilon_f{}^*} = \frac{\exp\left(-\frac{3}{2}\frac{\sigma_m}{\sigma_e}\right)}{\exp\left(\frac{1}{2}\right)} \quad \text{Equation 2-26}$$

Many researchers have used a stress-based failure criterion in their studies, with accurate results regardless of the pipe wall thickness. Recently, a stress-modified strain criterion (SMSC) has been reported to yield accurate results for thicker and low-level pipe grade (X42) [46], but less accurate results for mid-level X60 material.

3. A Review of Assessment Techniques

Over the past forty years, parameters that affect the remaining strength of the corroded pipe section have been investigated, and several assessment techniques have been developed. The parameters are [25]:

- Internal pressure
- Pipe design parameters (pipe outer diameter, pipe wall thickness)
- Defect parameters (depth and length of the defect)
- Material properties (yield strength and ultimate tensile strength)

In studies performed on pipe sections with different corrosion profiles (either machined or natural) the effect of the width of the corrosion has been assumed to be negligible [50]. Therefore, the parameter for corrosion width effect has not been included in any assessment method, for determining the remaining stress of pipes containing surface flaws.

It was recognized in early studies performed on pipe sections with defects that some amount of metal loss can be tolerated without removing the pipe from service [58]. Therefore, many studies have been performed to develop evaluations methods to be used by operators to assess whether the condition of the pipe section is safe under operating conditions so that a decision to repair or replace the pipe can be made in a timely manner. All assessment techniques are based on the NG-18 Ln-sec equation (Equation 3-1) for failure of the part-wall flaw, with the differences in approximation of the Folia's factor, the corrosion defect profile and flow stress.

$$\frac{C_v \frac{12}{A} E\pi}{8c\overline{\sigma}} = \ln \sec\left(\frac{\pi M \sigma_H}{2\overline{\sigma}}\right) \qquad \text{Equation 3-1}$$

Assessment techniques are used to predicting the remaining strength of a pipe section whose walls have been thinned by corrosion. This allows the pipeline operator to determine safe pressure levels for pipe sections affected by corrosion and make a decision if pipe repair or replacement is necessary. Three of the most widely used techniques are discussed below.

ASME B31G

The corrosion assessment codes in the United States, Canada and Europe are based on ASME B31G criterion for the evaluation of part-wall defects. These codes were established on full-scale burst experiments conducted by Keifner and Vieth on pipes containing longitudinal machined grooves [59].

In the B31G criterion assumes that failure is controlled by the hoop stress, which is the maximum principal stress. Because stress is inversely proportional to the cross-section of metal loss area, B31G, with given maximum defect parameters, assumes that the complex shape of the corrosion profile can be estimated by a parabola. Then, the hoop stress level at failure can be estimated with B31G criterion as [58]:

$$\sigma_H = \bar{\sigma}\left[\frac{1-\frac{2}{3}\left(\frac{d}{t}\right)}{1-\frac{2}{3}\left(\frac{d}{tM}\right)}\right] \quad \text{Equation 3-2}$$

$$\bar{\sigma} = 1.1\sigma_{m(YS)} \quad \text{Equation 3-3}$$

$$A = \frac{2}{3}\frac{d}{t} \quad \text{Equation 3-4}$$

$$M = \sqrt{1 + 0.8\left(L/Dt\right)^2} \quad \text{Equation 3-5}$$

For long corrosion grooves, when $\left(\frac{L}{\sqrt{Dt}}\right)^2 > 20$, the hoop stress is found by:

$$\sigma_H = \overline{\sigma}\left(1 - \frac{d}{t}\right) \quad \text{Equation 3-6}$$

The failure (burst) pressure (P_f) can be found by:

$$P_f = \frac{2t}{D}\sigma_H \quad \text{Equation 3-7}$$

The B31G is the most widely-used assessment technique among the pipe operators because of its simplicity. However, this approach is very conservative, because of the corrosion defect approximation. This can lead to unnecessary pipe repairs and removals, while pipe could still be safely operated.

ASME MB31G

To reduce the conservatism in the B31G criterion, several modifications have been introduced in the corrosion profile representation, Folia's factor and flow stress and a modified B31G (MB31G) criterion has been accepted [58].

$$\sigma_H = \overline{\sigma}\left[\frac{1\text{-}0.85\left(\frac{d}{t}\right)}{1\text{-}0.85\left(\frac{d}{tM}\right)}\right] \quad \text{Equation 3-8}$$

$$\overline{\sigma} = \sigma_Y + 68.9 \quad \text{Equation 3-9}$$

$$A = 0.85\frac{d}{t} \quad \text{Equation 3-10}$$

$$M = \sqrt{1 + 0.6275\left(\frac{L}{\sqrt{Dt}}\right)^2 - 0.003375\left(\frac{L}{\sqrt{Dt}}\right)^4} \quad \text{Equation 3-11}$$

For $\left(\frac{L}{\sqrt{Dt}}\right)^2 > 50$, $M = 3.3 + 0.032\left(\frac{L}{\sqrt{Dt}}\right)^2$ Equation 3-12

$$P_f = \frac{2t}{D}\sigma_H = \frac{2t}{D}\bar{\sigma}\left[\frac{1 - 0.85\left(\frac{d}{t}\right)}{1 - 0.85\left(\frac{d}{tM}\right)}\right]$$ Equation 3-13

RSTRENG

RSTRENG is the computer based software for prediction of P_f for pipelines containing external corrosion defects. The estimation of parameters is same as MB31G, with exception of the area of metal loss. RSTRENG uses as an effective area method, where area is calculated at every increment of the longitudinal length of the defect. Figure 3-1 shows corrosion profiles and the approximated corrosion shape used in the assessment tools B31G and RSTRENG.

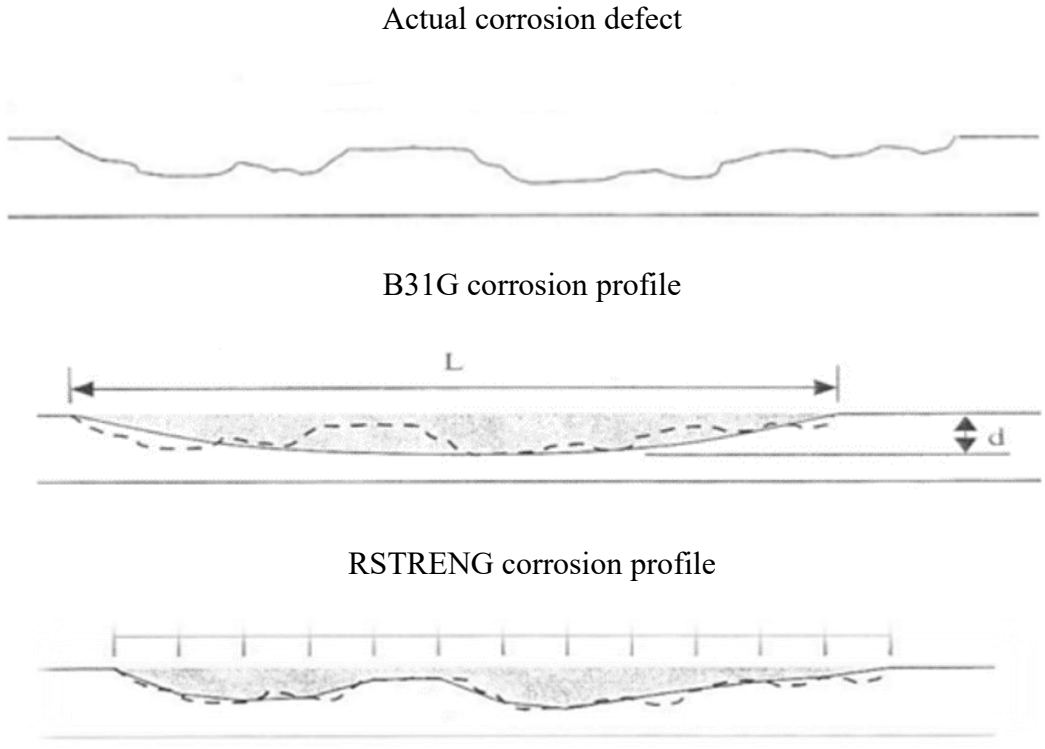

Figure 3-1 Corrosion profiles [25]

The conservatism level of various assessment criteria presented above as a function of complexity can be found in Figure 3-2.

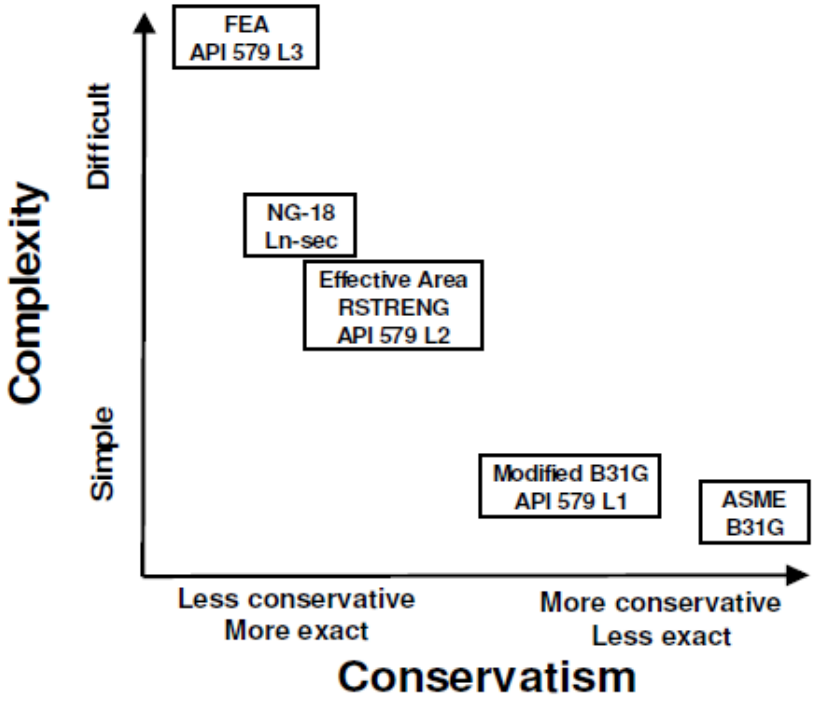

Figure 3-2 Complexity versus conservatism in assessment techniques for pipeline integrity

DNV-RP

The stress capacity equation for the DNV-RP method also has some minor changes in $\bar{\sigma}$, M and in rectangular corrosion profile representation.

$$\sigma_H = \bar{\sigma}\left[\frac{1-\left(\frac{d}{t}\right)}{1-\left(\frac{d}{tM}\right)}\right] \qquad \text{Equation 3-14}$$

$$\bar{\sigma} = \sigma_{TS} \qquad \text{Equation 3-15}$$

$$A = \frac{d}{t}$$ Equation 3-16

$$M = \sqrt{1 + 0.31\left(\frac{L}{\sqrt{Dt}}\right)^2}$$ Equation 3-17

The burst pressure is calculated differently than in other assessment techniques, and can be found by:

$$P_f = 1.05\frac{2t}{(D-t)}\sigma_H = 1.05\frac{2t}{(D-t)}\bar{\sigma}\left[\frac{1-\left(\frac{d}{t}\right)}{1-\left(\frac{d}{tM}\right)}\right]$$ Equation 3-18

Table 3-1**Error! Reference source not found.** presents the chronology of assessment techniques along with the important technical differences. Note that the NG-18 was issued first, and served as a base for the modern, simplified assessment techniques.

Table 3-1. Chronology of standard assessment techniques

	Fracture Mechanics	**Metal loss evaluation**			
	NG-18 Ln-Sec equation	ASME B31G	ASME MB31G	RSTRENG	DNV-RP
Year issued	1973	1984	1989	1990	1999
Charpy impact energy included?	Yes	No	No	No	No
Folia's factor	Exact	Simplified	Exact	Exact	Simplified
Flow stress	$\bar{\sigma}=\sigma_Y+68.9$ MPa	$\bar{\sigma}=1.1\sigma_Y$	$\bar{\sigma}=\sigma_Y+68.9$ MPa	$\bar{\sigma}=\sigma_Y+68.9$ MPa	$\bar{\sigma}=\sigma_{TS}$
Pit area	$A=\frac{\pi}{4}dL$	$A=2/3\left(\frac{d}{t}\right)$	$A=0.85\left(\frac{d}{t}\right)$	Exact profile	$A=\left(\frac{d}{t}\right)$
Fracture	Ductile and brittle	Ductile initiation	Ductile initiation	Ductile initiation	Ductile initiation

Calculation of the burst capacity of a corroded pipe section with the assessment techniques listed, is multistep process requiring input parameters such as a material's properties, pipe design and defect dimensions. After calculating the output pressure, the remaining strength of the pipe must

be compared to the minimum specified material parameter (e.g. specified minimum yield strength), so the operator can decide whether the pipe should be replaced or repaired. To make the evaluation easier, curves for each assessment method and pipe material type have been developed that allows the operator to quickly see if the defect length and depth threaten pipeline integrity. Figure 3-3 shows one such curve for the B31G, MB31G and DNV-RP assessment techniques, when X52 pipe operates at hoop level pressure equal to $100\%\sigma_{m(YS)}$. The operator uses the defect length and depth to locate a point on the graph. If the point is on or below the curve shown, the defect is "acceptable" (pipe can be operated at MOP). If the point is above the curve, the defect is "rejectable" and the pipe ***cannot*** operate at MOP and should be repaired or replaced. The equations for the curves can be found in Level 0 evaluation section below (Equation 3-19 - Equation 3-21).

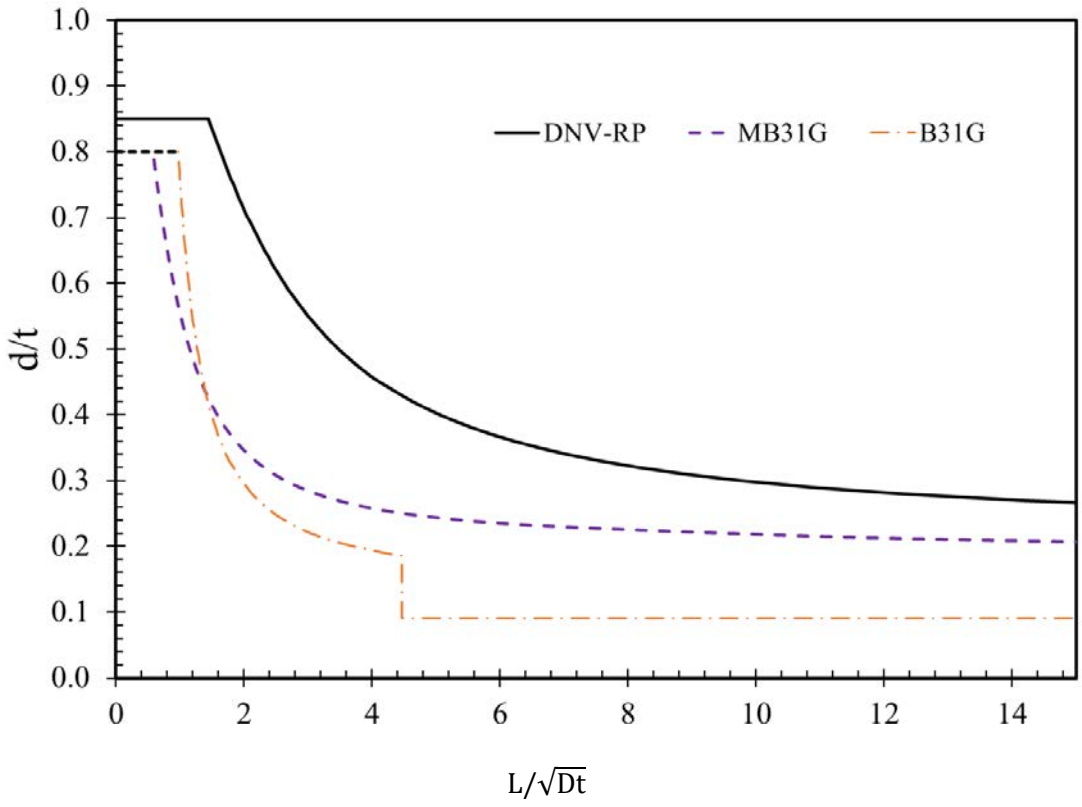

Figure 3-3 The normalized defect length function of normalized defect depth at $100\%\sigma_{m(YS)}$.

Evaluation methods

When the corroded area is evaluated, operators may choose a Level 0 through Level 3 analysis. The selection of the evaluation method is based on the type of available data. For all levels the specified minimum materials properties should be used unless actuals values are known with adequate confidence.

Level 0 evaluation

This evaluation level involves the use of the type of charts shown in Figure 3.3. These reference tables make it possible to determine maximum allowable defect length with depth with appropriate pipe sizes. This level of evaluation has been approved in the earlier edition of ASME B31G and can be found in Ref. [58]. In the charts used in level 0 evaluation were calculated from equations presented in Level 1, where the predicted level of σ_H =72% $\sigma_{m,(YS)}$ to obtain 1.39 factor of safety.

The criterion of acceptable combinations of the defect sizes can be written as:

B31G
$$\frac{1-\frac{2}{3}\frac{d}{t}}{1-\frac{2}{3}\frac{d}{tM}}=\frac{\sigma_{m(YS)}}{1.1\sigma_{m(YS)}}=0.91 \qquad \text{Equation 3-19}$$

MB31G
$$\frac{1-0.85\frac{d}{t}}{1-0.85\frac{d}{tM}}=\frac{\sigma_{m(YS)}}{\sigma_{m(YS)}+68.9MPa} \qquad \text{Equation 3-20}$$

DNV-RP-F101
$$\frac{1-\frac{d}{t}}{1-\frac{d}{tM}}=\frac{\sigma_{m(YS)}}{\sigma_{m(TS)}} \qquad \text{Equation 3-21}$$

In Table 3-2, presents a table for Level 0 evaluation from ASME B31G [58] for outer pipe diameters ranging between 762 mm, and 914 mm.

Table 3-2. Acceptable defect dimensions in accordance with pipe design parameters [58].

Depth,	Wall Thickness, t, mm						
d, mm	6.4	7.9	9.5	11.1	12.7	15.9	17.5
0.8	311.6	No limit	No limit	No limit	No limit	No limit	No limit
1.0	311.6	348.1	381.7	No limit	No limit	No limit	No limit
1.3	208.5	348.1	381.7	412.5	440.7	No limit	No limit
1.5	144.3	257.7	381.7	412.5	440.7	No limit	No limit
1.8	114.0	182.0	307.4	412.5	440.7	492.7	517.0
2.0	95.7	144.9	220.7	355.3	440.7	492.7	517.0
2.3	83.2	122.2	176.8	258.9	398.2	492.7	517.0
2.5	74.0	106.7	149.7	208.7	294.9	492.7	517.0
2.8	66.8	95.3	131.0	177.3	239.3	481.8	517.0
3.0	61.0	86.3	117.2	155.6	204.1	366.3	517.0
3.3	56.1	79.1	106.5	139.4	179.5	300.9	401.9
3.6	51.9	73.1	97.8	126.9	161.2	258.4	331.9
3.8	48.3	68.0	90.6	116.8	146.9	228.2	285.8
4.1	45.1	63.6	84.6	108.4	135.4	205.5	252.9
4.3	42.2	59.7	79.3	101.3	125.8	187.8	228.1
4.6	39.6	56.2	74.7	95.1	117.7	173.4	208.6
4.8	37.1	53.1	70.6	89.8	110.8	161.5	192.8
5.1	34.9	50.3	66.9	85.0	104.7	151.3	179.6
5.3	...	47.7	63.6	80.8	99.3	142.7	168.5
5.6	...	45.2	60.6	77.0	94.5	135.1	158.9
5.8	...	43.0	57.8	73.5	90.2	128.4	150.6
6.1	...	40.9	55.2	70.3	86.2	122.4	143.2
6.4	...	...	52.8	67.4	82.6	117.0	136.6
6.6	...	...	50.6	64.6	79.3	112.2	130.7
6.9	...	...	48.4	62.1	76.3	107.7	125.4
7.1	...	...	46.5	59.7	73.4	103.6	120.5
7.4	...	...	44.6	57.5	70.8	99.9	116.0
7.6	...	...	42.8	55.4	68.3	96.4	111.9
7.9	...	...	...	53.4	65.9	93.2	108.1
8.1	...	...	...	51.5	63.7	90.1	104.5
8.4	...	...	...	49.7	61.6	87.3	101.2
8.6	...	...	...	48.0	59.6	84.6	98.1
8.9	...	...	...	46.3	57.7	82.1	95.2
9.1	...	...	...	...	55.9	79.7	92.5
9.4	...	...	...	...	54.2	77.4	89.8
9.7	...	...	...	...	52.5	75.3	87.4
9.9	...	...	...	...	50.9	73.2	85.0
10.2	...	...	...	...	49.4	71.3	82.8
10.4	...	...	...	...	...	69.4	80.7
10.7	...	...	...	...	...	67.6	78.6
10.9	...	...	...	...	...	65.8	76.7
11.2	...	...	...	...	...	64.2	74.8
11.4	...	...	...	...	...	62.5	73.0
11.7	...	...	...	...	...	61.0	71.3
11.9	...	...	...	...	...	59.5	69.6
12.2	...	...	...	...	...	58.0	68.0
12.4	...	...	...	...	...	56.6	66.4
12.7	...	...	...	...	...	55.2	64.9
13.0	...	...	...	...	...	...	63.5
13.2	...	...	...	...	...	...	62.0
13.5	...	...	...	...	...	...	60.6
13.7	...	...	...	...	...	...	59.3
14.0	...	...	...	...	...	...	58.0

As an example, in Table 3-3 presents a case study with all pipe design and defect parameters along with burst pressure experiment information:

Table 3-3 Burst pressure experiment data

D (mm)	t (mm)	d (mm)	L (mm)	w (mm)	σ_Y (MPa)	S_{TS} (MPa)	$P_{f\text{-}exp.}$ (MPa)	σ_H (MPa)	$\%\sigma_{m(YS)}$
762.00	9.53	3.71	139.70	149	414.10	534.04	12.68	507.20	141.47

From Table 3-2, the maximum acceptable defect length for the case from Table 3-3, is approximately equal to 94 mm, when the hoop stress is 72% $\sigma_{m(YS)}$. But the pipe section affected by corrosion, could withstand 141.47%$\sigma_{m(YS)}$, when length of the defect is 139.7 mm.

Level 1 evaluation

This level relies on simple calculations with the single measurement of the maximum defect dimensions. The equations for a residual stress estimation of the corroded area, used in assessment techniques, are presented in Equation 3-2 through Equation 3-17 from sections above.

Level 2 evaluation

Level 2 combines more details than previous levels, for a more accurate estimation of residual strength. This method relies on several detailed measurements of the corroded profile throughout the metal loss area. As the method includes repetitive computations, computer based software could be used. One of the well-known software packages for the effective area evaluation is RSTRENG.

Level 3 evaluation

This level of evaluation involves a detailed analysis, such as FEA of the metal loss area. The analysis should be performed as accurately as possible, considering all factors, loadings and boundary conditions, along with the material's stress- strain properties.

Nonlinear FEA of corrosion defect in pipelines and pressure vessels

The regions affected by corrosion can be assessed using an elastic-plastic nonlinear finite element analysis. The steps used in almost all studies [27], [46], [60], for plastic collapse prediction are as follows:

1. Modeling – create FEM with information available for pipe geometry and defect dimensions;
2. Material properties – stress-strain properties of the material should be introduced with adequate accuracy, along with other properties;
3. Mesh design – the finite element mesh should be designed as fine as possible at the areas of interest, so the mesh would not have significant effect on stress results;
4. Reproduce test conditions with applied structure constraint and loads;
5. Perform a non-linear analysis;
6. Based on chosen failure criterion examine the local variation of the stress or strain states.

4. Research Questions and Plan

Based on the discussion provided above, the following research questions were developed:

- Which constitutive model should be used for pipeline steels?
- In FEM studies, which failure criterion provides better results?
- Do analytical models in literature, such as ASME B31G, MB31G and DNV-RP-F101, provide reliable results?
- Does the width of the corrosion affect the burst capacity of the pipe section?
- Do common techniques of using machined grooves, in lieu of real corrosion defects, give reliable results?

These research questions will be answered below in five phases. In Phase 1, constitutive equations will be compared by using data from the literature for two pipeline grade steels. In Phase 2, a preliminary FEM study will be conducted by using experimental data from the literature to compare two failure criteria. By using the results in Phases 1 and 2, an FEM study will be conducted in Phase 3 to replicate experimental data from real corrosion cases with all dimensions known. The results developed in Phase 3 will be extended to replicating experimental data with real corrosion but missing dimensions in Phase 4. In addition, the effect of the corrosion pit width will be investigated by a FEM study. In Phase 5, the assessment methods will be evaluated by using real and synthetic corrosion data.

5. Phase 1: Evaluation of the Constitutive Equations for Work Hardening

Constitutive Equations

True stress-true plastic strain data in the plastic regions of X42 [46] and X60 [45] specimens were used to assess the fits of the four constitutive equations. To determine the best fits, the Newton-Raphson method was used to minimize the root mean square error, RMSE;

$$\mathrm{RMSE} = \sqrt{\frac{\Sigma_{i=1}^{n}\left(y_{exp(i)} - \hat{y}_{(i)}\right)}{n - a}} \qquad \text{Equation 5-1}$$

where a is the number of parameters to be fitted and n is the number of data points. The coefficient of determination, R^2, was also found for each fit;

$R^2 = 1 - \frac{SS_e}{SS_{tot}}$	Equation 5-2
$SS_E = \sum_{i=1}^{n}\left(P_{if-exp} - P_{if-predicted}\right)^2$	Equation 5-3
$SS_E = \sum_{i=1}^{n}\left(P_{f-exp} - \overline{P_{f-exp}}\right)^2$	Equation 5-4
$\overline{P_{f-exp}} = \frac{1}{n}\sum_{i=1}^{n}\left(P_{f-exp}\right)_i$	Equation 5-5

The values of the estimated parameters for the four constitutive equations, as well as RMSE and R^2 for each fit to X42 and X60 data are presented in Table 5-1. The R^2 values in each case exceed 0.97, indicating that all constitutive equations can be used to characterize the true stress–true strain relationships

The fits provided by each constitutive equation to the X42 and X60 data are provided in Figure 5-1. In Figure 5-1 a, the Voce equation provides a better fit, as indicated by higher R^2 in Table 5-1. However, the Hollomon equation follows the initial part of the curve more closely until the true stress corresponding to the ultimate tensile strength. For X60, the constitutive equations with three parameters provide almost the same fit in Figure 5-1 b and therefore their R^2 values are essentially identical. The Hollomon equation still provides a very respectable fit. Based on this analysis, all four-constitutive equation can be used to represent true stress-true strain curves. The Hollomon equation, with two parameters, was chosen for its simplicity.

Table 5-1. Estimated parameters for the constitutive equations for X42 and X60 with calculated RMSE and R^2 of each fit.

		X42			X60		
Equations	**Parameters**	**Estimate**	**RMSE (MPa)**	**R^2**	**Estimate**	**RMSE (MPa)**	**R^2**
Hollomon	**K_H (MPa)**	644.0	11.85	0.974	1107.6	34.82	0.972
	n_H	0.118			0.229		
Voce	**σ_∞ (MPa)**	622.4	8.98	0.986	1801.7	13.68	0.996
	σ_0 (MPa)	387.5			587.4		
	K_V	5.33			0.64		
Swift	**K_S (MPa)**	644.2	12.77	0.971	1007.0	12.83	0.997
	ε_S	0.005			0.339		
	n_S	0.121			0.509		
Ludwik	**σ_L (MPa)**	133.5	13.11	0.969	533.6	12.73	0.997
	n_L	0.156			0.698		
	K_L (MPa)	511.4			632.6		

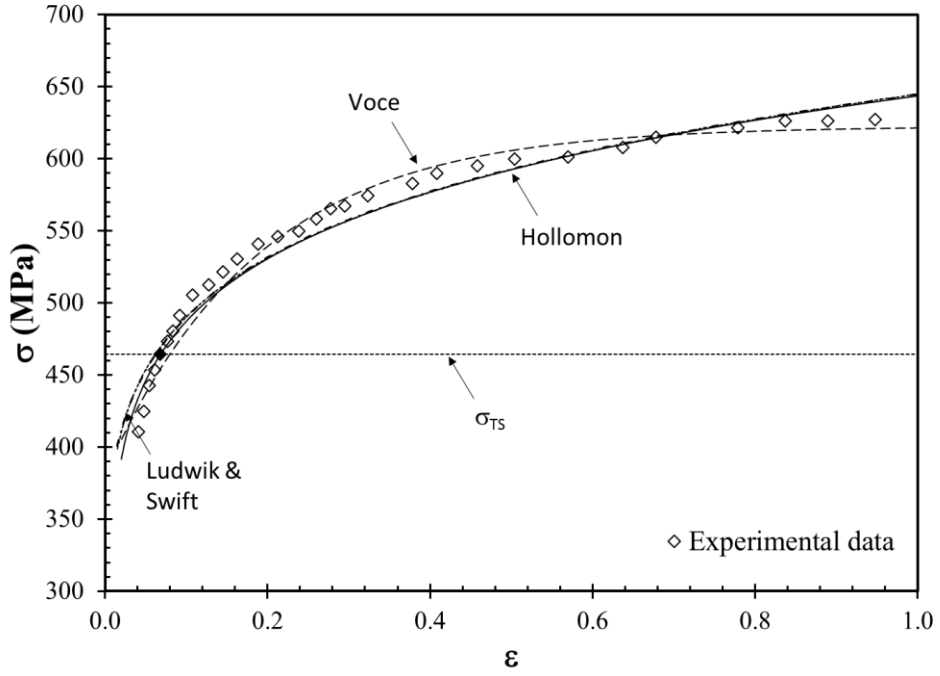

(a)

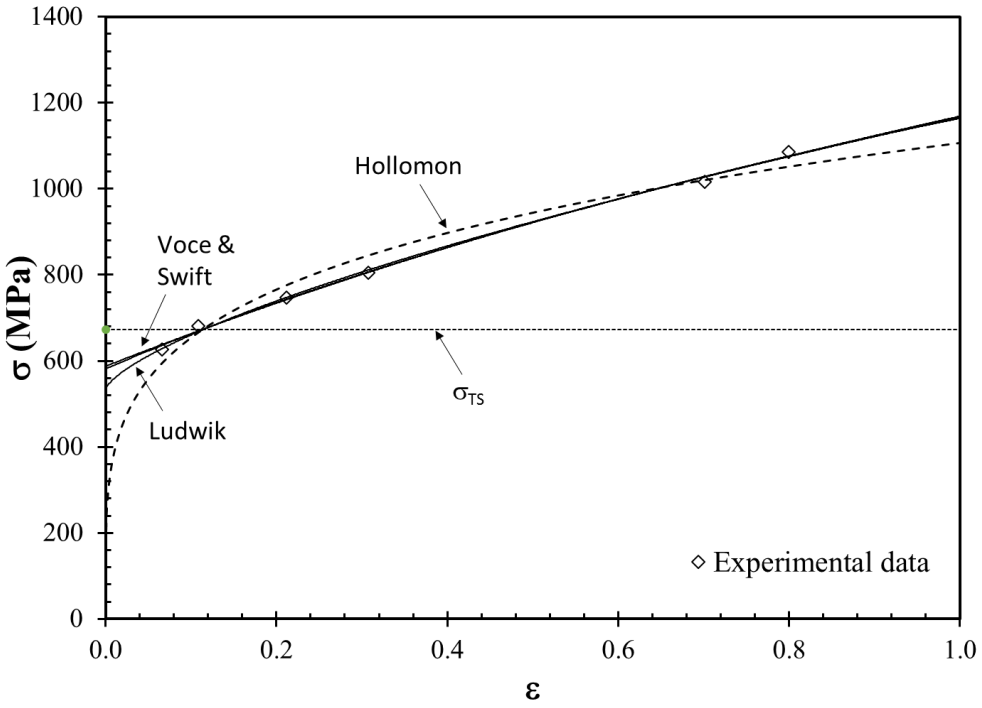

(b)

Figure 5-1. The fits of constitutive equations to experimental data for (a) X42, and (b) X60.

6. Phase 2: Evaluation of Failure Criteria

Three failure criteria have been found in the literature, indicating pipes will burst when:

1. True stress reaches 90% of true ultimate tensile strength, i.e., σ_{TS},
2. True stress reaches σ_{TS}
3. True strain reaches stress modified critical strain, ε_f.

The first one was proposed by Chiodo et al. [61] without any theoretical basis and therefore was not investigated further in this study. Criteria 2 and 3 were evaluated by using data from the literature.

The burst pressure data reported in the literature for low and mid-grade pipe steels, namely X42 and X60, were used for comparing FEA results with experimental data. Burst experiments with API X42 pipe were conducted by Alang et al. [46] with various longitudinal machined defects to simulate corrosion damage. The rectangular defect shapes on the pipe surface were machined using a Computer Numerical Control (CNC) machining center. Detailed dimensions of the pipes with artificial (machined) defects are given in Table 6-1 with corresponding failure pressure values. The nominal outer diameter of the pipe was 60 mm and the pipe section length was kept constant at 600 mm.

Table 6-1. Burst test data for X42 [46]

Test ID	Material	D (mm)	t (mm)	d (mm)	L (mm)	σ_y(MPa)	P_b(MPa)
EX1	X42	60.00	5.80	4.10	49.70	284.70	54.00
EX2	X42	60.00	5.60	3.50	49.80	284.70	61.00
EX3	X42	60.00	5.55	4.00	69.70	284.70	46.00
EX4	X42	60.00	5.62	4.50	50.00	284.70	44.00

*Test ID's are consistent with those used in Ref. [46]

Burst tests were conducted by Mok et al. [62] for 20 vessels with different orientation defects in X60 grade pipes. The nominal outside diameter was 508 mm and wall thickness was 6.4 mm.

Similarly, single and multiple defects with various sizes and orientations were machined on the pipes. Only five pipes with a single longitudinal defect (rectangular shape) were included for analysis in the present study. The details are presented in Table 6-2.

Table 6-2. Burst test data for X60 [62]

Test ID	Material	D (mm)	t (mm)	d (mm)	L (mm)	σ_Y(MPa)	P_b(MPa)
10	X60	508.00	6.40	2.56	381.00	540.00	11.25
11	X60	508.00	6.40	2.56	1016.00	540.00	11.55
12	X60	508.00	6.40	3.46	900.00	540.00	8.00
13	X60	508.00	6.40	3.20	1000.00	540.00	8.40
14	X60	508.00	6.40	2.18	900.00	540.00	11.80

*Test ID's are consistent with those used in Ref. [62]

For criterion 2, the reported values of 464.4 MPa [46] and 672.5 MPa [62] were used for X42 and X60, respectively. Based on the true stress-strain data presented in Figure 5-1, the value of $\varepsilon_f{}^*$ for X42 and X60 is 1.05 and 0.8, respectively. Consequently, A_f is calculated by using Equation 2-25 as 1.732 and 1.319 for X60 and X42, respectively.

To predict burst pressure of pipes with defects geometries outlined in Table 6-1 and Table 6-2, finite element analyses were conducted to calculate local stresses and strains. In FEA, the evolution of stress and strain can be displayed over the loading history, allowing the stress triaxiality and equivalent strain to be calculated by using Equation 2-22 through Equation 2-24. Subsequently, the true fracture strain can be estimated from Equation 2-25. Failure pressure is then determined as the pressure that causes the equivalent strain to reach the fracture strain. Similarly, failure pressure that causes the local stress to reach σ_{TS} can be determined.

A commercial Finite Element software, Siemens NX [63], was used to simulate stress and strain generation while internal pressure was increased in the pipe containing an external surface flaw. The model was meshed with hexahedral elements. As failure of the pipe in experimental works was noticed in remaining ligament of thinned wall, the FE mesh was applied sufficiently

small around the defect area. To ensure that the mesh is sufficiently fine, a preliminary mesh convergence study was performed until the stress variation between runs fell below 5%. The quarter of the pipe with sufficiently fine mesh is shown in Figure 6-1.

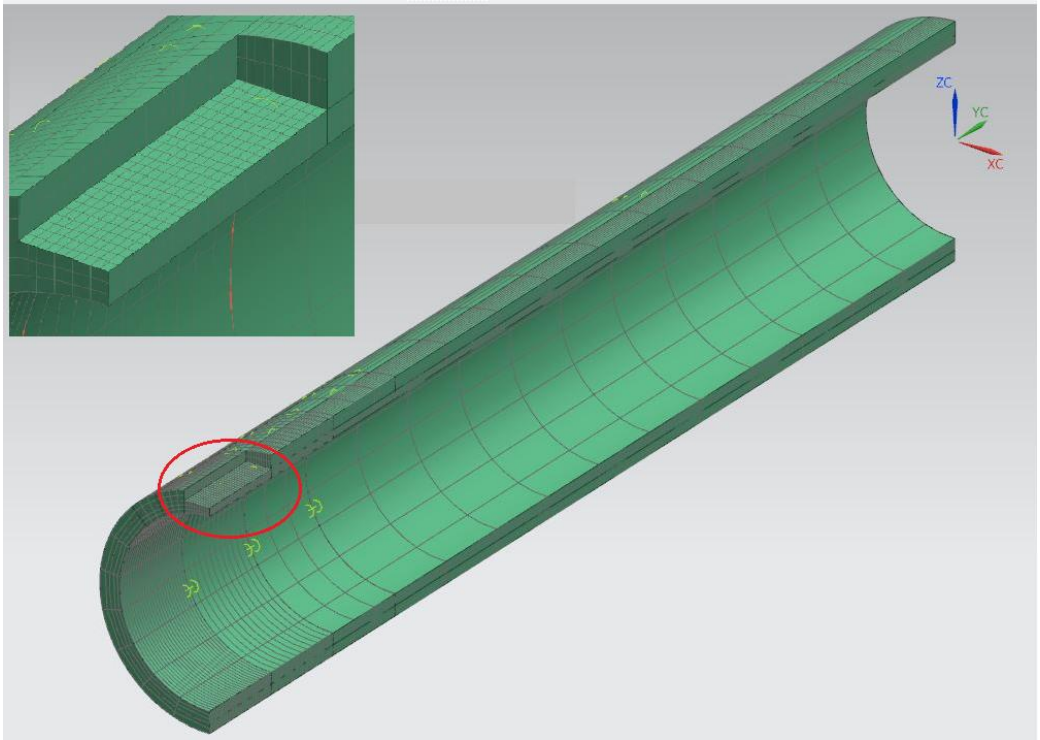

Figure 6-1. Quarter of the pipe model with applied mesh on it

The symmetry conditions were applied on symmetry planes of the quarter model (X=0, Y=0). It is sufficient to fix (Z=0) the nodes far away from the defect-interest area to eliminate rigid body motion. Failure pressure analysis was studied for internal pressure loading only. For each pipe model, the internal pressure load was applied normal to pipe inner surface and monotonically increasing throughout the analysis. Except of atmospheric pressure, external loadings were not considered.

FEA results

For case studies EX1 through EX4 pipe section length (L) was kept 600mm for all case experiments. The stress distribution along the quarter pipe section is shown in Figure 6-2. After certain distance along the pipe axis, the stresses can be assumed to be significantly lower than the critical stress. Therefore, the pipe section investigated in FEA can be reduced while maintaining reliable results.

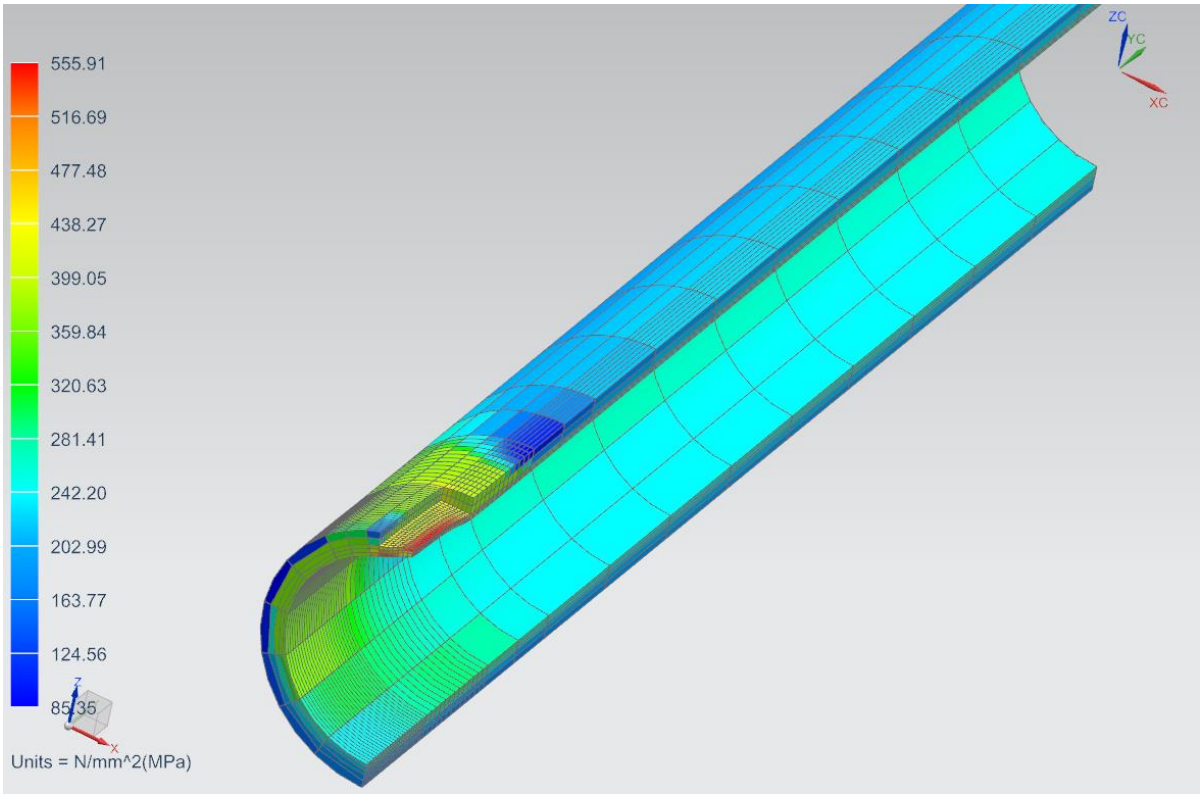

Figure 6-2. Stress distribution along the pipe axes.

Pipe section length was reduced to two times of the outer diameter, as suggested by an expert from industry [64]. Hence with an outer diameter of 60 mm, the pipe section modeled was 120 mm long. The comparison of the failure pressure results between two pipe section lengths is presented in Table 6-3, which shows identical results for lengths of 600 and 120 mm pipe lengths.

Consequently, subsequent FE analyses were performed on pipe section length equal to two times the outer diameter.

Table 6-3. FEA results for full and reduced pipe section length.

Case No.	$P_{f\text{-}experimental}$, MPa	$P_{f,l=600mm}$, MPa	$P_{f,l=120mm}$, MPa
EX2	61.00	61.95	61.95

The results of the FEA for X42 and X60 data for the failure criterion based on stress are presented in Figure 6-3, with experimental and predicted burst pressures. Note that the coefficient of determination, R^2, is 0.79 and 0.90 for X42 and X60 data, respectively. Therefore, the criterion that failure takes place when the local stress reaches σ_{TS} is reliable and can be used in other FEA studies. In comparison, the burst pressure results obtained for both datasets by using the stress-modified critical strain criterion are presented in Figure 6-4. Although the R^2 for X42 is 0.80 and therefore respectable, there is a significant lack of fit for X60, resulting in $R^2 < 0$. Based on these results, the failure criterion based on stress performs better in FEA. Hence, this criterion was used in Phases 3-5.

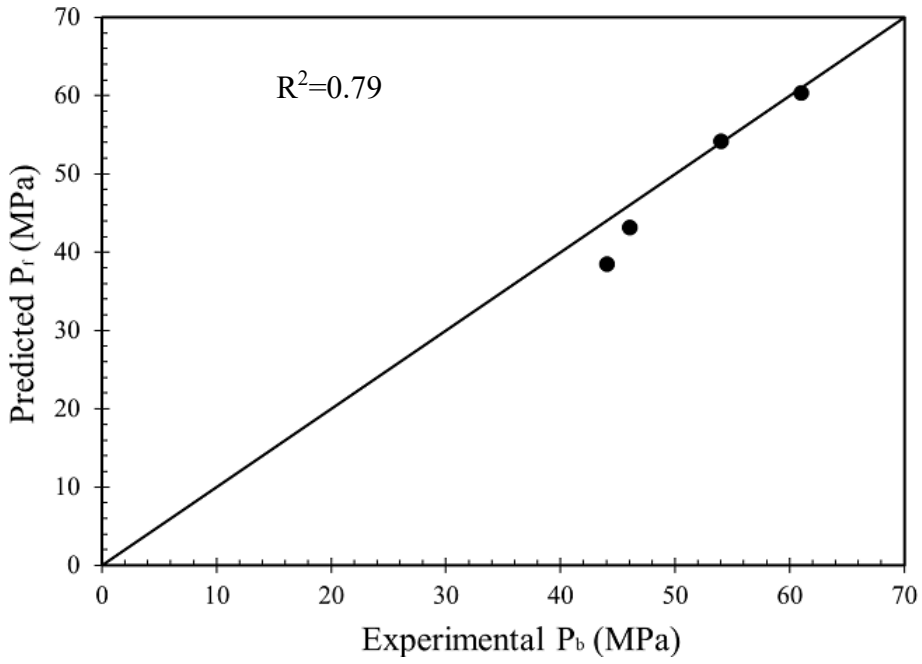

(a)

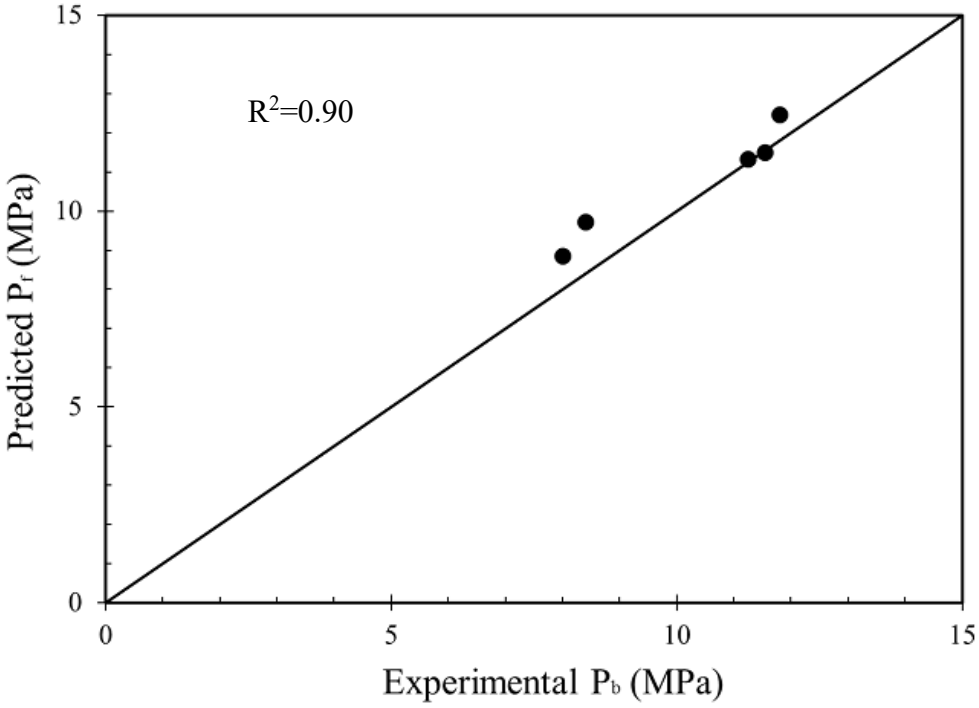

(b)

Figure 6-3. Experimental vs. predicted failure pressure using FEA for (a) X42 and (b) X60 by using the stress failure criterion.

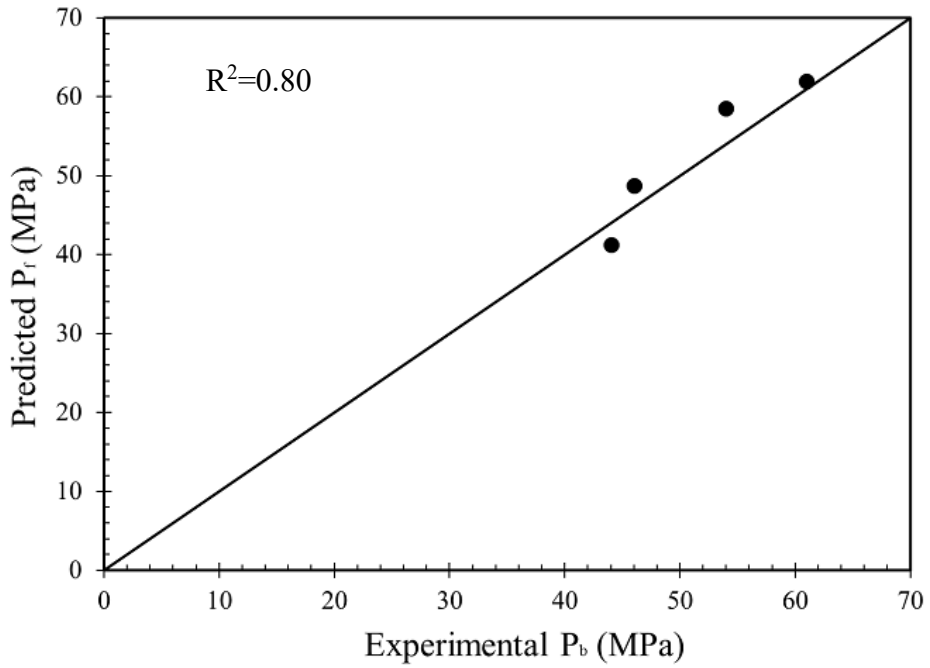

(a)

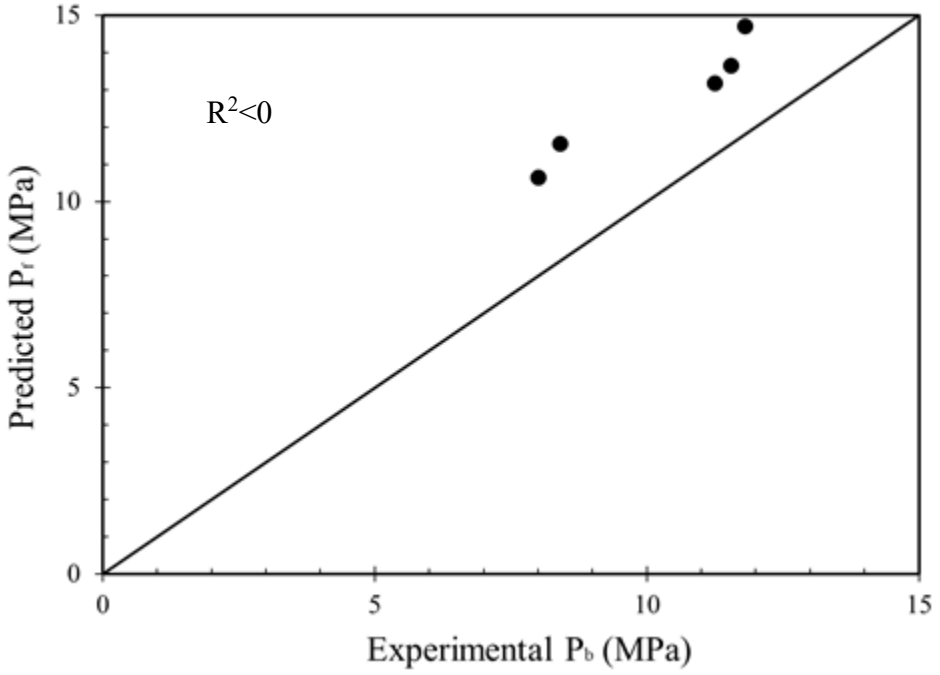

(b)

Figure 6-4. Experimental versus predicted failure pressure using FEA for (a) X42 and (b) X60 by using the stress-modified critical strain criterion.

7. Phase 3 – FEA of Real Corrosion Data

Data used for the research

In almost all investigations on the effect of surface defects on fracture properties of steel pipes, artificial (machined) defects have been used [25], [45]- [46], [60], [65]- [66]. These studies have provided valuable insights for FEA techniques that are used in the current study. However, design engineers need data based on real corrosion damage on the performance of pipes.

To the author's knowledge, only very limited data are available in the literature for real corrosion and characterization of corrosion damage in the form of pit contours. One of the rare studies with such data is described in PRCI report No: L51689 [28]. The database contains 124 test results, for real corrosion as well as machined defects. The first 86 test correspond to those presented in Ref. [67], In Ref. [67] some differences exist from those presented in L51689. Specifically,

- Some differences in actual yield strength
- Some wall thickness values may differ as much as 3%
- Some of the values of SMYS are given wrong in [67]
- Major failure pressure difference in case 51

Based on these differences, the data listed in Ref. [28] were used in the current study. A short introduction to the data and experimental tests is given below:

Cases 1-25

Experiments were conducted on corroded pipe specimens by Texas Eastern Transmission Corporation. Experimental cases 9 through 25 were conducted repeatedly on one specimen with successive leak repairs. The defects dimensions are given in terms of longitudinal profile. However, for these cases the contour maps were never developed.

Cases 26-31

These experimental cases were conducted on six separate pressure vessel specimens, fabricated from line pipes removed from service due to the presence of corrosion defects. Contours maps were provided for these cases and are presented in Appendix C from PRCI Report [28].

Case 32-92

The test specimens were made from corroded line pipe samples contributed by various pipeline operators. Cases 32 through 42 were conducted with PRCI funding. All specimens contained external corrosion defects except case 83, which contains internal corrosion. Failure pressures for the cases 48-51, 79-81, 83-86, were recorded, while pipe sections were in service. Defect contour maps are available for some cases and can be found in Appendix C from PRCI Report [28].

Finite element analysis

For FEA, eight cases for pipe X52 were selected from the data described above. For the cases 27-31, 51, 80 and 81, the contour maps were provided, and were used in determining the average defect width of corrosion pits. For the cases 27 - 31, 68-78 and 88 the tensile strength of the pipe materials was not recorded. So, from the cases 1-5, 51, 80, 81, 92, where full material properties were given for X52, a linear relationship between σ_Y and S_T was found, as presented in Figure 7-1. This linear relationship can be written as:

$$S_{TS}(\text{MPa})=0.697\sigma_Y+246.24 \qquad \text{Equation 7-1}$$

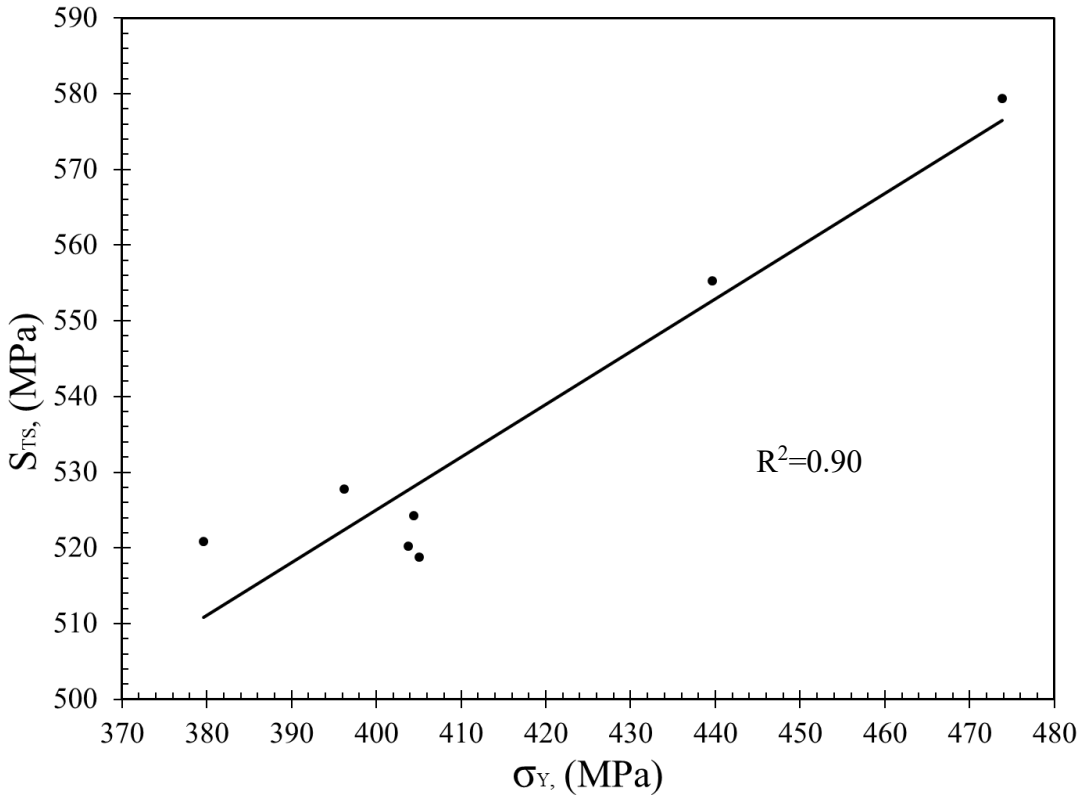

Figure 7-1 The plot describing the linear relationship between σ_Y and S_{TS}

As discussed above, constitutive equation by Hollomon [37] was used to represent the σ-ε curve in FEA. By definition, necking begins when the Considere criterion is met, at which the maximum engineering stress, i.e., ultimate tensile strength is achieved. By definition, the Considere criterion is met when the work hardening rate is equal to true stress. Hence,

$$\sigma_{TS}=\frac{d\sigma}{d\varepsilon}=\frac{d(K\varepsilon^n)}{d\varepsilon} \quad \text{Equation 7-2}$$

$$K\varepsilon_{TS}^{n}=\mathrm{n}K\varepsilon_{TS}^{n-1} \quad \text{Equation 7-3}$$

Therefore,

$$\varepsilon_{TS}=n \quad \text{Equation 7-4}$$

and

$$\sigma_{TS}=Kn^{n} \quad \text{Equation 7-5}$$

Then, ultimate tensile strength can be written as:

$$\sigma_{TS}=\frac{Kn^{n}}{e^{n}} \quad \text{Equation 7-6}$$

and yield strength as:

$$\sigma_{Y}=K\left(0.002+\frac{\sigma_{Y}}{E}\right)^{n} \quad \text{Equation 7-7}$$

Hence, K and n parameters were calculated from given σ_Y and S_{TS}. The experimental data to be replicated in FEA are provided in Table 7-1.

Table 7-1 Full-scale experiment cases for numerical and FEA

Case	D (mm)	t (mm)	d (mm)	L (mm)	w (mm)	σ_Y (MPa)	S_{TS} (MPa)	K (MPa)	n	$P_{f\text{-}exp}$ (MPa)
27	762.00	9.53	3.71	139.70	149	414.10	534.04*	761.83	0.11	12.68
28	762.00	9.53	2.92	114.30	87.5	418.90	537.43*	764.22	0.11	13.06
29	762.00	9.53	5.84	101.60	79	446.50	556.94*	777.78	0.10	12.23
30	762.00	9.53	5.31	40.60	30.5	476.80	578.35*	792.31	0.09	14.75
31	762.00	9.53	5.31	50.80	50	449.20	558.85	779.09	0.10	13.78
51	508.00	7.75	5.33	266.70	152.4	379.60	520.90	768.15	0.13	8.06
80	762.00	9.27	5.82	406.40	203	403.80	520.20	797.96	0.10	6.80
81	762.00	9.53	6.22	685.80	295	473.80	579.40	764.81	0.11	6.84

* Estimated with Equation 7-1.

Model generation

The experiments on the pipe section were conducted in laboratories, except of case 51, 80, 81 which were failed while pipe was in service. Consequently, two different types of the FEM were analyzed:

1. End-capped pipe sections
2. Open end pipe sections

Because the pressure vessel end cap dimensions were not provided in the original report, so the following assumptions were made:

- Hemispherical cap end was used
- Cap was of the same material as the pipe section, i.e., X52
- The dimensions were those demonstrated in Figure 7-2.

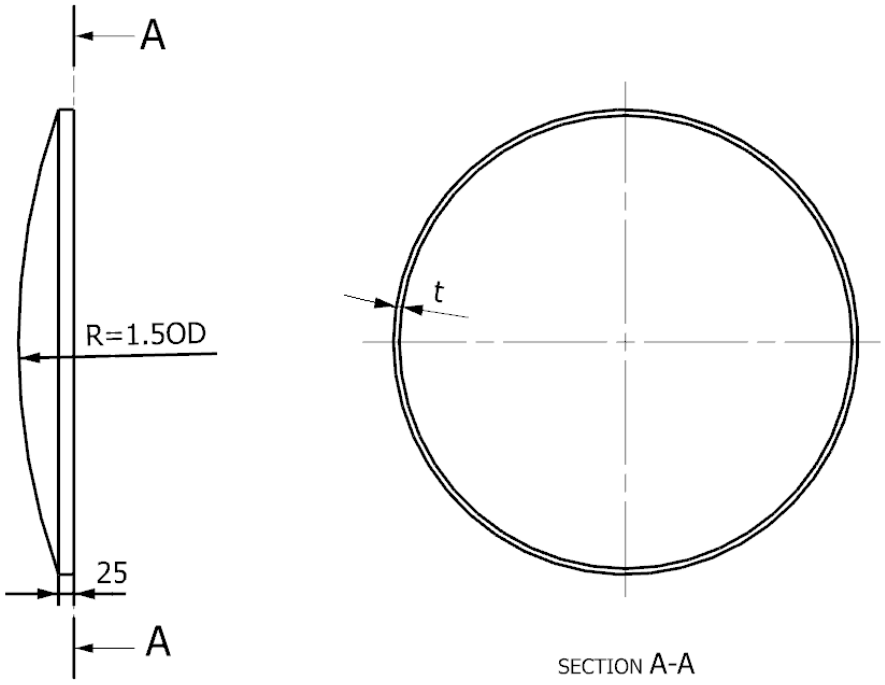

Figure 7-2 Dimensions assumed for hemispherical end.

As before, the commercial Finite Element Software Siemens NX [63] was used to simulate the failure pressure of the line pipe containing external surface flaws. The pipe section length was taken as twice the outer diameter of the pipe section being analyzed, as demonstrated previously. For time efficiency, the quarter of the pipe was modeled as shown in Figure 7-3 for both end-capped and open-end pipes. The real corrosion defect profile was simplified to an elliptical shape,

where the maximum defect dimensions (axial length, depth and circumferential width) were retained.

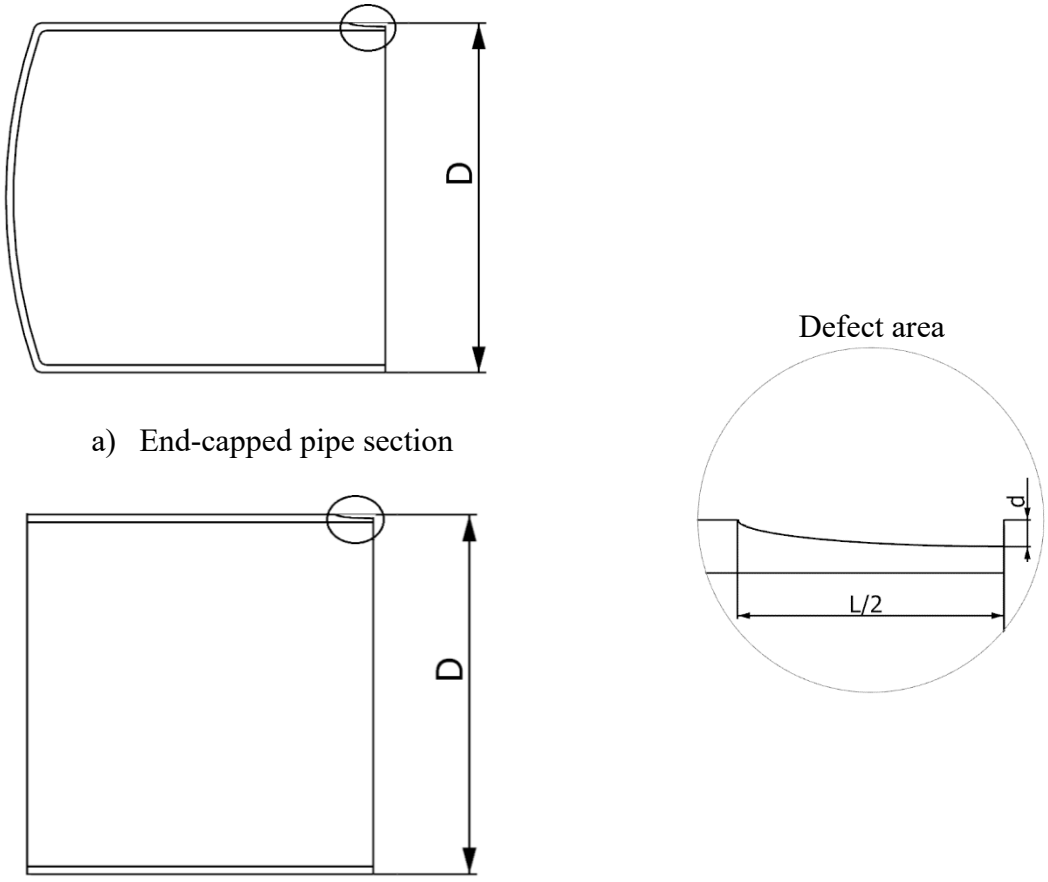

a) End-capped pipe section

b) Open-end pipe section

Figure 7-3 The sketch of quarter closed pipe used for FEM.

Material properties

The Finite Element software requires the stress- true strain curve of the material for more accurate analysis and results. For that reason, the Hollomon fit, with calculated K and n parameters for each data, was used. All analyses were undertaken using E = 207 GPa and υ =0.3 [46], [50], which are common values for steels.

FE Mesh

The quarter of the pipe was meshed with the second order eight noded hexahedral elements. As reported previously, the FE mesh was applied sufficiently fine around the defect area. In the literature, different numbers of elements are recommended through the remaining ligament of the pipe wall. For example, BS 7910 Annex G [27] suggested at least four elements through the remaining thickness, while Cronin [68], [69] stated that two elements will suffice. At first, FEA was conducted with four elements through the remaining ligament. During the analysis, it was observed that stresses differed significantly from one element to another. Hence a mesh convergence study was necessary. In this study, however, this step was bypassed by selecting the number of elements such that the ratio between the elemental nodal Von-Mises and elemental Von-Mises stresses was approximately 1, leading to reliable results. The criteria of choosing the element number was based on the d/t ratio:

- For $0 \leq \frac{d}{t} < 0.5$, fifteen elements
- For $0.5 \leq \frac{d}{t} \leq 1$, ten elements

Loads

Failure pressure analysis was studied for internal pressure loading only. For each pipe model, the internal pressure load was applied normal to pipe inner surface while monotonically increasing throughout the analysis. Except the atmosphere pressure, other external loadings were not considered.

Boundary conditions

The symmetry boundary conditions were applied on symmetry planes, constraining the translation degrees of freedom. Along with symmetry, the edge far away from the defect was constrained to eliminate the rigid body motion.

Failure Criterion

Stress based failure criterion, which was found earlier in this study to be reliable and effective, was used to predict the burst pressure of the pipe. Because of the software does not show the necking, failure was assumed to occur when the von-Mises stresses in the defect area reached the reference stress.

Finite Element Analysis

Finite element models were developed for the cases with actual corrosion width measured from surface plots. The cases are: 27-31, 51, 80 and 81. The mesh and the stress results for the Case 27 are presented in Figure 7-4. In Figure 7-4.c, it can be noticed that elemental von Mises stresses change their color gradually, providing further evidence that results can be expected to be accurate with the given mesh. Throughout iterations, elemental von Mises stresses were measured. At the point where the stresses reached σ_{TS}, the internal pressure was recorded as a failure (burst) pressure (Figure 7-5). For all other cases, the results are provided in Appendix 2.

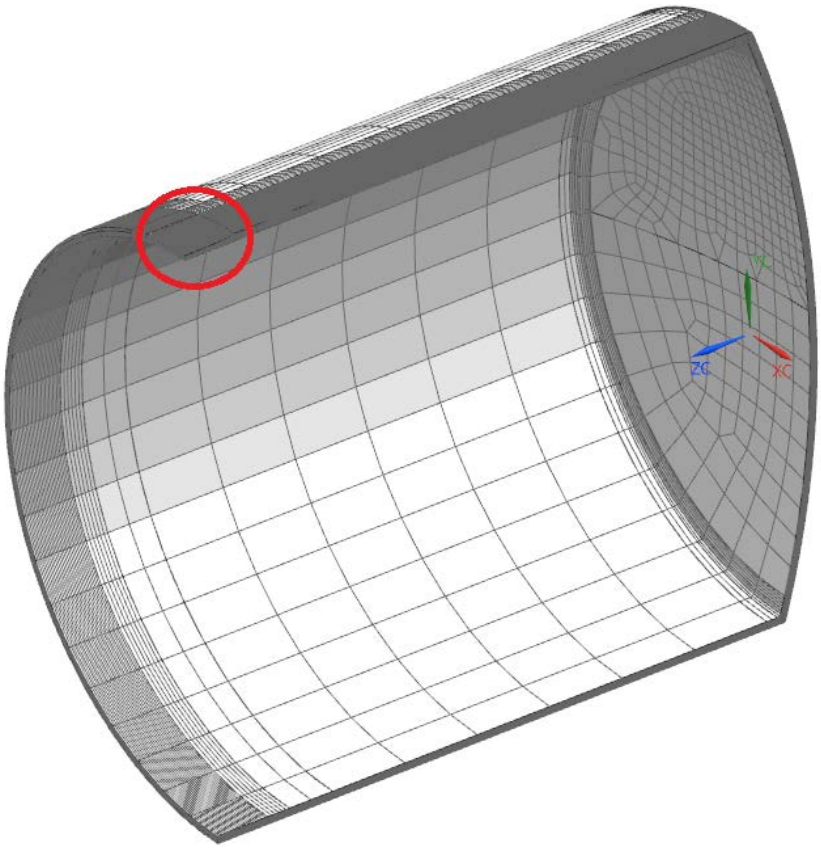

a) Quarter of the pipe with applied mesh on it

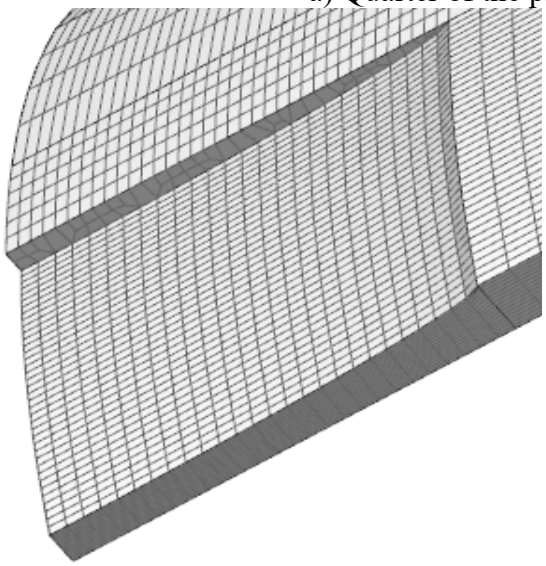

b) Area of the defect

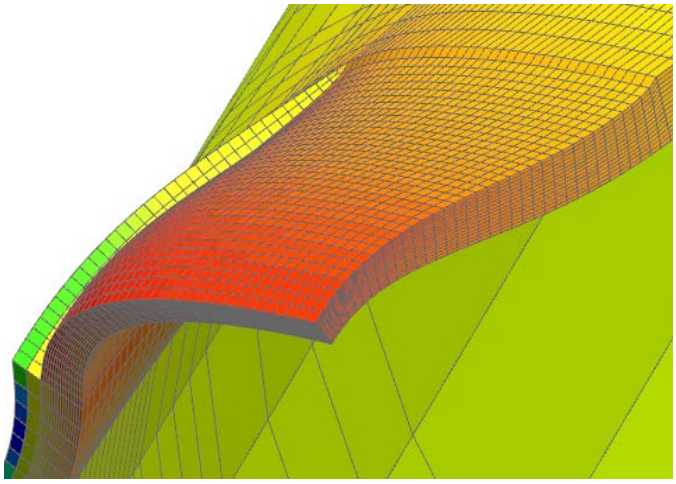

c) The stress distribution in the defect area

Figure 7-4 Case 27, pipe section model used for FEA.

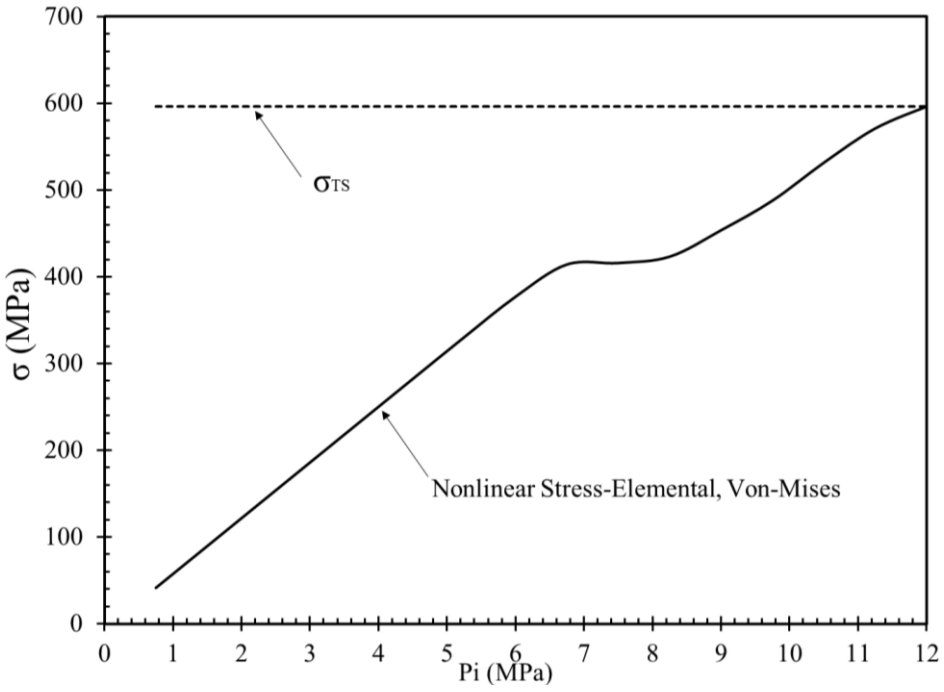

Figure 7-5 Variation of the von Mises stresses with applied load.

The predicted values of P_f and corresponding value of %errors are presented in Table 7-2. Note that the highest error is 15.64% with a majority of errors under ±5%. The R^2 for the fit is 0.959.

Table 7-2 FEM results for the cases with actual width.

Case	$P_{f\text{-}exp.}$ (MPa)	$P_{f\text{-}FEM}$ (MPa)	$\%error = \frac{P_{f-exp.} - P_{f-FEM}}{P_{f-exp}} \cdot 100$
27	12.68	12.00	-5.35
28	13.06	13.46	3.09
29	12.23	11.67	-4.58
30	14.75	14.28	-3.15
31	13.78	13.85	0.51
51	8.06	6.80	-15.64
80	6.80	6.31	-7.21
81	6.84	6.62	-3.15

The experimental versus predicted burst pressure values are presented in Figure 7-6. Note that there is a strong agreement between the FEM results and experimental data, as indicated by the high R^2 value.

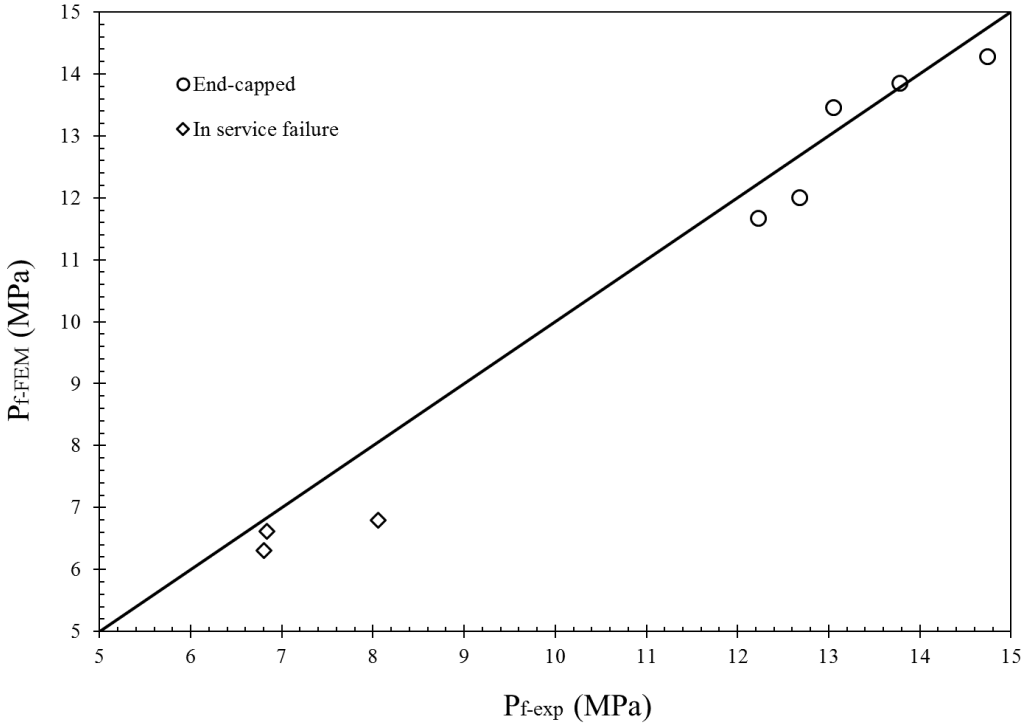

Figure 7-6. Comparison of experimental vs predicted data.

8. Phase 3. FEA for Corrosion Pits with Unknown Widths

The cases with contour plots available have been investigated for any possible pit width and length correlation. The results are shown in Figure 8-1. The data indicate a curvilinear relationship with the best fit obtained as:

$$w=2.3661\cdot L^{0.7452} \qquad \text{Equation 8-1}$$

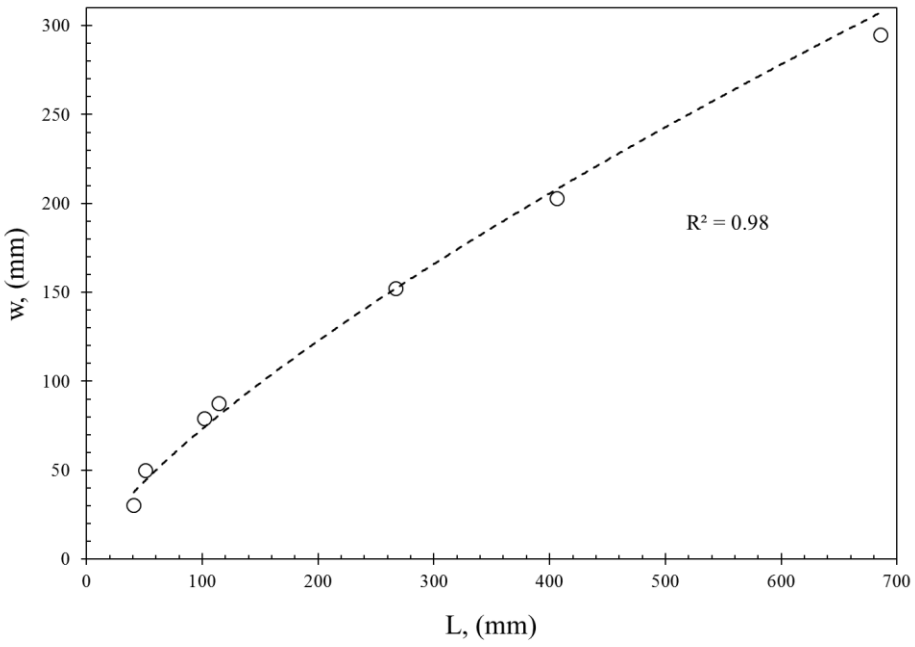

Figure 8-1 w versus L plot and fitted curve

The data used in this phase with missing widths are outlined in Table 8-1, including burst pressure, estimated S_T (as in Phase 2 with Equation 7-1) and w (estimated and Equation 8-1).

Table 8-1 Full-scale experiment cases for numerical and FEA

Case	D (mm)	t (mm)	d (mm)	L (mm)	w (mm) **	σ_Y (MPa)	S_{TS} (MPa)	K (MPa)	n	$P_{f\text{-}exp}$ (MPa)
1	762.00	9.53	3.71	63.50	52.17	404.4	524.3	747.99	0.11	11.182
2	762.00	9.53	3.71	57.20	48.27	404.4	524.3	747.99	0.11	11.162
3	762.00	9.53	3.99	108.00	77.51	404.4	524.3	747.99	0.11	11.713
4	762.00	9.53	6.10	139.70	93.89	439.6	555.3	780.77	0.10	11.506
5	762.00	9.53	5.31	120.70	84.20	405.1	518.8	734.15	0.11	10.507
68	762.00	9.45	3.30	914.40	380.78	409.30	531.52*	759.44	0.11	12.71
69	762.00	9.55	5.84	304.80	167.93	372.70	506.01*	740.99	0.12	10.44
70	762.00	9.53	3.56	304.80	167.93	406.50	529.57*	758.04	0.11	12.51
71	762.00	9.70	3.68	508.00	245.72	428.60	544.97*	769.02	0.11	13.11
72	762.00	9.55	3.30	508.00	245.72	387.20	516.12*	748.34	0.12	12.30
73	762.00	9.60	2.79	838.20	356.87	438.90	552.15*	774.07	0.10	13.20
74	762.00	9.63	4.32	355.60	188.37	440.30	553.13*	774.76	0.10	12.23
75	762.00	9.60	4.32	203.20	124.14	412.70	533.89*	761.14	0.11	11.85
76	762.00	9.58	4.06	304.80	167.93	416.80	536.75*	763.18	0.11	12.33
77	762.00	9.47	2.79	228.60	135.52	405.80	529.08*	757.69	0.11	12.68
78	762.00	9.45	3.30	914.40	380.78	409.30	531.52*	738.97	0.11	12.71
86	558.80	6.35	3.76	152.40	100.18	420.10	539.05*	786.95	0.11	558.80
88	762.00	9.22	3.05	198.16	121.83	425.90	551.20*	765.62	0.12	762.00
92	609.60	7.93	2.29	481.90	236.25	396.20	527.80*	747.99	0.11	609.60

*: Estimated with Equation 7-1 **: Estimated with Equation 8-1

Finite Element analyses

Same model generation concepts as in Phase 2 were used to conduct the study for estimated corrosion width. The predicted values of P_f and corresponding value of %error can be found in Table 8-2. Note that a large majority of the errors exceed ±10%. The plot showing the comparison between the experimental and predicted data can be found in Figure 8-2. The plot clearly shows that the unexplained variation is much higher than, which is shown as data points are located further from the slope of one

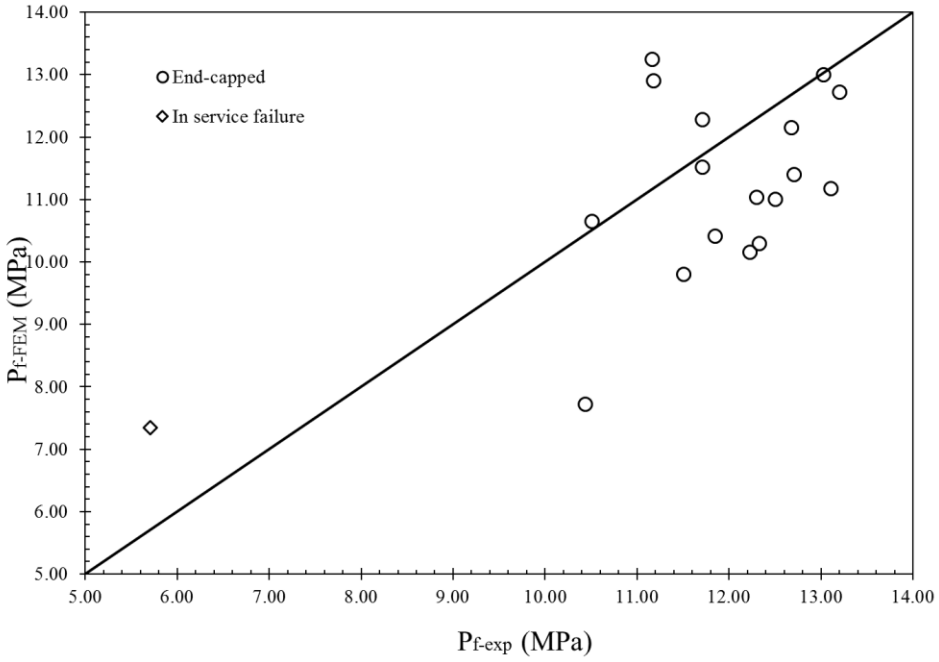

Figure 8-2. Comparison of experimental vs predicted data

Table 8-2 FEM results for the cases with estimated width.

Case	$P_{f\text{-}exp.}$ (MPa)	$P_{f\text{-}FEM}$ (MPa)	$\%error = \frac{P_{f-exp.} - P_{f-FEM}}{P_{f-exp}} \cdot 100$
1	11.18	12.90	15.36
2	11.16	13.25	18.71
3	11.71	12.28	4.84
4	11.51	9.80	-14.83
5	10.51	10.65	1.36
68	12.71	11.40	-10.27
69	10.44	7.72	-26.04
70	12.51	11.00	-12.04
71	13.11	11.17	-14.77
72	12.30	11.03	-10.32
73	13.20	12.72	-3.64
74	12.23	10.16	-16.93
76	11.85	10.41	-12.16
77	12.33	10.30	-16.44
78	12.68	12.15	-4.16
86	5.71	7.35	28.83
88	11.71	11.52	-1.65
92	13.03	13.00	-0.22

Statistical analyses

The errors for FEA data from models with estimated widths are presented in Table 8-3, along with that for data with actual widths. Note that sum of square for error in data with estimated widths is much higher, leading to lower R^2.

Table 8-3. Analysis of error FEM results for Phases 2 and 3.

w	SS_E	MS_E	SS_T	R^2
Known	3.03	0.43	73.93	0.959
Estimated	40.99	2.41	49.18	0.164

To compare whether the difference in error between the two datasets is significant, further statistical analysis was necessary. To test the hypothesis that the error is (or alternatively, is not) the same in the two datasets, the F-test was used. The hypothesis test procedure outlined in Table 8-4 was followed. The sample sizes for the "estimated" and "known" width datasets (n_1 and n_2) were 18 and 8, respectively. Mean square for error, MS_E is found by diving SS_E by the degrees of freedom of the dataset, i.e., n-1.

Table 8-4 Variance equality hypotheses test of two normal distributions

Null Hypothesis, H_0	$\sigma_1^2 = \sigma_2^2$
Alternate Hypothesis, H_A	$\sigma_1^2 \neq \sigma_2^2$
Test Statistic	$F_0 = \frac{MS_{E(1)}}{MS_{E(2)}}$
Rejection region	$F_o > F_{\frac{\alpha}{2},n_1-1,n_2-1}$ or $F_o < F_{1-\frac{\alpha}{2},n_1-1,n_2-1}$

To test hypothesis for the variance equality, the residuals, i.e., the difference between the observed value and estimated data need to be tested for normality. Residuals, e, are calculated by:

$$e_i = y_i - \hat{y_i} = P_{f-exp.} - P_{f-pred.} \qquad \text{Equation 8-2}$$

The residuals for the two datasets are given in Table 8-5 along with results of a goodness-of-fit hypothesis test, using the Anderson-Darling (AD) test statistic [70]. Note that the P-values for both datasets exceed 0.05, the default level for α-error (Type I). Therefore, the hypotheses that residuals for both "known" and "estimated" width datasets are normally distributed cannot be rejected. Minitab Software was used to check whether residuals from both datasets are normally distributed. The normal probability plot for both datasets is shown in Figure 8-3, along with results of a goodness-of-fit hypothesis test, using the Anderson-Darling (AD) test statistic [70]. Note that the P-values for both datasets exceed 0.05, the default level for α-error (Type I). Therefore, the hypotheses that residuals for both "known" and "estimated" width datasets are normally distributed cannot be rejected.

Table 8-5 Residuals for the two datasets.

Known	Estimated
-0.68	1.72
0.40	2.09
-0.56	0.57
-0.47	-1.71
0.07	0.14
-1.26	-1.31
-0.49	-2.72
-0.22	-1.51
	-1.94
	-1.27
	-0.48
	-2.07
	-1.44
	-2.03
	-0.53
	1.65
	-0.19
	-0.03

$$F_0 = \frac{S_1^{\,2}}{S_2^{\,2}} = 5.57$$

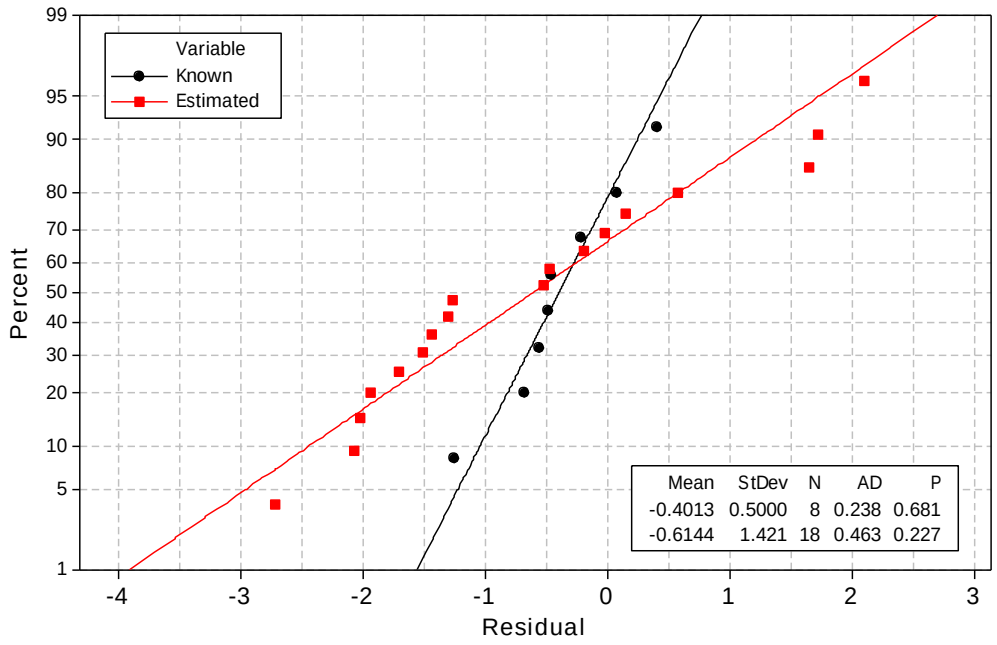

Figure 8-3 The normal probability plot of the residuals for known and estimated corrosion width.

The F-test can now be conducted. Because $F_{0.975,17,7} = 4.52$, test statistic (F_0=5.56) is larger than the critical F-value. Therefore, the hypothesis that the mean square error of the two datasets is the same can be rejected. Consequently, there is evidence that (i) knowing the actual width is important in FEA studies, and (ii) contrary to what is assumed in the literature, the width of corrosion pits may affect the burst pressure. To investigate this further a parametric study was conducted. Case 86, which had the largest error (28.83%), was chosen. Five different defect widths were simulated to investigate the possible effect of corrosion pit width on failure pressure of a corroded pipe. The axial length and depth of the corrosion pit were kept constant at 152.4 mm and 3.76 mm, respectively. The results are presented in Table 8-6 and in Figure 8-4.

Table 8-6. The results of the parametric study results for the Case 86.

Case	w (mm)	$P_{f\text{-}FEM}$ (MPa)
86	100.18	7.35
86-1	20	8.65
86-2	50	8.15
86-3	75	7.67
86-4	150	7.28
86-5	200	7.28

It can be noticed that the width does affect the burst pressure, especially at low widths. With increasing pit width, failure pressure is reduced linearly until a plateau is reached. For the case 86, the asymptotic relationship has been found based on the Figure 8-4 below:

$$\begin{aligned} &\text{if } w \le w_c \quad \text{then, } P_f = P_0 - C_{fc} \cdot w \\ &\text{if } w > w_c \quad \text{then, } P_f = 7.28 \text{ MPa} \end{aligned} \qquad \text{Equation 8-3}$$

where $w_c = 104.23$ mm, $P_0 = 8.95$ MPa, and $C_{fc} = 0.16$ MPa/mm.

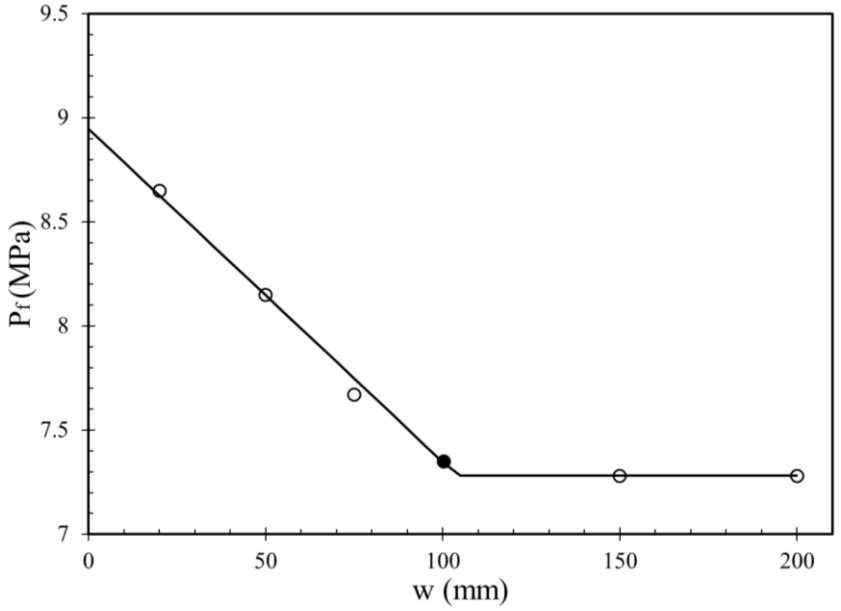

Figure 8-4 The effect of the defect width on failure pressure and the fitted equation (Equation 8-3).

To determine whether the same effect can be observed in other cases, Case 31 and Case 80 were chosen for FEM with various width dimensions, while pit length and depth were kept the same as

previously given in Table 7-1 . The results are given in Table 8-7 and Figure 8-5. Note that the same behavior, i.e., linear decrease in burst pressure with pit width is observed in Case 80. However, such a plateau is not reached with the widths tested for Case 31.

Table 8-7 Parametric study results for the Case 31 and 80

Case	w (mm)	$P_{f\text{-}FEM}$ (MPa)
31	50	14.1
31-1	20	14.23
31-2	75	13.85
31-3	100	13.55
31-4	150	13.05
31-5	200	12.8
80	203	6.31
80-1	20	7.04
80-2	40	6.96
80-3	75	6.6
80-4	100	6.33
80-5	150	6.32

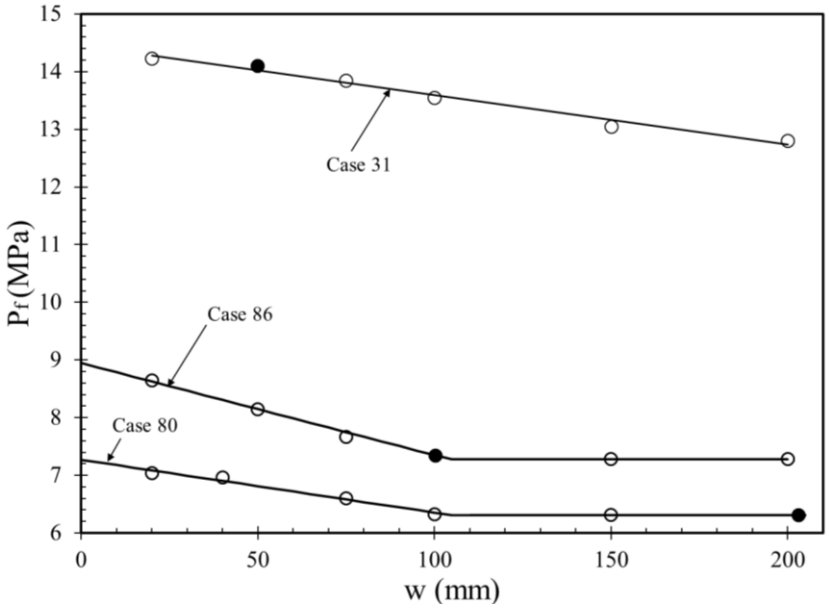

Figure 8-5 The asymptotic and linear relationships for the cases chosen in parametric study

For Case 31, P_0=14.45 MPa and C_{fc}=0.0086 MPa/mm. For Case 80, P_0=7.27 MPa, C_{fc}=0.01 MPa/mm. At a w_c=104.93 mm, the plateau of P_f=6.31 MPa is reached. Analysis of these results for a potential relationship between w_c, L and d did not yield results.

9. Phase 5: Determination of Type I and II errors

A Type I (α) error occurs when the null hypothesis is rejected when it, in fact, should not have been. Conversely, a Type II (β) error is committed when the null hypothesis is not rejected when in reality, it should be. For the pipes with corrosion defects, the null hypothesis was stated as:

H_o: The corrosion defect is "safe".

This means for a pipeline operating at certain P_i and therefore σ_H, the pipe section affected by corrosion will fail above that level. The test basis is presented in Table 9-1.

Table 9-1. Type I and II errors defined.

	Actual situation	
Decision	Defect is safe	Defect is not safe
Defect is safe	No error	β
Defect is not safe	α	No error

In this study, the effectiveness of three assessment techniques, ASME B31G, MB31G and DNV-RP at Level 0 evaluation was tested. The data from in-service failures in X52 steel pipes due to real corrosion pits in the PRCI Report [28] were first used and are presented in Table 9-2. To reduce the conservatism embodied in Level 0 evaluation, σ_H was assumed to be equal to $\sigma_{m(YS)}$. Corrosion defects were plotted according to their unique defect depth and length. According to the level of the σ_H at the moment of failure, it was determined whether each defect was "safe" or not.

Table 9-2. Data used for evaluation of assessment techniques.

Case	D (mm)	t (mm)	d (mm)	L (mm)	$P_{f\text{-}exp}$ (MPa)	$L/\sqrt{Dt}$	d/t	$\%\sigma_{Y(SM)}$
1	762	9.53	3.71	63.50	11.18	0.75	0.39	124.8
2	762	9.53	3.71	57.20	11.16	0.67	0.39	124.6
3	762	9.53	3.99	108.00	11.71	1.27	0.42	130.8
4	762	9.53	6.10	139.70	11.51	1.64	0.64	128.5
5	762	9.53	5.31	120.70	10.51	1.42	0.56	117.3
27	762	9.53	3.71	139.70	12.68	1.64	0.39	141.5
28	762	9.53	2.92	114.30	13.06	1.34	0.31	145.8
29	762	9.53	5.84	101.60	12.23	1.19	0.61	136.5
30	762	9.53	5.31	40.60	14.75	0.48	0.56	164.6
31	762	9.53	5.31	50.80	13.78	0.60	0.56	153.8
51	508	7.75	5.33	266.70	8.06	4.25	0.69	73.8
68	762	9.45	3.30	914.40	12.71	10.78	0.35	143.0
69	762	9.55	5.84	304.80	10.44	3.57	0.61	116.2
70	762	9.53	3.56	304.80	12.51	3.58	0.37	139.6
71	762	9.70	3.68	508.00	13.11	5.91	0.38	143.6
72	762	9.55	3.30	508.00	12.30	5.96	0.35	137.0
73	762	9.60	2.79	838.20	13.20	9.80	0.29	146.2
74	762	9.63	4.32	355.60	12.23	4.15	0.45	135.1
76	762	9.60	4.32	203.20	11.85	2.38	0.45	131.3
77	762	9.58	4.06	304.80	12.33	3.57	0.42	136.9
78	762	9.47	2.79	228.60	12.68	2.69	0.29	142.3
80	762	9.27	5.82	406.40	6.80	4.84	0.63	78.0
81	762	9.53	6.22	685.80	6.84	8.05	0.65	76.3
86	558.8	6.35	3.76	152.40	5.71	2.56	0.59	70.1
88	762	9.22	3.05	198.16	11.71	2.36	0.33	135.1
92	609.6	7.925	2.29	481.9	13.03	6.93	0.29	139.9

The Level 0 evaluation for pipe material X52 from in service failures reported in the PRCI Report [28] is presented in Figure 9-1. The area inside (to the left of) each curve is what the specific assessment technique designates as the "safe" region, while outside (to the right) is the "unsafe" region. For each assessment method, the hoop stress was calculated and subsequently plotted in Figure 3-3, with its normalized defect length and width. In Figure 9-1, the "unfilled green circles" represent an "acceptable" defect, i.e., that which caused failure above $\sigma_{m(YS)}$. The "cross red marks" represent those defects which led to failure below $\sigma_{m(YS)}$, representing "not acceptable" defects.

Note that there are only four “not acceptable” defects. These defects are above the curves for ASME B31G and MB31G. For DNV-RP, three of the defects are above the curve and one is below.

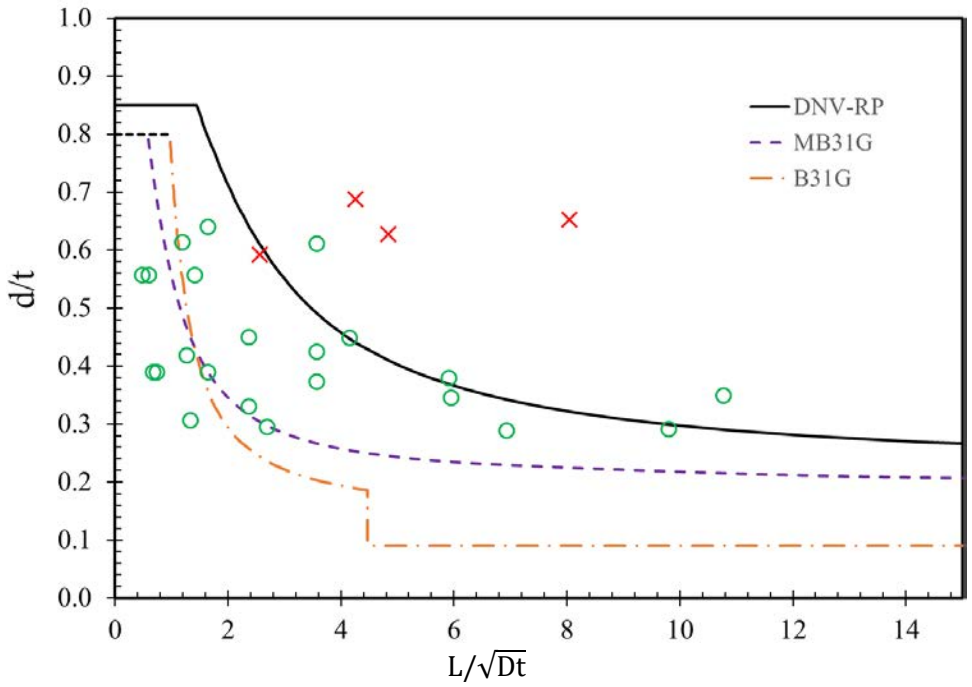

Figure 9-1. Level 0 evaluation for the X52 pipe material containing external corrosion flaw.

The null hypothesis stated above was tested. The number of data points with Type I and II errors are summarized in Table 9-3 for B31G, Table 9-4 MB31G and Table 9-5 for DNV-RP-F101. A Type II error was committed by DNV-RP, but not ASME B31G nor MB31G.

Table 9-3. Type I and II errors for B31G

	Actual situation	
Decision	Defect is safe	No
Defect is safe	6	0
Defect is not safe	16	4

Table 9-4. Type I and II errors for MB31G

	Actual situation	
Decision	Defect is safe	Defect is not safe
Defect is safe	9	0
Defect is not safe	13	4

Table 9-5. Type I and II errors for DNV-RP-F101

	Actual situation	
Decision	Defect is safe	Defect is not safe
Defect is safe	19	1
Defect is not safe	3	3

Parametric Study

Because FEM for case 29 produced an accurate prediction of the burst pressure, it was chosen for a parametric study at Level 0. Keeping design parameters and the defect width constant, the length and depth were changed in order to fill the gaps around assessment curves for ASME B31G, MB31G and DNV-RP. The results are given in Table 9-6 and plotted in Figure 9-2.

Table 9-6. Results of the parametric study.

Case	D (mm)	t (mm)	d (mm)	L (mm)	$P_{f\text{-}FEM}$ (MPa)	$L/\sqrt{Dt}$	d/t	$\%\sigma_{Y(SM)}$
29-1	762	9.53	4.30	340.8	10.10	4.00	0.45	112.8
29-2	762	9.53	2.86	1020.0	11.65	11.97	0.30	130.1
29-3	762	9.53	4.76	681.6	9.06	8.00	0.50	101.1
29-4	762	9.53	7.14	170.0	6.63	2.00	0.75	74.0
29-5	762	9.53	7.14	100.0	9.24	1.17	0.75	103.2
29-6	762	9.53	7.14	110.0	8.68	1.29	0.75	96.9

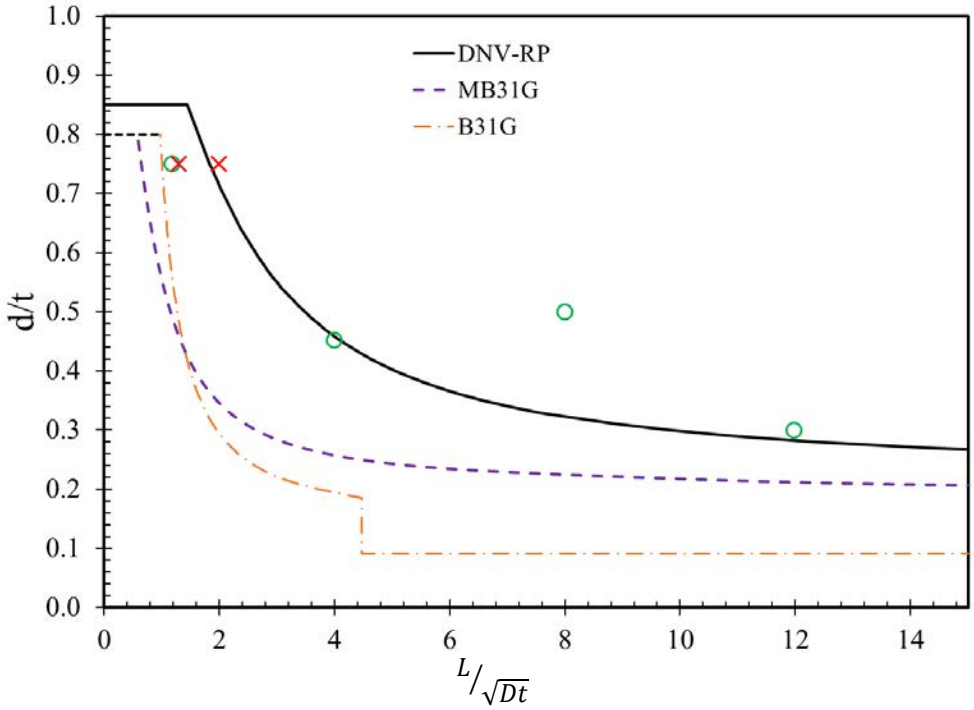

Figure 9-2. Evaluation of assessment techniques for synthetic data.

From the parametric study, it can be concluded, that for the d/t=0.5, the pipe can withstand the pressure even with longer defects. The DNV-RP represents more accurately for the part where, d/t=0.5. For the deep defect, the length can be a very critical parameter. As can be noticed, for a normalized defect depth of 0.75, the acceptable normalized length will be 1.17, but 1.29 can be critical. Further analysis is necessary for deep defects.

Conclusions

Research Question 1: Which constitutive model should be used for pipeline steels?

For X42 and X60, Hollomon, Ludwik, Voce and Swift constitutive equations have been compared to represent the material properties. The R^2 values in each case exceed 0.97, indicating that all constitutive equations can be used to characterize the true stress – true strain relationships. Although, Voce equation provides a better fit (R^2=0.986), the Hollomon constitutive equation has been used for material's stress-strain curve representation because of its simplicity in FEA for X52 pipe material for real corrosion data.

Research Question 2: In FEM studies, which failure criterion provides better results?

SMSC and stress based criterion showed respectable fits for X42, thick wall pipe. However, there is a significant lack of fit for X60, resulting in $R^2 < 0$, when the SMSC criterion is used. In conclusion it can be said, that the stress based criterion is most reliable, independent of pipe material and thickness. Hence, this criterion has been used for the FEA conducted on X52 pipe material.

Research Question 3: Does width of the corrosion affect the burst capacity of the pipe section?

Throughout the analyses, it has been noticed that the better fit to the model resulted when the data for the circumferential defect extension was known as opposed to "unknown." Even when a reliable correlation (R^2=0.98) has been found between L and w from the cases with available contour plots, in FEA with an unknown width of corrosion, a large majority of the errors exceeded ±10%.

Statistical F-test, has also shown that knowing the actual width is important in FEA studies, and the width of corrosion pits may affect the burst pressure. Parametric studies on width for the cases 31, 80, 81 have also give very strong proof that width does affect the burst pressure, especially at low widths.

Research Question 4: Do common techniques of using machined groove, in lieu of real corrosion defects, give reliable results?

Based on the studies mentioned Research Question 3, the researchers investigating burst capacity with machined grooves should consider in their study the width parameter.

Research Question 5: Do analytical models in literature, such as ASME B31G, MB31G and DNV-RP-F101, provide reliable results?

Three most commonly used assessment techniques have been investigated. Although, ASME B31G is the most conservative technique, it is more reliable for short defects than MB31G and DNV-RP. But after $L/\sqrt{Dt}$=1.38 and d/t=0.4, the B31G becomes much more conservative. The DNV-RP is the least conservative assessment criterion. However, this method produced a β error, i.e., the method predicted a "safe" operating pressure which would actually have resulted in the pipe section failing. Therefore, DNV-RP is not recommended for Level 0 evaluation of steel pipes, specifically X52 pipes.

Recommendations for Future Research

- This study has been limited to X52 pipe material type. For future research, it will be necessary to investigate other pipe material types, and their response to fracture.

- A more in-depth study of w/L ratio is required, for different corrosion depth, d, and pipe design dimensions, such as diameter, D, and wall thickness, t.

- As previous analytical methods have been developed based on machined grooves, the width of defect has not been considered. Therefore, a new analytical method is necessary for real corrosion profiles and the width.

References

[1] T. Anthony, "Pipeline transport," Wikimedia Foundation, Inc., 24 June 2016. [Online]. Available: https://en.wikipedia.org/wiki/Pipeline_transport. [Accessed 27 July 2017].

[2] G. A. Papadakis, "Major hazard pipelines: a comparative study of onshore transmission accidents," *Journal of Loss Prevention in the Process Industries* , vol. 12, no. 1, pp. 91-107, 1999.

[3] "U.S. Energy Information Administration," U.S. Energy Mapping System, [Online]. Available: https://www.eia.gov/state/maps.php.

[4] ASTM, *ANSI/ ASME B31.1 Standard for Power Piping,* New York: ANSI/ ASME, 2004.

[5] ASTM, *ANSI/ ASME B31.3, Standard for Chemical Plant and Petroleum Refinary Piping,* New York: ANSI/ ASME, 2002.

[6] ASTM, *Standard for Liquid Transportation Systems for Hydrocarbons, Liquid Petroleum Gas, Anhydrous Ammonia, and Alcohols,* New York: ANSI/ASME, 2002.

[7] ASTM, *Standard for Gas Transmission and Distribution Piping Systems,* New York: ANSI/ ASME, 2014.

[8] E. S. MENON, Transmission Pipeline Calculations and Simulations Manual, Oxford: Elsevier Inc. , 2015.

[9] American Petroleum Institute, "API 5L: Specification for line pipe. 49CFR192.113," API Publishing Services, Washington D.C., 2004.

[10] I. R. Vilarouco, R. Soares de CastroI, Y. P. Yadava and R. A. Ferreira, "Study of phase transformations In API 5L X80 Steel in order to increase its fracture toughness," *Materials Research,* vol. 16, no. 2, pp. 489-496, 2013.

[11] G. O. Brown, "The history of the Darcy-Weisbach equation for pipe flow resistance," in *Environmental and Water Resources History Sessions at ASCE Civil Engineering Conference and Exposition*, Washington D.C., 2002.

[12] C. F. Colebrook, "Turbulent flow in pipes, with a particular reference to the transition region between the smooth and rough pipe laws," *Journal of the Institute of Civil Engineers,* vol. 11, no. 4, pp. 133-156, 1939.

[13] A. Mayberry, "Class Location Requirements for Gas Pipelines," PHMSA, 2014.

[14] Spectra Energy Corp, "Natural Gas Pipeline Construction," Spectra Energy, 2017. [Online]. Available: http://www.spectraenergy.com/Operations/US-Natural-Gas-Operations/New-Projects-US/Our-Process-Interstate/Pipeline-Construction/.

[15] E. Cruz, Director, *Basic Pipeline Construction.* [Film]. USA: Youtube, 2010.

[16] R. Abusoufeh, Interviewee, *Design priciples on piping systems.* [Interview]. 13 June 2017.

[17] C. Irwin, "Energy News Roundup: South Stream Deals Breach EU Law," 19 December 2013. [Online]. Available: http://breakingenergy.com/2013/12/19/energy-news-roundup-south-stream-deals-breach-eu-law/.

[18] Department of Transportation and Homeland Security, "Electronic Code of Federal Regulations,Title 49," U.S. Government Publishing Office, 2014.

[19] Enduro, "Pipeline Pigging with Smart Pigs," A Pipeline Pigging Resource, 2012. [Online]. Available: http://smartpigs.net/. [Accessed 8 August 2017].

[20] PHMSA, "The State of The National Infrastructure," US Department of Transportation, 2011.

[21] Pipeline Hazardous Materials Safety Administration, "Significant Incidents," United States Department of Transportation, 2017.

[22] D. Lyons, "Western european cross-country oil pipelines 30-year performance statistics," CONCAWE, Brussels, 2002.

[23] Baker and Keifner&Associates, "Mechanical Damage, Final report," Michael Baker, Jr. Inc., 2009.

[24] R. L. Norton, Machine Design: An integrated approach, Worcester. Massachuetts: Prentice Hall, 2011.

[25] S. A. Hosseini , *Assessment of Crack in Corrosion Defects in Natural Gas Transmission Pipelines,* Waterloo, Ontario, Canada: A thesis presented to the University of Waterloo, 2010.

[26] M. Hasan, "Pitting Corrosion and Crevice Corrosion," LinkeIn Corporation, Turkyurdu, 2014.

[27] The British Standards Institution, *Guide to methods for assessing the acceptability of flaws in metallic structures,* London: BSI Standards Limited, 2013.

[28] J. F. Kiefner and P. H. Vieth , "Database of Corroded Pipe Tests, PR-218-9206, Prepared for the Pipeline Corrosion Supervisory Committee, Pipeline Research Committee of Pipeline Research Council International, Inc. PRCI Catalog No. L51689," Technical Toolboxes, Inc., Texas, 1993.

[29] M. Cerit, K. Genel and S. Eksi, "Numerical investigation on stress concentration of corrosion pit," *Engineering Failure Analysis,* vol. 16, no. 7, pp. 2467-2472, 2009.

[30] J. F. Keifner, "Fracture Initiation," in *American Gas Association, Fourth Symposium on Line Research*, Dallas, 1969.

[31] L. Gajdos and M. Sperl, "Critical conditions of Pressuarized Pipes," *Engineering Mechanics: International Journal of Theoretical and Applied Mechanics,* vol. 20, no. 5, pp. 401-412, 2013.

[32] D. S. Dugdale, "Yielding of steel sheets containing slits," *Journal of Mechanics and Physics of Solids,* vol. 8, no. 2, pp. 100-104, 196.

[33] E. S. Folias, "The stresses in a cylidrical shell containing an axial crack," *International Journal of Fracture Mechanics,* vol. 1, no. 2, pp. 104-113, October 1965.

[34] G. T. Hahn, M. Sarrate and A. R. Rosenfield, "Criteria for crack extension in cylidrical pressure vessels," *international Journal of fracture,* vol. 5, no. 3, pp. 187-210, 1969.

[35] A. R. Duffy, G. M. McClure , W. A. Maxey and T. J. Atterbury, "Study of feasibility of basing natural gas pipeline operating pressure on actual yield determined by hydrostatic test, Catalogue No. L30050," American Gas Association Inc, 1968.

[36] Keifner Associates Inc. and PHMSA, "Validity of standard defect assessment methods for the alliance pipeline operating 80% of SMYS," US DoT, Columbus, 2006.

[37] J. H. Hollomon, "Tensile deformation," *AIME TRANS,* vol. 12, no. 4, pp. 1-22, 1945.

[38] E. Voce, "A practical strain-hardening function," *Metallurgia,* vol. 51, no. 307, pp. 219-226, 1955.

[39] P. Ludwik, Elemente der Technologischen Mechanik, Berlin: Springer Berlin Heidelberg, 1909, p. 32.

[40] H. W. Swift, "Plastic instability under plane stress," *Journal of the Mechanics and Physics of Solids,* vol. 1, no. 1, pp. 1-18, 1952.

[41] J. M. Story, W. H. Hunt Jr., R. H. Wagoner and D. J. Lege, "Novel techniques in metal deformation testinf," in *The Minerals, Metals, Materials Society*, Metals Park, Ohio, 1983.

[42] M. Tiryakioglu, J. T. Staley and J. Campbell, "A comparative study of the constituve equations to predict the work hardening characteristics of cast Al-7wt.%Mg alloys," *journal of Materials Science Letters,* vol. 19, no. 24, pp. 2179-2181, 2000.

[43] O. Unal and M. Tiryakioglu, "Characterization of Tensile Deformation in AZ91D Mg Alloy Castings," in *In Shape Casting: 6 th international Symposium*, Nashville, 2016.

[44] B. K. Choudhary, E. I. Samuel, S. R. Bhanu and S. L. Mannan, "Tensile stress-strain and work hardening behaviour of 316LN austenitic stainless steel," *Materials Science and technology,* vol. 17, no. 2, pp. 223-231, 2001.

[45] D. H. Mok, R. J. Pick, A. G. Glover and R. Hoff, "Bursting of Line Pipe with Long External Corrosion," *International Journal of Pressure Vessels and Piping,* vol. 46, no. 2, pp. 195-216, 1991.

[46] N. A. Alang, N. A. Razak, K. A. Shafie and A. Sulaiman, "Finite Element Analysis on Burst Pressure of Steel Pipes with Corrosion Defects," in *13th International Conference on Fracture*, Beijing, China, 2013.

[47] Y. K. Leel, Y. P. Kim, W. H. Bang, K. H. Ohl and W. S. Kim, "The prediction of failure pressure of gas pipeline with multi corroded region," *Materials Science Forum,* Vols. 475-479, pp. 3323-3326, 2005.

[48] T. A. Netto , U. S. Ferraz and S. F. Estefen, "The effect of corrosion defects on the burst pressure of pipelines," *Journal of Construction Steel Research,* vol. 61, no. 8, pp. 1185-1204, 2005.

[49] L. Y. Xu and Y. F. Cheng, "Reliability and failure pressure prediction of various grades of pipeline steel in presence of corrosion defects and pre-strain," *International Journal of Pressure Vessels and Piping,* vol. 89, pp. 75-84, 2012.

[50] M. S. Chiodo and C. Ruggieri, "Failure assessments of corroded pipelines with axial defects using stress-based criteri: Numerical studies and verification analyses," *International Journal of Pressure Vessels and Piping,* vol. 86, no. 2-3, pp. 164-176, 2009.

[51] J. R. Rice and D. A. Tracey, "On ductile enlargment of voids in triaxial stress fields," *Journal Mechanics and Physics of Solids,* vol. 17, no. 3, pp. 201-217, 1969.

[52] A. L. Gurson, "Continuum theory of ductile rupture by void nucleation and growth: Part I - yield criteria and flow rules for porous ductile media," *Journal of Engineering Materials and Technology,* vol. 99, no. 1, pp. 2-15, 1977.

[53] J. A. Lamaitre, "Continuous damage mechanics model for ductile fracture," *Journal of Engineering Materials and technology,* vol. 107, no. 1, pp. 83-89, 1985.

[54] J. W. Hancock and A. C. Mackenzie, "On the mechanics of ductile failure in high-strength steels subjected to multi-axial stress-states," *Journal Mechanics and Physiscs of Solids,* vol. 24, no. 2-3, pp. 147-169, 1976.

[55] C. K. Oh, Y. J. Kim, J. H. Baek, Y. P. Kim and W. S. Kim, "A phenomenological model of ductile fracture for API X65 steel," *International Journal of Mechanics Sciences,* vol. 49, no. 12, pp. 1399-1412, 2007.

[56] C. K. Oh, Y. J. Kim, J. M. Park, J. H. Baek and W. S. Kim, "Development of stress-modified fracture strain for ductile failure of API X65 steel," *International Journal of Fracture,* vol. 143, no. 119, pp. 119-133, 2007.

[57] J. W. Hancock and A. C. Mackenzie, "On the mechanisms of ductile failure in high-strenght steels subjected to multi-axial stress-states," *Journal of Mechanics and Physics Solids,* vol. 24, no. 2-3, pp. 147-160, 1976.

[58] ASTM, "ASME B31G. Manual for determining the remaining strenght of corroded pipelines, A Supplement to ASME 831 Code for Pressure Piping," ASME, New York , 2012.

[59] B. A. Chouchaoui and R. J. Pick, "Behaviour of circumferentially aligned corrosion pits," *International journal of pressure vessels and piping,* vol. 57, no. 2, pp. 131-251, 1994.

[60] Advantica and PRCI, *Corrosion assessment guidance for high strength steels, Catalog No. L52294,* Houston: Technical Toolboxes, Inc., 2008.

[61] M. S. Chiodo and C. Ruggieri, "Failure assessments of corroded pipelines with axial defects using stress based criteria: Numerical studies and verification analyses," *International Journal of Pressure Vessels and Piping,* vol. 86, no. 2-3, pp. 164-176, 2009.

[62] D. R. Mok, R. J. Pick and A. G. Glover, "Behavior of line pipe with long external corrosion," *International Journal of Pressure Vessels and Piping,* vol. 46, no. 2, pp. 195-216, 1991.

[63] K. Jaecheol , *Siemens NX 9 Design Fundamentals A Step by Step Guide,* ONSIA Inc, 2014.

[64] B. Zhu, *Answers for questions asked by Jennet Orasheva,* Houston: Google Mail, 2016.

[65] J. Freire, R. Vieira, J. Castro and A. Benjamin, "Burst tests of pipeline with extensive longitudinal metal loss," *Experimetal techniques,* vol. 30, no. 6, pp. 60-65, 2006.

[66] M. Leandro de Silva and H. Silva da Costa Mattos, "Prediction of the burst pressure for metallic pipelines with localized corrosion defects," in *International Symposium on Solid Mechanics*, Porto Alegre, Rio Drande do Sul, Brazil, 2013.

[67] J. F. Keifner, P. H. Vieth and I. Roytman, "Continued Validation of RSTRENG. PR-218-9304, Prepared for the Line Pipe Research Supervisory Committee, Pipeline Research Committee of Pipeline Research Council International, Inc. PRCI Catalog No. L51749," Technical Toolboxes, Inc., Texas, 1996.

[68] D. Cronin, "Assessment of corrosion defects in pipelines," Waterloo, 2000.

[69] D. S. Cronin and R. J. Pick, "Experimental database for corroded pipe: evaluation of RSTRENG and B31," in *Proceedings of the 2000 International Pipeline Conference*, 2000, pp. 757-767.

[70] T. W. Anderson and D. A. Darling, "A test of goodness of fit," *Journal of American Statistical Association,* vol. 49, no. 268, pp. 765-769, 1954.

10. Appendix

Appendix 1. Available contour maps of corrosion pits [28].

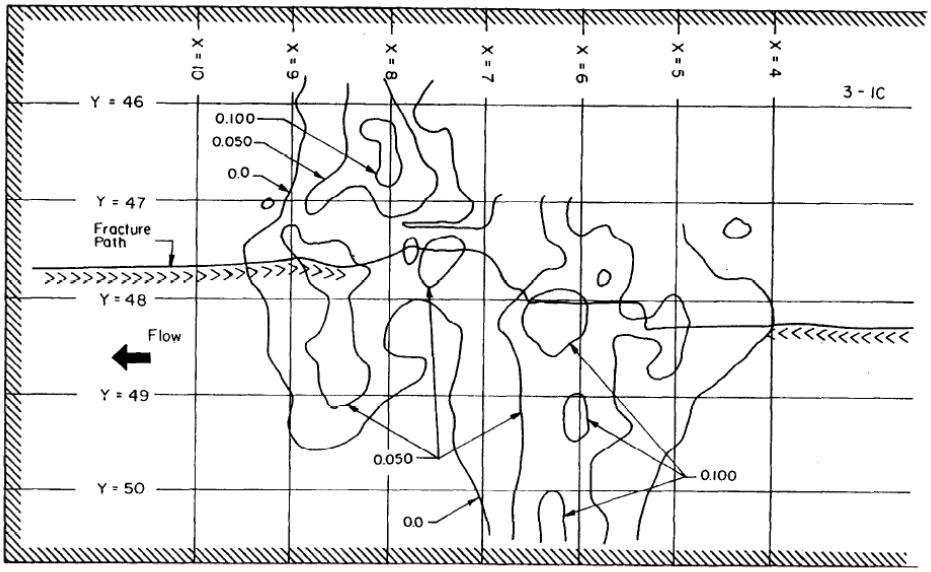

Figure 10-1. Surface map for case 27

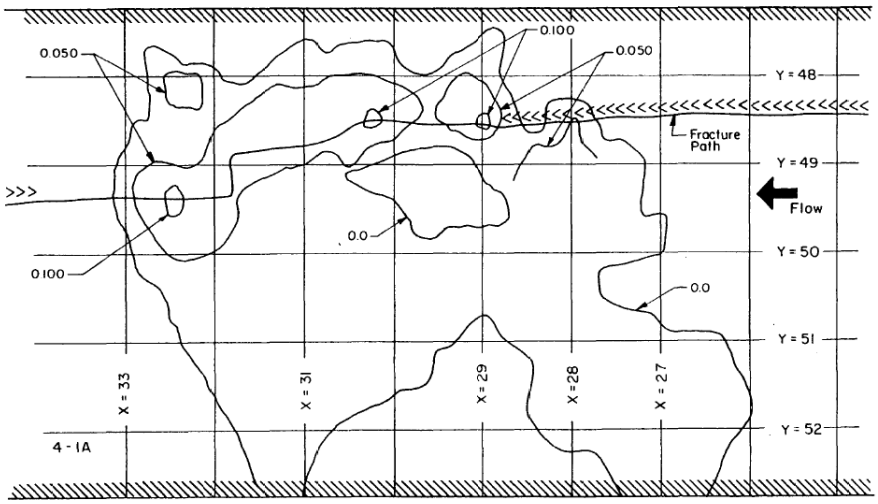

Figure 10-2. Surface map for case 28

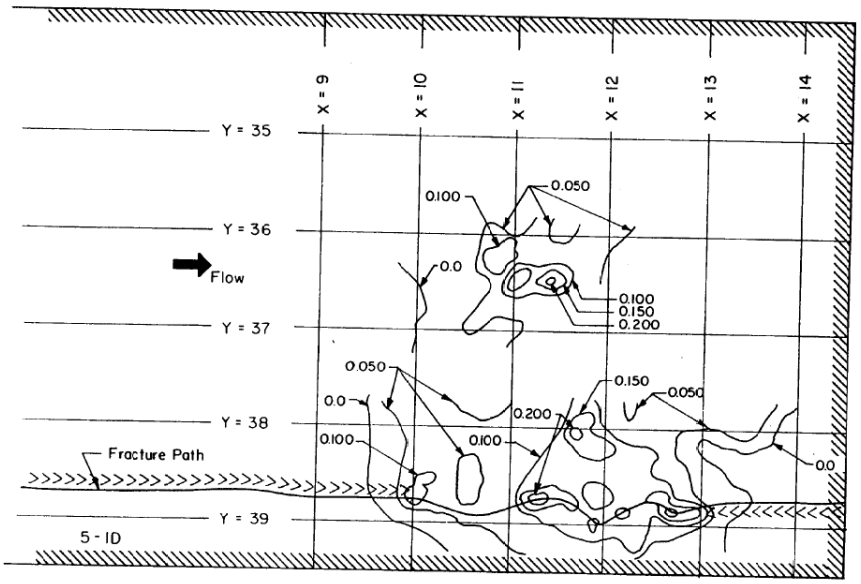

ORIGIN OF RUPTURE IN DIGOUT NO. 5

CASE 29

Figure 10-3. Surface map for case 29

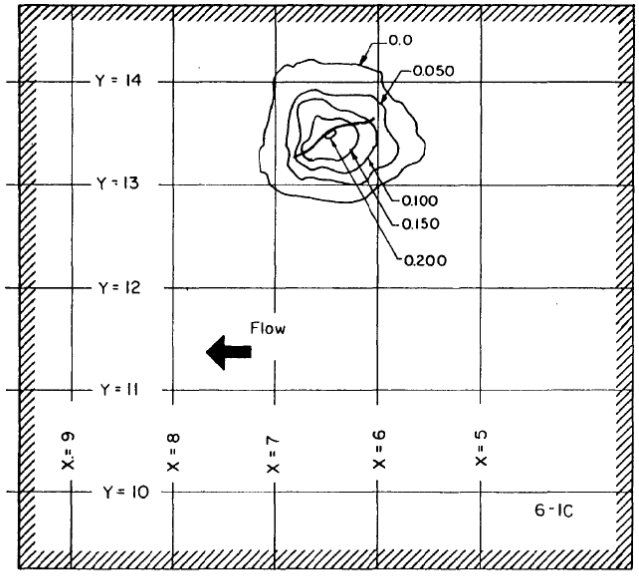

LOCATION OF LEAK IN DIGOUT NO. 6

CASE 30

Figure 10-4. Surface map for case 30

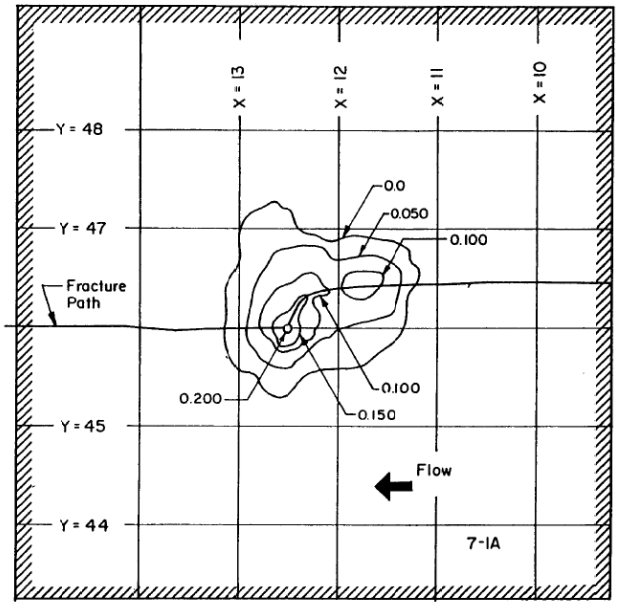

ORIGIN OF RUPTURE IN DIGOUT NO. 7

CASE 31

Figure 10-5. Surface map for case 31

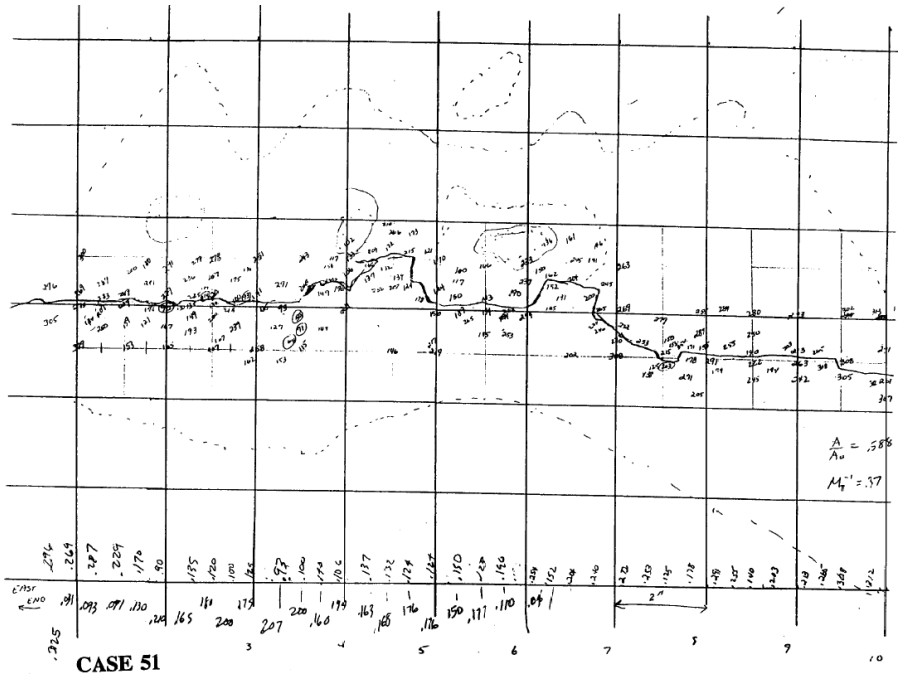

Figure 10-6. Surface map for case 51

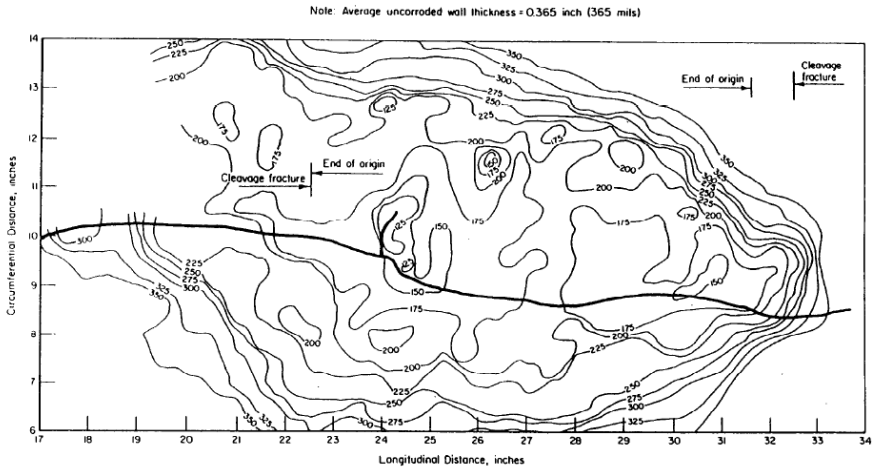

CONTOURS OF REMAINING WALL THICKNESS IN ORIGIN REGION

CASE 80

Figure 10-7. Surface map for case 80

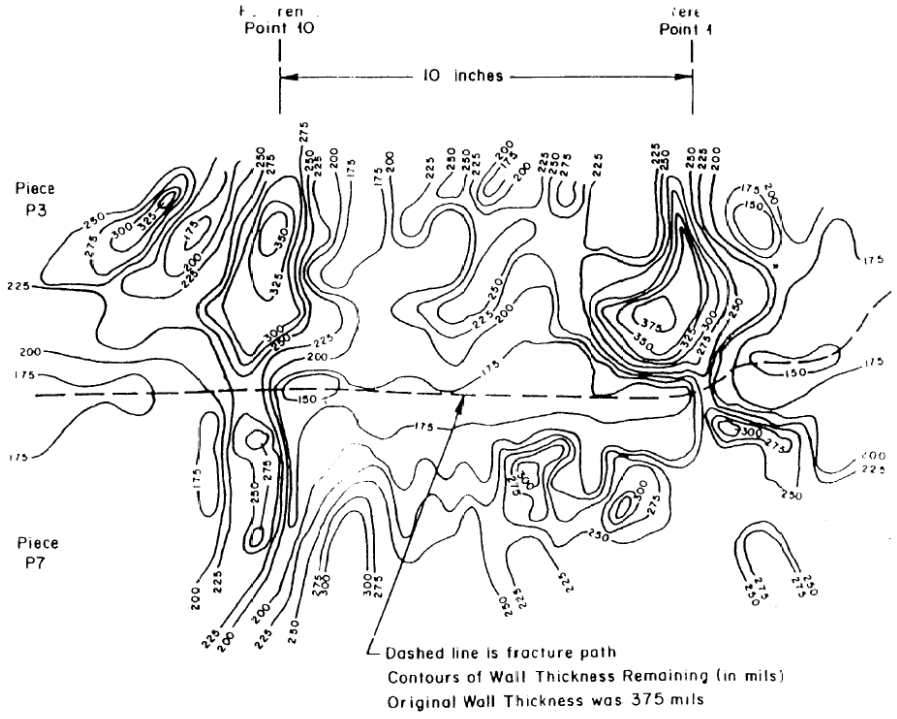

CONTOURS OF REMAINING WALL THICKNESS AT ORIGIN REGION

CASE 81

Figure 10-8. Surface map for case 81

Appendix 2. FEA results for the Cases 28-31, 51, 80 and 81

Case 28

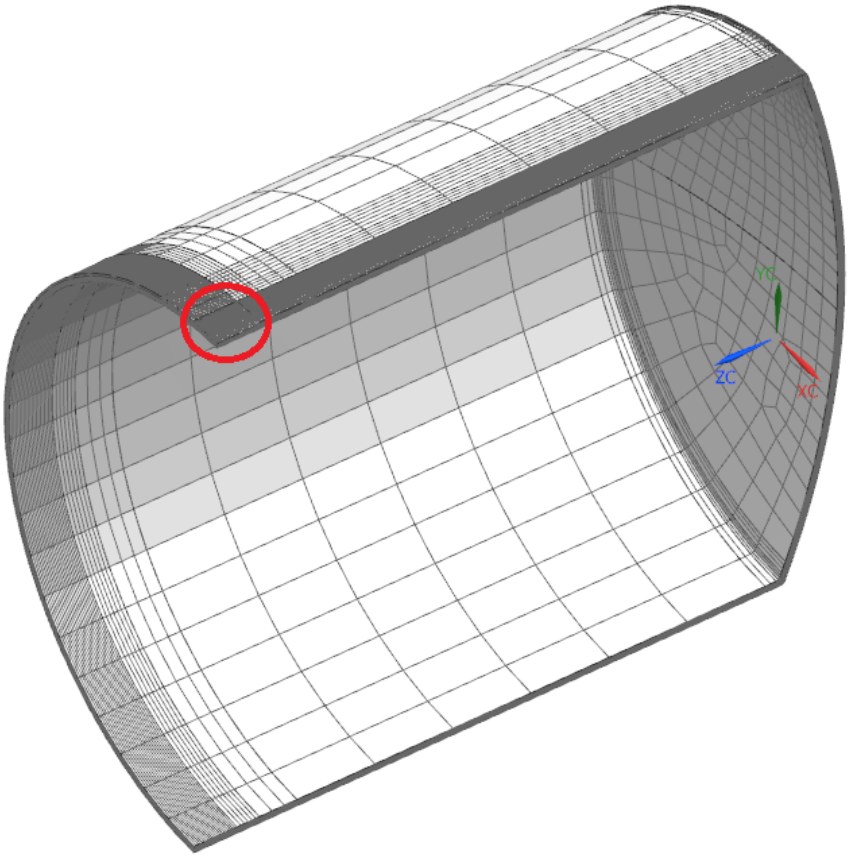

a) Quarter of the pipe with applied mesh on it

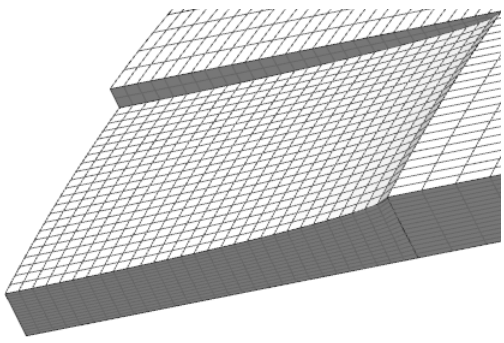

b) Area of the defect

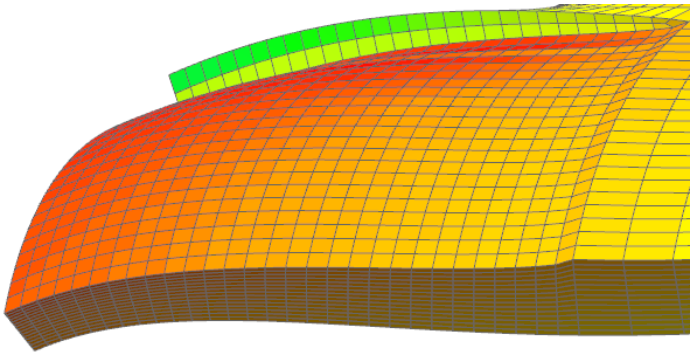

c) The stress distribution in the defect area

Figure 10-9. Case 28, pipe section model used for FEA.

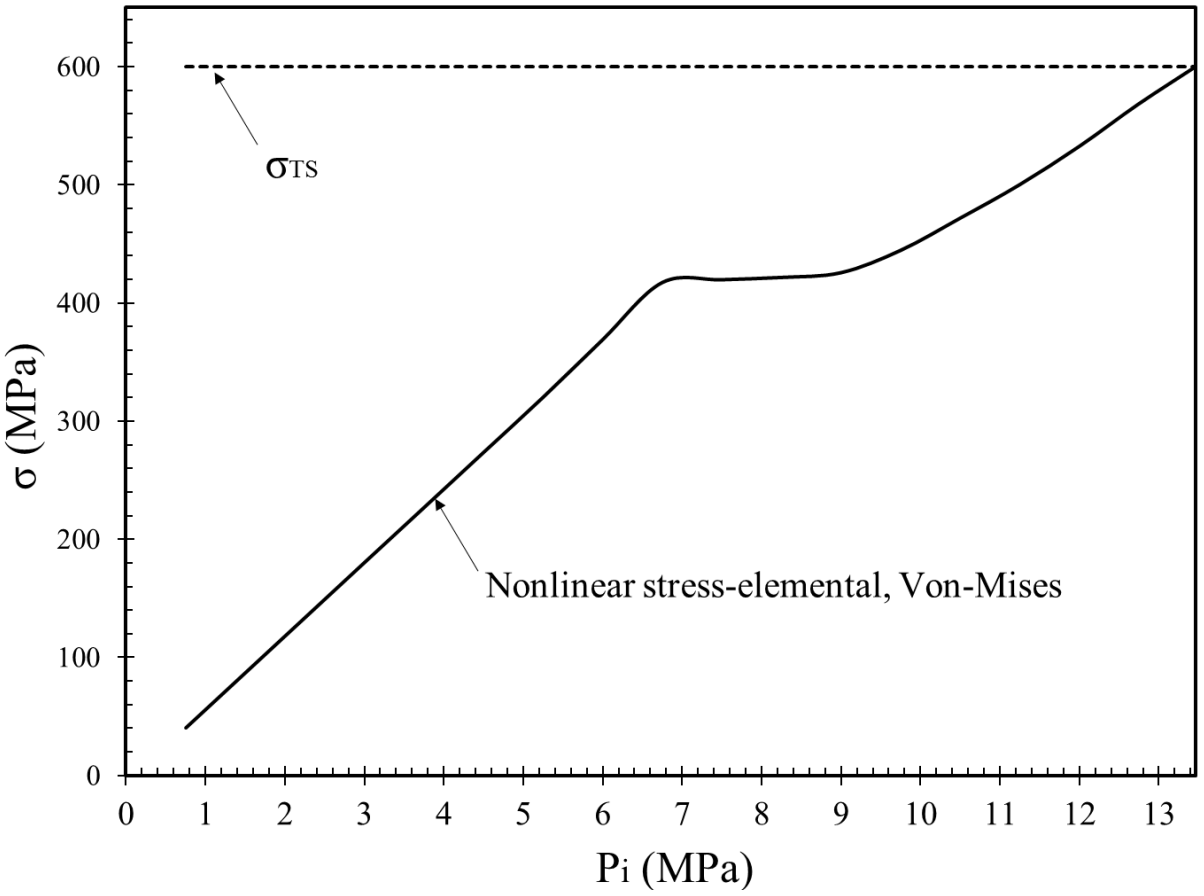

Figure 10-10. Variation of the Von Mises stresses with applied load.

Case 29

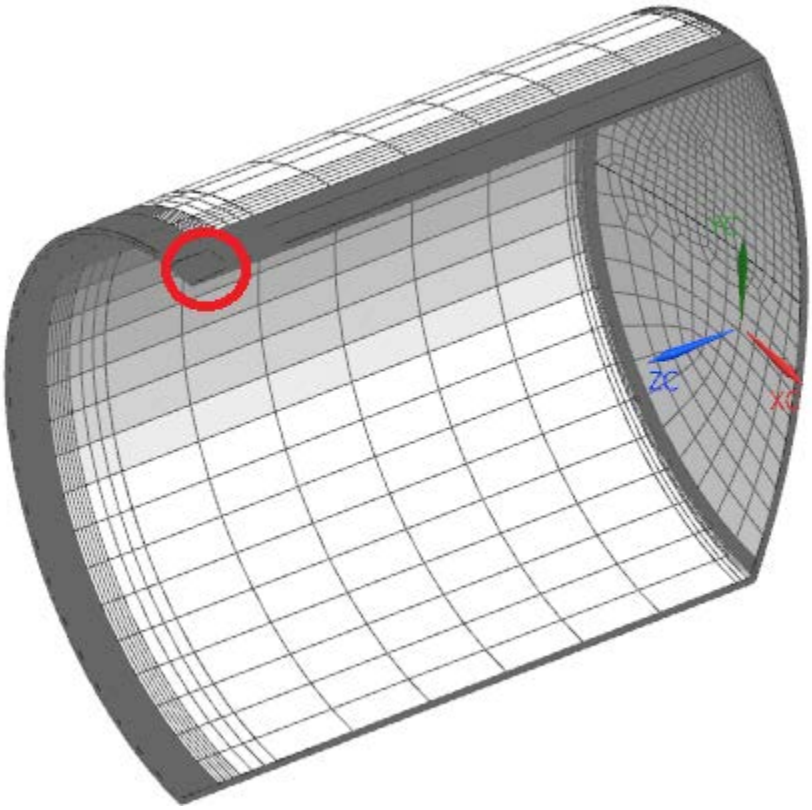

a) Quarter of the pipe with applied mesh on it

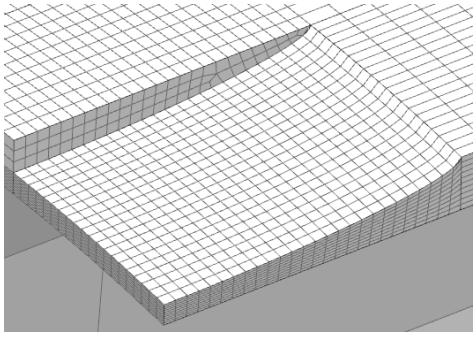

b) Area of the defect

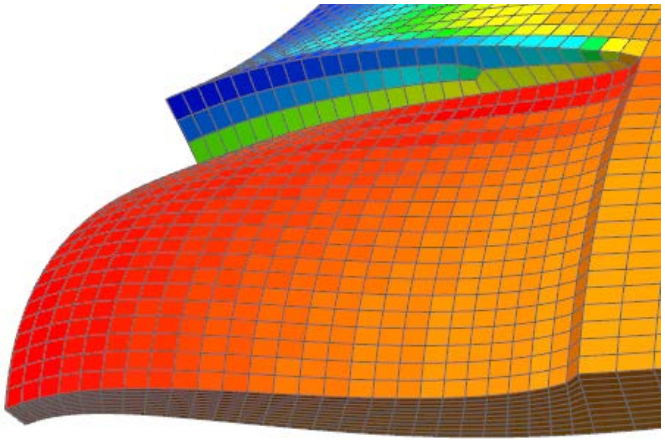

c) The stress distribution in the defect area

Figure 10-11. Case 29, pipe section model used for FEA.

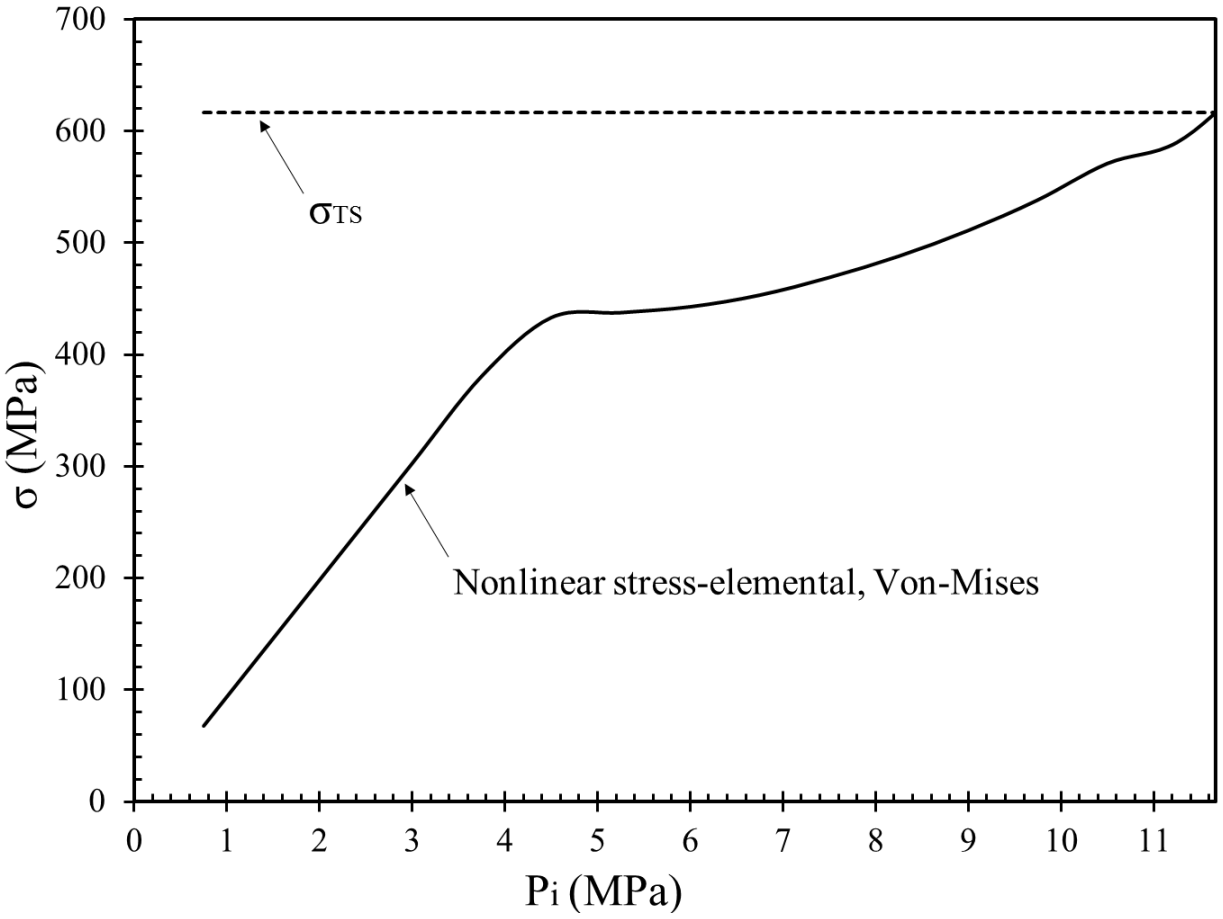

Figure 10-12. Variation of the Von Mises stresses with applied load.

Case 30

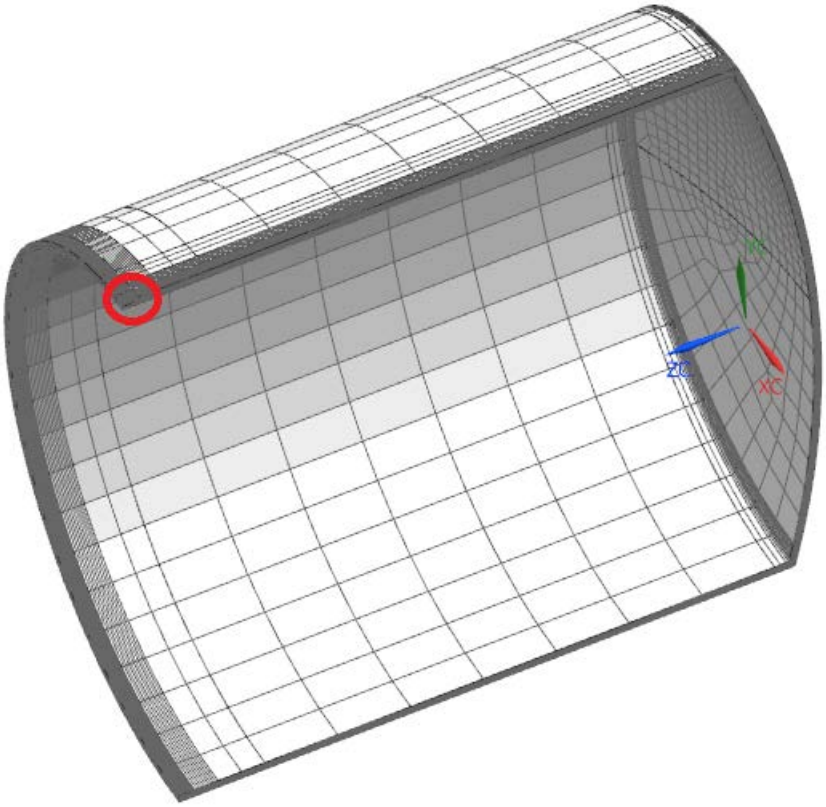

a) Quarter of the pipe with applied mesh on it

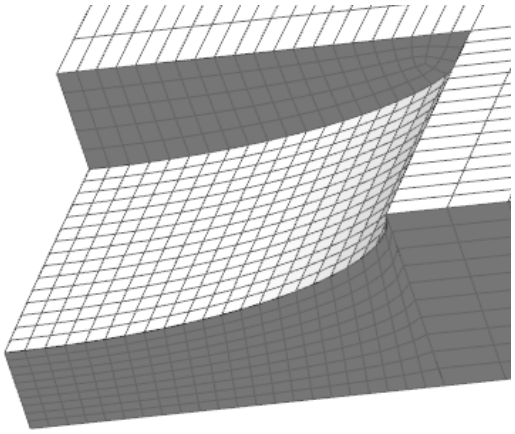

b) Area of the defect

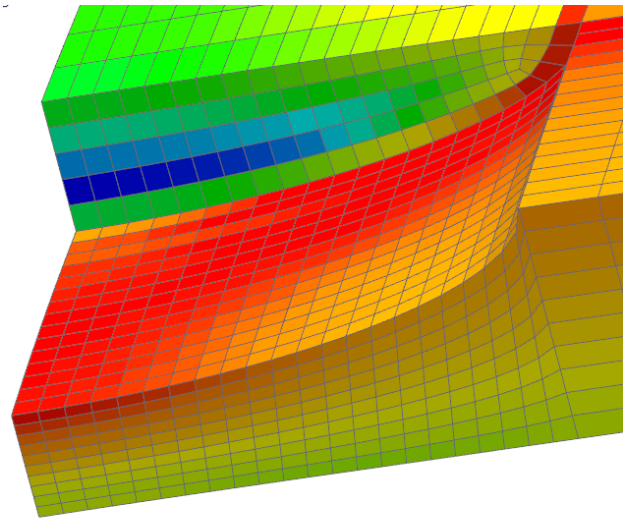

c) The stress distribution in the defect area

Figure 10-13 Case 30, pipe section model used for FEA.

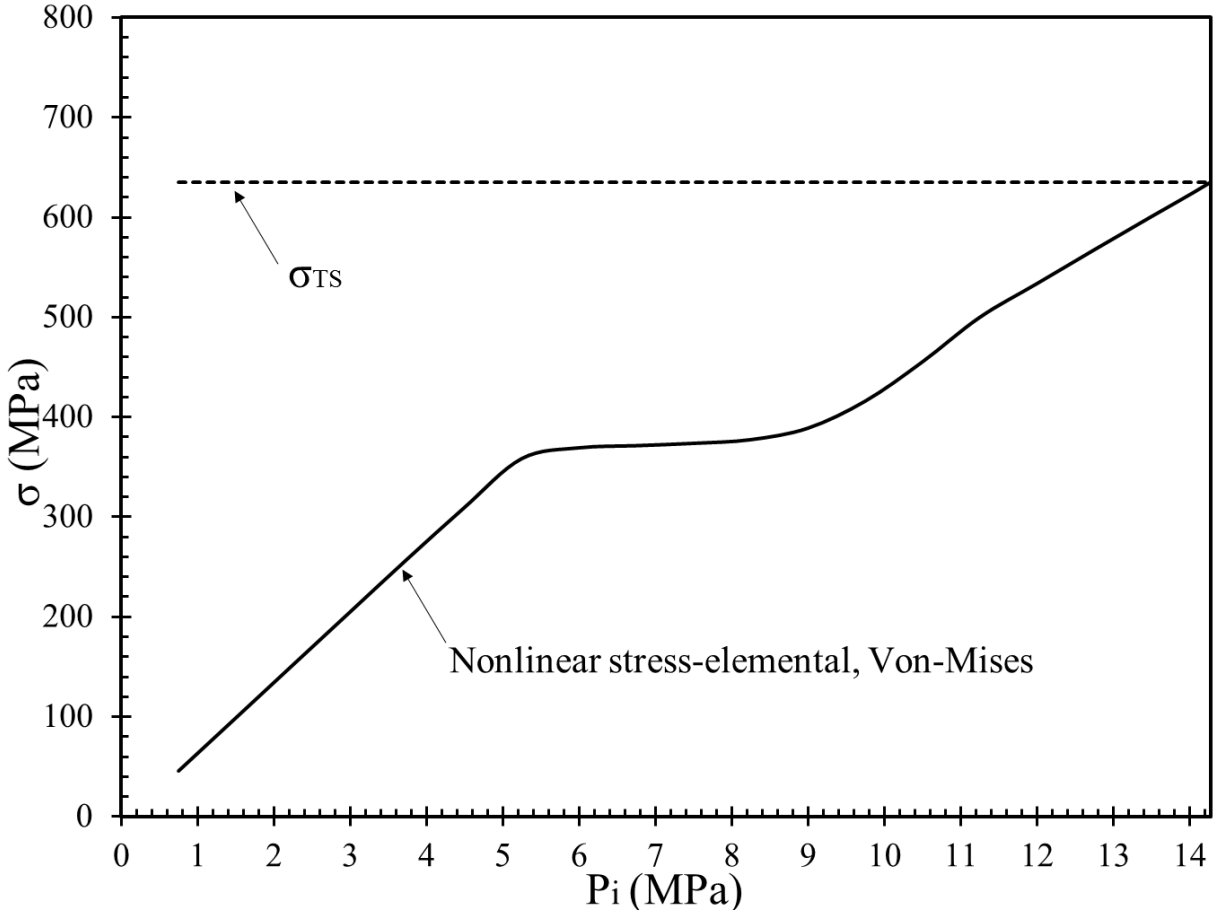

Figure 10-14 Variation of the Von Mises stresses with applied load, Case 30

Case 31

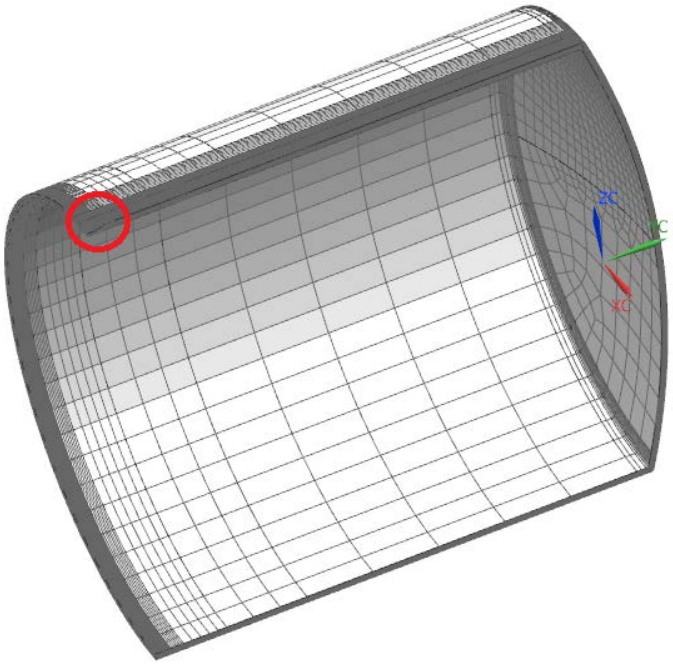

a) Quarter of the pipe with applied mesh on it

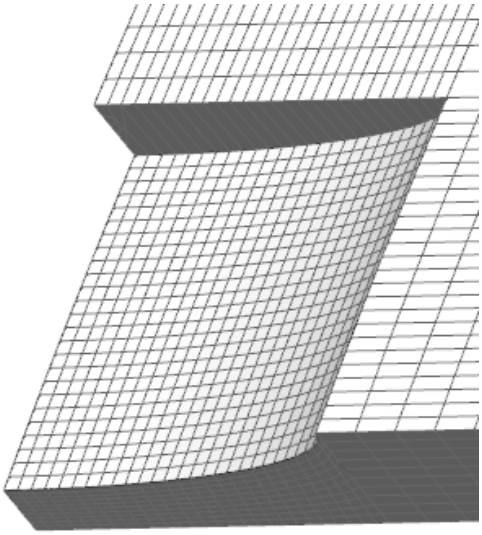

b) Area of the defect

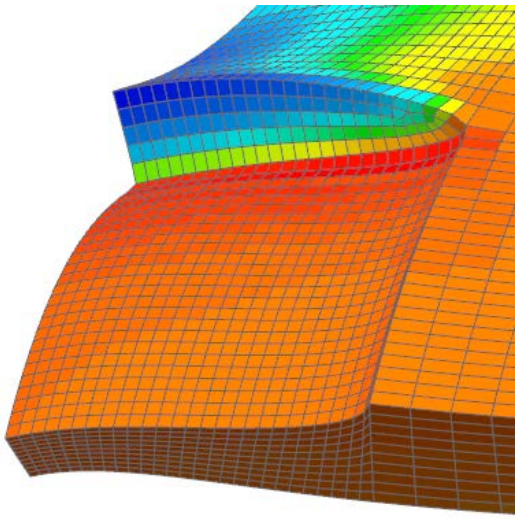

c) The stress distribution in the defect area

Figure 10-15 Case 31, pipe section model used for FEA

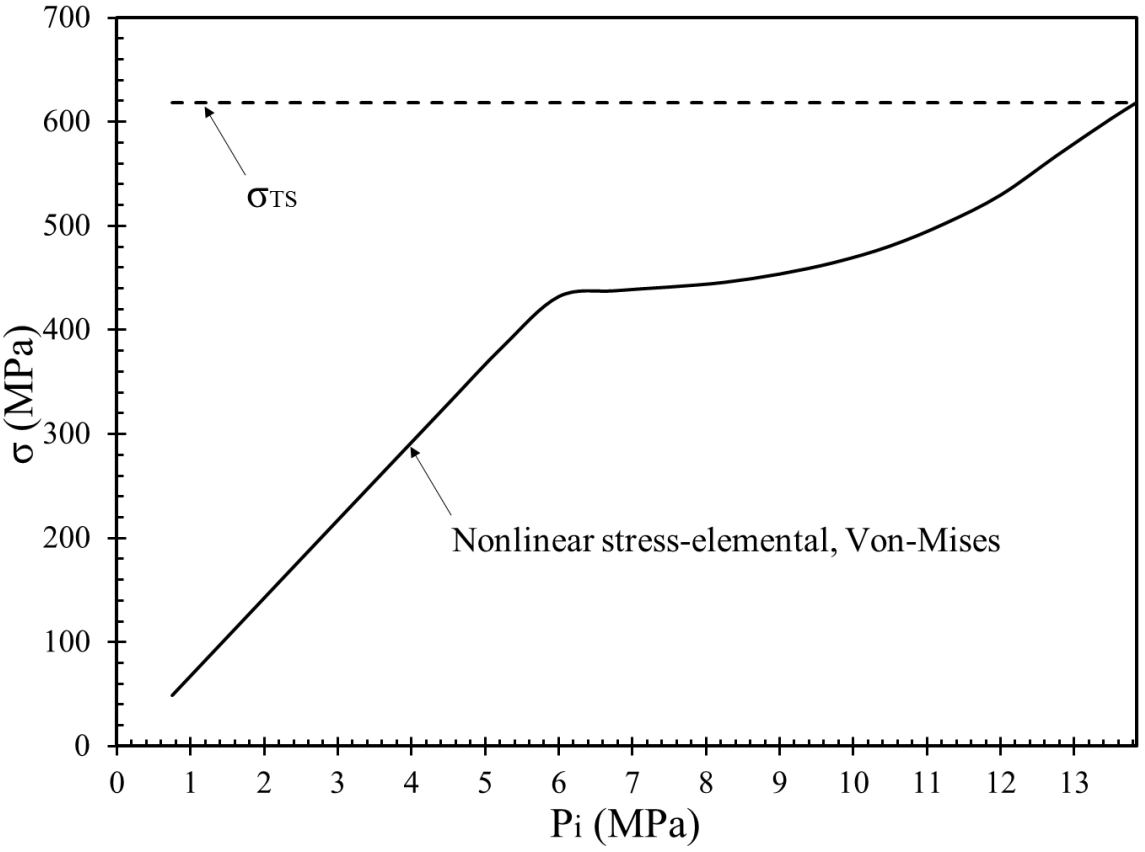

Figure 10-16 Variation of the Von Mises stresses with applied load, Case 31

Case 51

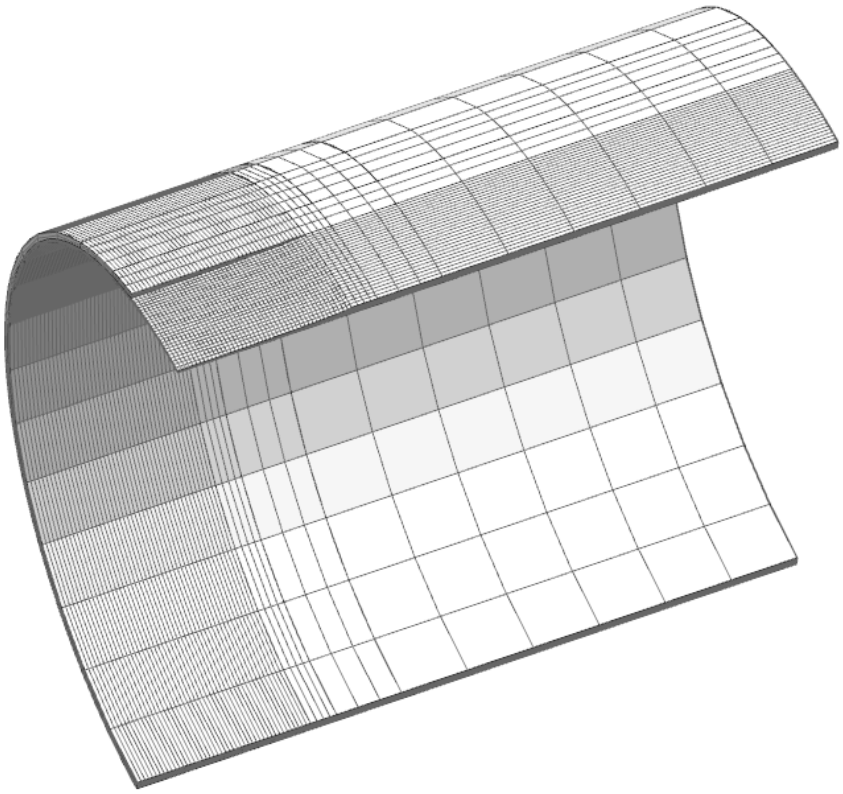

a) Quarter of the pipe with applied mesh on it

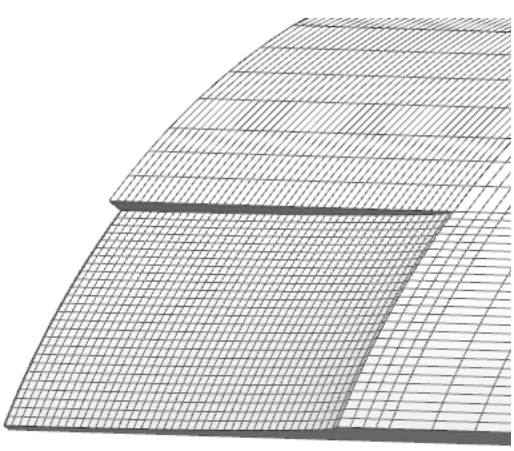

b) Area of the defect

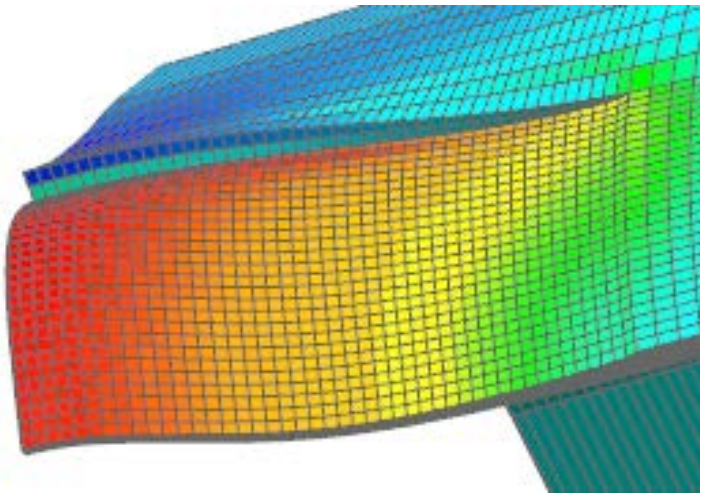

c) The stress distribution in the defect area

Figure 10-17 Case 51, pipe section model used for FEA

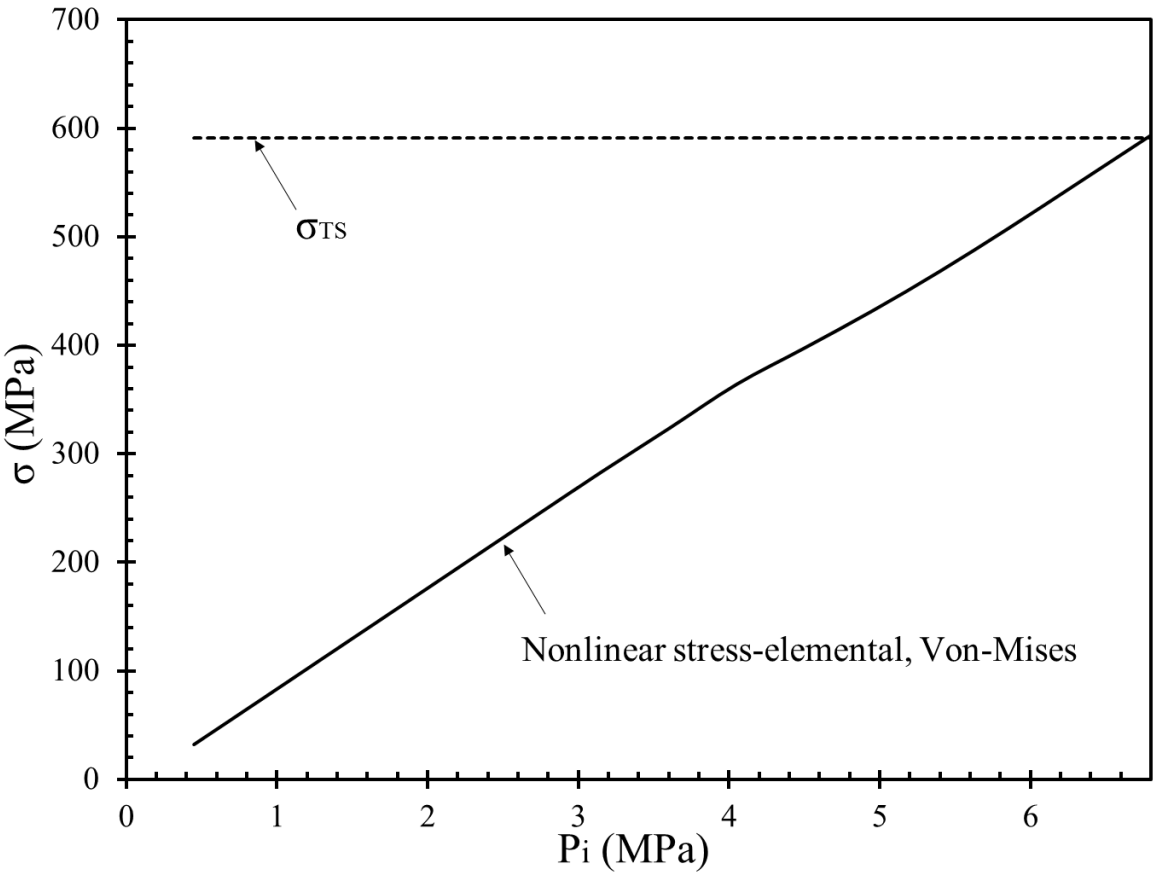

Figure 10-18 Variation of the Von Mises stresses with applied load, Case 51

Case 80

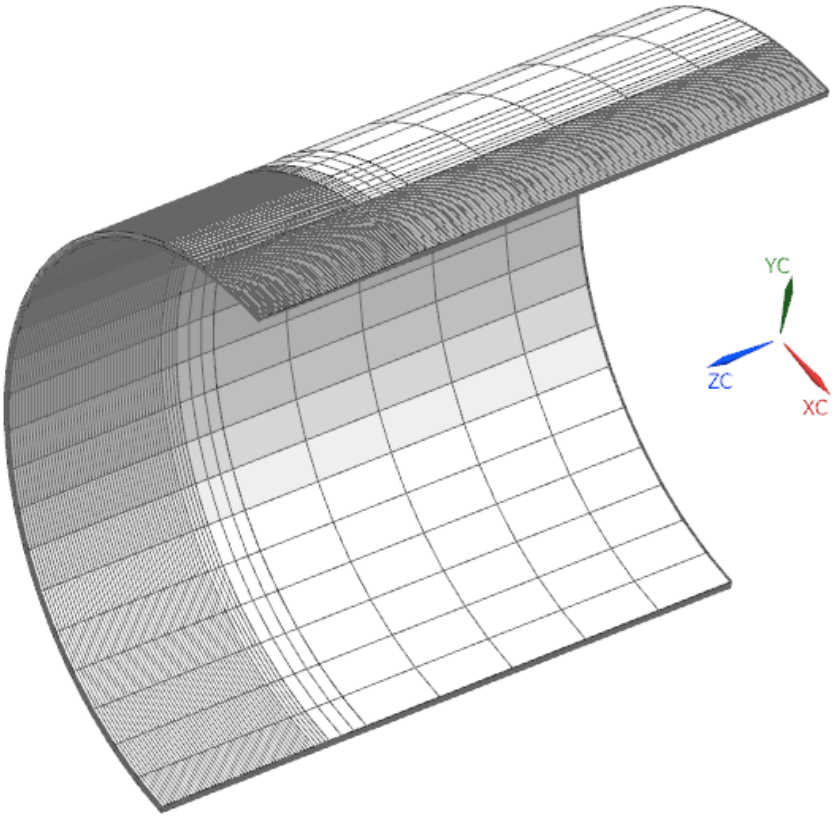

a) Quarter of the pipe with applied mesh on it

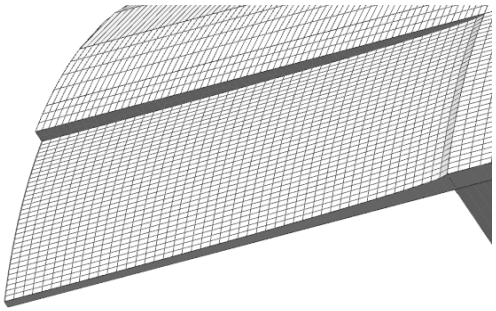

b) Area of the defect

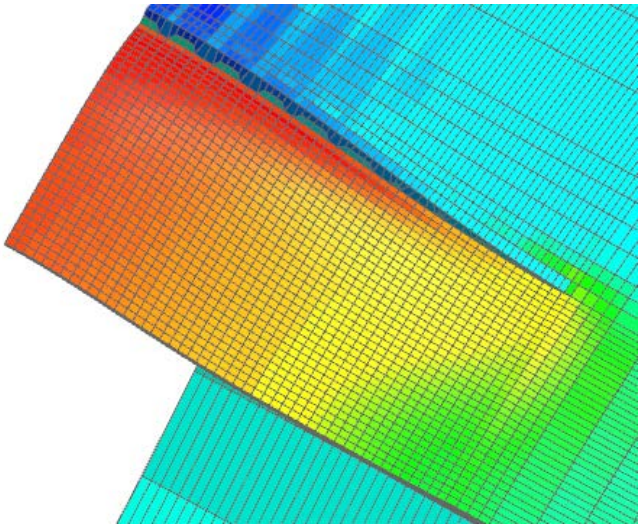

c) The stress distribution in the defect area

Figure 10-19 Case 80, pipe section model used for FEA

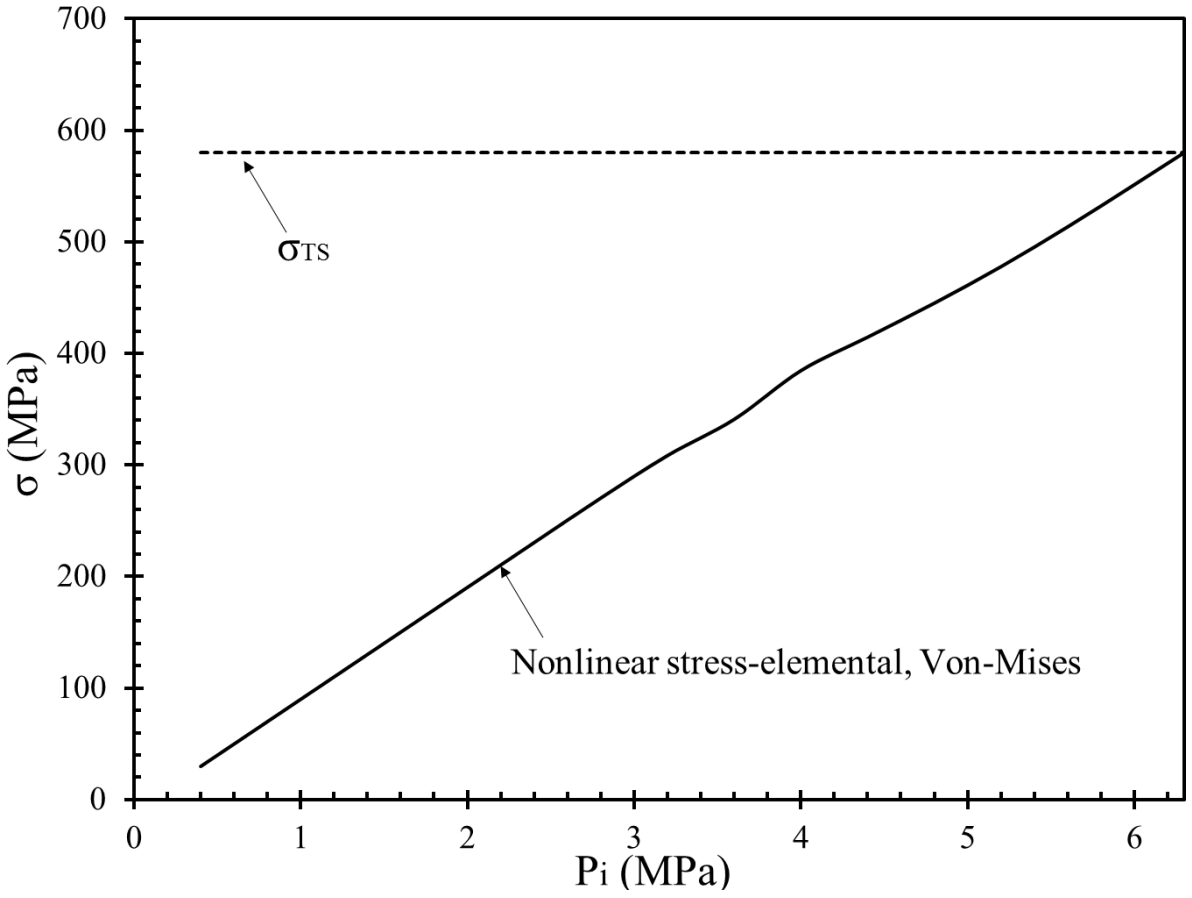

Figure 10-20 Variation of the Von Mises stresses with applied load, Case 80

Case 81

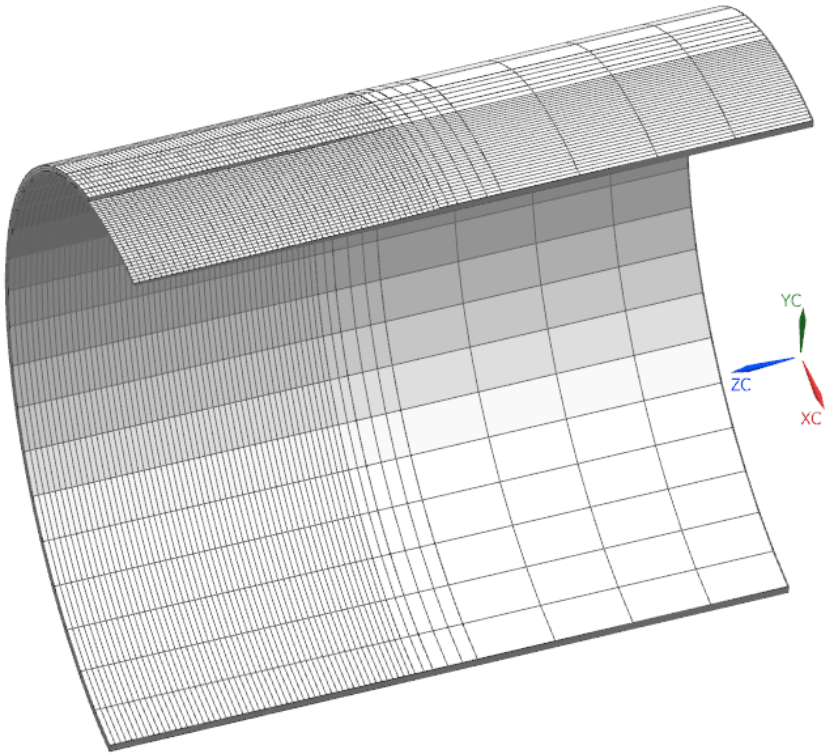

a) Quarter of the pipe with applied mesh on it

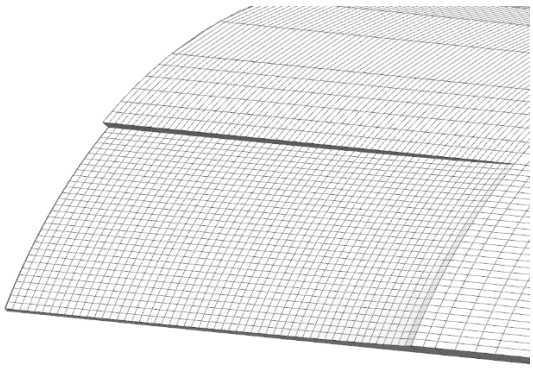

b) Area of the defect

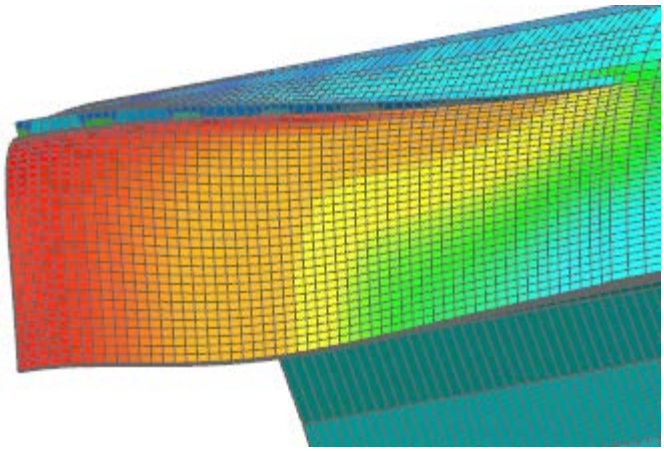

c) The stress distribution in the defect area

Figure 10-21 Case 81, pipe section model used for FEA

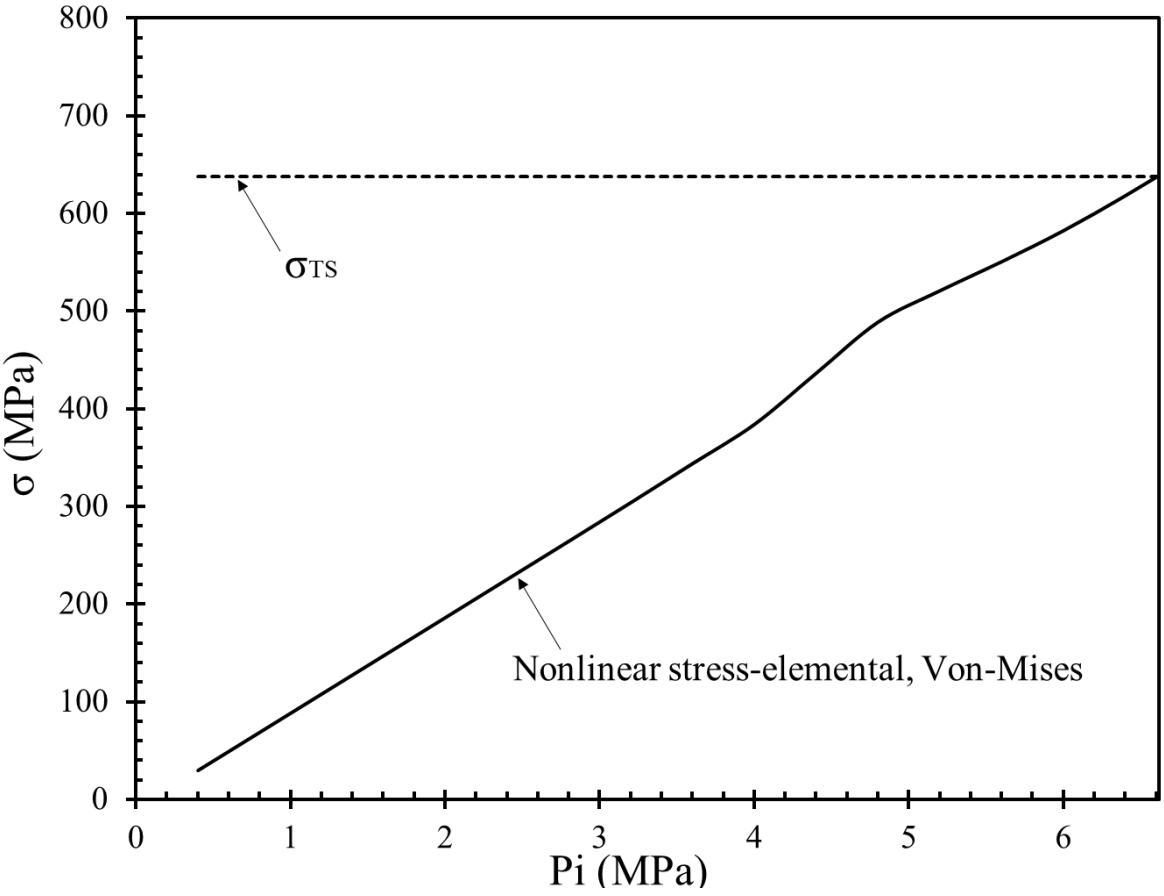

Figure 10-22 Variation of the Von Mises stresses with applied load, Case 81